Applied rheology for melt blown technology

Jiří Drábek

Bachelor thesis
2011

Tomas Bata University in Zlín
Faculty of Technology

Univerzita Tomáše Bati ve Zlíně

Fakulta technologická

Ústav výrobního inženýrství

akademický rok: 2010/2011

ZADÁNÍ BAKALÁŘSKÉ PRÁCE
(PROJEKTU, UMĚLECKÉHO DÍLA, UMĚLECKÉHO VÝKONU)

Jméno a příjmení:	**Jiří DRÁBEK**
Osobní číslo:	**T08589**
Studijní program:	**B 3909 Procesní inženýrství**
Studijní obor:	**Technologická zařízení**
Téma práce:	**Applied rheology for melt blown technology**

Zásady pro vypracování:

1. Prepare the literature overview for the given research subject.
2. Perform rheological evaluation of two different polypropylene melts having extremely low viscosity by suitable experimental techniques.
3. Describe obtained experimental data by an appropriate rheological model.
4. Evaluate the flow behavior of tested polymer samples with respect to nanofiber production by the melt blown technology.

Rozsah bakalářské práce:

Rozsah příloh:

Forma zpracování bakalářské práce: **tištěná/elektronická**

Seznam odborné literatury:

1. Wang, X., Zhao, Q., Effect of processing parameters on the uniformity of adhesive meltblown web , Polymer Engineering and Science 48, 2143–2146 (2008).
2. Chen, T., Zhang, C., Chen, X., Li, Q., Numerical computation of the fiber diameter of melt blown nonwovens produced by the inset die , Journal of Applied Polymer Science 111, 1775–1779 (2009).
3. Tan, D. H., Zhou, Ch., Ellison, Ch. J., Kumar, S., Macosko, Ch. W., Bates, F. S., Meltblown fibers: Influence of viscosity and elasticity on diameter distribution, Journal of Non–Newtonian Fluid Mechanics, 165, 892–900 (2010).
4. Joseph, E. G., Structure and properties of multi–layer melt blown microfiber non-wovens, Annual Technical Conference – ANTEC, Conference Proceedings, 1092–1095 (2010).
5. Macosko, CH.W.: Rheology : Principles, Measurements and Applications. New York, 1994.
6. Zatloukal, M.: A simple phenomenological non–Newtonian fluid model, Journal of Non–Newtonian Fluid Mechanics, 165, 592–595 (2010).
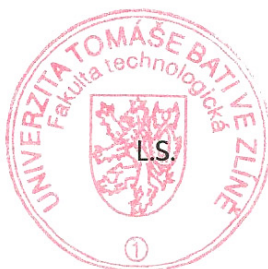
Vedoucí bakalářské práce: **prof. Ing. Martin Zatloukal, Ph.D.**
                                 Centrum polymerních materiálů

Datum zadání bakalářské práce: **14. února 2011**

Termín odevzdání bakalářské práce: **3. června 2011**

Ve Zlíně dne 11. ledna 2011
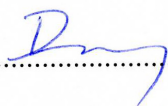
doc. Ing. Petr Hlaváček, CSc.   L.S.   doc. Ing. Miroslav Maňas, CSc.
        děkan   *ředitel ústavu*

Příjmení a jméno: Drábek Jiří   Obor: Technologická zařízení

P R O H L Á Š E N Í

Prohlašuji, že

- beru na vědomí, že odevzdáním diplomové/bakalářské práce souhlasím se zveřejněním své práce podle zákona č. 111/1998 Sb. o vysokých školách a o změně a doplnění dalších zákonů (zákon o vysokých školách), ve znění pozdějších právních předpisů, bez ohledu na výsledek obhajoby [1)];
- beru na vědomí, že diplomová/bakalářská práce bude uložena v elektronické podobě v univerzitním informačním systému dostupná k nahlédnutí, že jeden výtisk diplomové/bakalářské práce bude uložen na příslušném ústavu Fakulty technologické UTB ve Zlíně a jeden výtisk bude uložen u vedoucího práce;
- byl/a jsem seznámen/a s tím, že na moji diplomovou/bakalářskou práci se plně vztahuje zákon č. 121/2000 Sb. o právu autorském, o právech souvisejících s právem autorským a o změně některých zákonů (autorský zákon) ve znění pozdějších právních předpisů, zejm. § 35 odst. 3 [2)];
- beru na vědomí, že podle § 60 [3)] odst. 1 autorského zákona má UTB ve Zlíně právo na uzavření licenční smlouvy o užití školního díla v rozsahu § 12 odst. 4 autorského zákona;
- beru na vědomí, že podle § 60 [3)] odst. 2 a 3 mohu užít své dílo – diplomovou/bakalářskou práci nebo poskytnout licenci k jejímu využití jen s předchozím písemným souhlasem Univerzity Tomáše Bati ve Zlíně, která je oprávněna v takovém případě ode mne požadovat přiměřený příspěvek na úhradu nákladů, které byly Univerzitou Tomáše Bati ve Zlíně na vytvoření díla vynaloženy (až do jejich skutečné výše);
- beru na vědomí, že pokud bylo k vypracování diplomové/bakalářské práce využito softwaru poskytnutého Univerzitou Tomáše Bati ve Zlíně nebo jinými subjekty pouze ke studijním a výzkumným účelům (tedy pouze k nekomerčnímu využití), nelze výsledky diplomové/bakalářské práce využít ke komerčním účelům;
- beru na vědomí, že pokud je výstupem diplomové/bakalářské práce jakýkoliv softwarový produkt, považují se za součást práce rovněž i zdrojové kódy, popř. soubory, ze kterých se projekt skládá. Neodevzdání této součásti může být důvodem k neobhájení práce.

Ve Zlíně 30.5.2011   ....

[1] zákon č. 111/1998 Sb. o vysokých školách a o změně a doplnění dalších zákonů (zákon o vysokých školách), ve znění pozdějších právních předpisů, § 47 Zveřejňování závěrečných prací:

(1) Vysoká škola nevýdělečně zveřejňuje disertační, diplomové, bakalářské a rigorózní práce, u kterých proběhla obhajoba, včetně posudků oponentů a výsledku obhajoby prostřednictvím databáze kvalifikačních prací, kterou spravuje. Způsob zveřejnění stanoví vnitřní předpis vysoké školy.

(2) Disertační, diplomové, bakalářské a rigorózní práce odevzdané uchazečem k obhajobě musí být též nejméně pět pracovních dnů před konáním obhajoby zveřejněny k nahlížení veřejnosti v místě určeném vnitřním předpisem vysoké školy nebo není-li tak určeno, v místě pracoviště vysoké školy, kde se má konat obhajoba práce. Každý si může ze zveřejněné práce pořizovat na své náklady výpisy, opisy nebo rozmnoženiny.

(3) Platí, že odevzdáním práce autor souhlasí se zveřejněním své práce podle tohoto zákona, bez ohledu na výsledek obhajoby.

[2] zákon č. 121/2000 Sb. o právu autorském, o právech souvisejících s právem autorským a o změně některých zákonů (autorský zákon) ve znění pozdějších právních předpisů, § 35 odst. 3:

(3) Do práva autorského také nezasahuje škola nebo školské či vzdělávací zařízení, užije-li nikoli za účelem přímého nebo nepřímého hospodářského nebo obchodního prospěchu k výuce nebo k vlastní potřebě dílo vytvořené žákem nebo studentem ke splnění školních nebo studijních povinností vyplývajících z jeho právního vztahu ke škole nebo školskému či vzdělávacího zařízení (školní dílo).

[3] zákon č. 121/2000 Sb. o právu autorském, o právech souvisejících s právem autorským a o změně některých zákonů (autorský zákon) ve znění pozdějších právních předpisů, § 60 Školní dílo:

(1) Škola nebo školské či vzdělávací zařízení mají za obvyklých podmínek právo na uzavření licenční smlouvy o užití školního díla (§ 35 odst. 3). Odpírá-li autor takového díla udělit svolení bez vážného důvodu, mohou se tyto osoby domáhat nahrazení chybějícího projevu jeho vůle u soudu. Ustanovení § 35 odst. 3 zůstává nedotčeno.

(2) Není-li sjednáno jinak, může autor školního díla své dílo užít či poskytnout jinému licenci, není-li to v rozporu s oprávněnými zájmy školy nebo školského či vzdělávacího zařízení.

(3) Škola nebo školské či vzdělávací zařízení jsou oprávněny požadovat, aby jim autor školního díla z výdělku jím dosaženého v souvislosti s užitím díla či poskytnutím licence podle odstavce 2 přiměřeně přispěl na úhradu nákladů, které na vytvoření díla vynaložily, a to podle okolností až do jejich skutečné výše; přitom se přihlédne k výši výdělku dosaženého školou nebo školským či vzdělávacím zařízením z užití školního díla podle odstavce 1.

ABSTRAKT

Tato práce se věnuje problematice experimentálního a teoretického hodnocení tokového chování dvou odlišných polymerů s velmi vysokým indexem toku taveniny, a to s ohledem na výrobu polymerních nanovláken pomocí technologie melt blown.

Klíčová slova: polymerní nanovlákna, technologie melt blown, smyková viskozita, elongační viskozita, aplikovaná reologie, zpracovatelství polymerů

ABSTRACT

In this work, two different melt blown polymer samples with very high melt flow indexes have been rheologically characterized by using suitable experimental technique and theoretical tools and the results have been discussed from the polymeric nanofiber production point of view.

Keywords: polymeric nanofibers, melt blown technology, shear viscosity, extensional viscosity, applied rheology, polymer processing

ACKNOWLEDGEMENTS

I would like to express my sincere gratitude to all people who supported me during the work on the thesis.

I am especially grateful to my supervisor, prof. Ing. Martin Zatloukal, Ph.D. for his patience, guidance and support throughout the process of measuring and analyzing data and writing the thesis.

I am also indebted to Ing. Luboš Rokyta for his advice concerning about 3D figures which are use in this thesis and its presentation.

I would like to extend my gratitude to my family and all my true friends for their support.

I declare that surrender release bachelor thesis and recorded in the electronic version of IS/STAG are identical.

I agree that the results of my Bachelor Thesis can be used by my supervisor's decision. I will be mentioned as a co-author in the case of any publication.

I declare I worked on this Bachelor Thesis by myself and I have mentioned all the used literature.

Zlín, May 23, 2011

Jiří Drábek
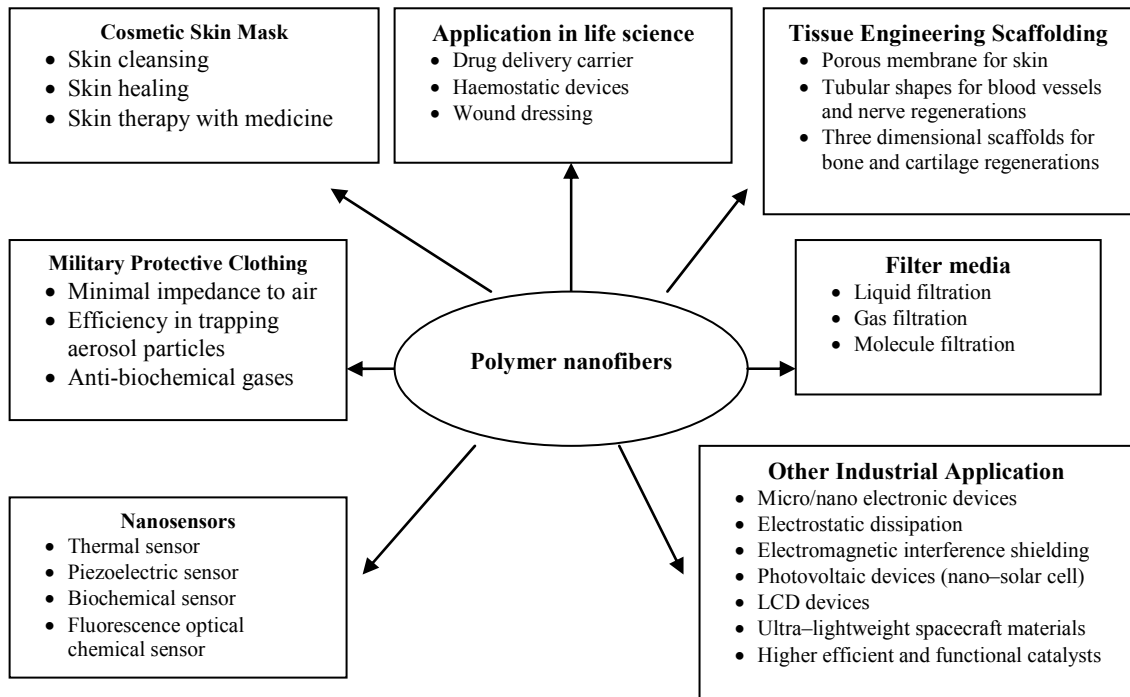
CONTENTS

INTRODUCTION

One of the key problem in the polymer processing operations optimization is unknown relationship between equipment design, processing conditions and rheological characteristics of the polymers. In order to assess such relationships, the modeling of the polymer processing is widely utilized for which the rheological characteristics of the polymer melts determined at the particular temperature range represents crucially important material input data. However, the selection of the proper constitutive equation for the polymer melt, which is able to represent the measured rheological data mathematically, is required to reach fully predictive capabilities of the performed polymer processing simulations. Thus, the polymer processing operation at which the full rheological polymer sample characterization is very complicated or practically impossible by standard rheological tools is difficult to optimize. The melt blown technology for the polymeric nanofibers production is one of them. In more detail, polymer melt viscosity during the nanofiber production has to decrease considerably (melt index > 1600 g/10 min). As the result, the measurement of basic rheological characteristics at the processing deformation rates for the melt blown polymer samples is challenging task.

With the aim to extend the current knowledge in such a research field, the work is focused on the rheological evaluation of two different PP melt blown samples by using capillary rheometer in order to find out the way in which shear as well as extensional viscosities can be determined experimentally at wide range of deformation rates. In the second part of this work, fitting capabilities of two different constitutive equations for the melt blown polymer melts are tested and the obtained results are evaluated with respect to polymer nanofiber production.

I. THEORY

1 POLYMERIC NANOFIBERS

Nanotechnology has enjoyed unprecedented global research and development support over the last few years. Their unusual physicochemical characteristics are primarily governed by their very high surface area to volume ratio or the ratio of surface atoms to the interior atoms in cluster (see Figure 1) [1].

Cosmetic Skin Mask
- Skin cleansing
- Skin healing
- Skin therapy with medicine

Application in life science
- Drug delivery carrier
- Haemostatic devices
- Wound dressing

Tissue Engineering Scaffolding
- Porous membrane for skin
- Tubular shapes for blood vessels and nerve regenerations
- Three dimensional scaffolds for bone and cartilage regenerations

Military Protective Clothing
- Minimal impedance to air
- Efficiency in trapping aerosol particles
- Anti-biochemical gases

Polymer nanofibers

Filter media
- Liquid filtration
- Gas filtration
- Molecule filtration

Nanosensors
- Thermal sensor
- Piezoelectric sensor
- Biochemical sensor
- Fluorescence optical chemical sensor

Other Industrial Application
- Micro/nano electronic devices
- Electrostatic dissipation
- Electromagnetic interference shielding
- Photovoltaic devices (nano–solar cell)
- LCD devices
- Ultra–lightweight spacecraft materials
- Higher efficient and functional catalysts

Fig. 1. The diversity of applications for polymer nanofibers [1]

Nanofiber mats, having fiber diameter typically in order of tens and hundred nanometers, are very well suited for air filtration because low solidity and acceptable mechanical strength can be obtained. During the past decades, significant process has been done in the area of filtration science and technology, which follows increased needs of many advanced industries dealing with electronics, medical, pharmaceutical and biology to maintain clean room manufacturing environments. The increase in air velocity, viscosity and air pressure leads to filtration efficiency decrease, because of increased drag/lift forces and reduced Brownian motion intensity, where as the increase in the air temperature and particle-fiber fiction coefficient leads to filtration efficiency enhancement due to increased Brownian motion intensity and reduced particle-slip, respectively, and vice versa [2]. Nanofibers are characterized by a very large surface area to volume ratio, which significantly increases the probability of the aerosol particles deposition on the fiber surface and thus, the filter effi-

ciency can be significantly increased. Future growth and diversification of the nonwoven industry depends on the capability of producing nonwoven fibers with an average diameter less than 1μm commonly called nanofibers. Nanofibers offer a smaller average pore size, which can enhance performance in filtration applications. There are several techniques capable of generating nanofibers, such as electrospinning, melt blowing, jet blowing and laser-assisted supersonic drawing. Moreover, many different types of polymers can be utilized for the nanofiber production by using these techniques [3]. Probably the most popular techniques to produce continuously nanofibers from the polymer melt is melt blown technology [4]. The melt blown technique may allow making large quantities of such fibers at low cost, which will considerably increase their commercial applications [5].

2   MELT BLOWN TECHNOLOGY

The first attempt to develop microfiber was in 1939, by Carlton Francis, who pictured a spray gun as a process in which textile like microfiber can be developed [6]. The melt blown technology (MB) is one-step process for converting polymer into a microfiber structure web that dates back to the 1950s [7]. In the early 1950s, the United States Army Chemical Warfare Laboratories continued Dow research to produce microfibers to collect radioactive particles [6]. MB webs have fiber diameters generally in the range of 2 to 4 μm. MB webs produced from different polymer systems are extensively used in a wide range of applications. One of disadvantages of melt blown webs is its lack of mechanical strength [8]. It has become an important industrial technique because of its ability to produce fabrics of microfiber structure [9].
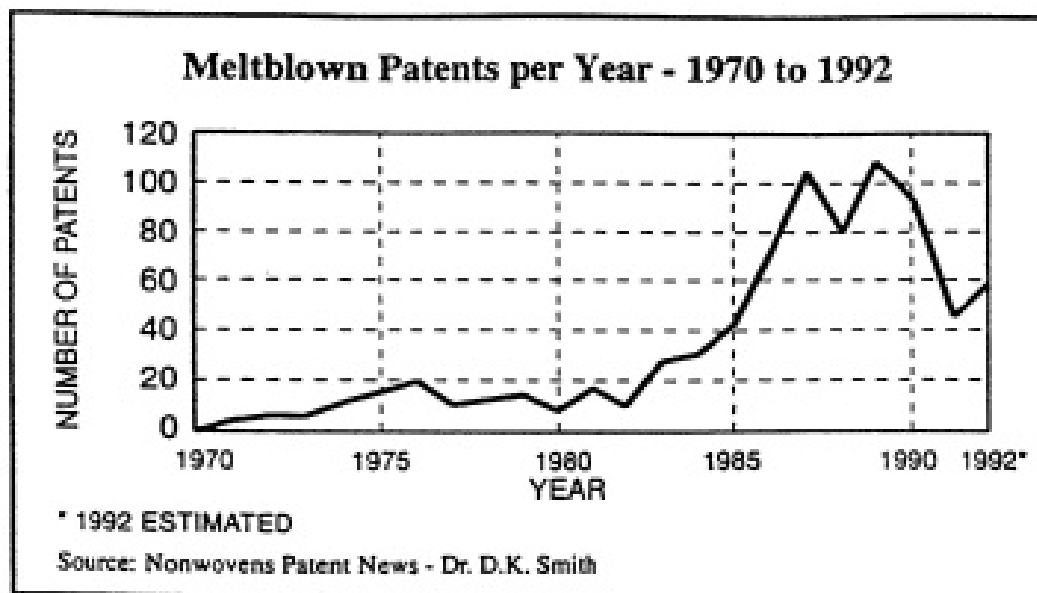
Fig. 2. Plot of the number of melt blown patents granted between 1970 and 1992 [10]

The rapid grow of the applied patents in area of melt blown technology granted between 1970 and 1992 (see Figure 2) and over 2500 patent applications processed between 2000 and 2009 [10] indicates research as well as industrial importance of this technology.

2.1 Melt blown line
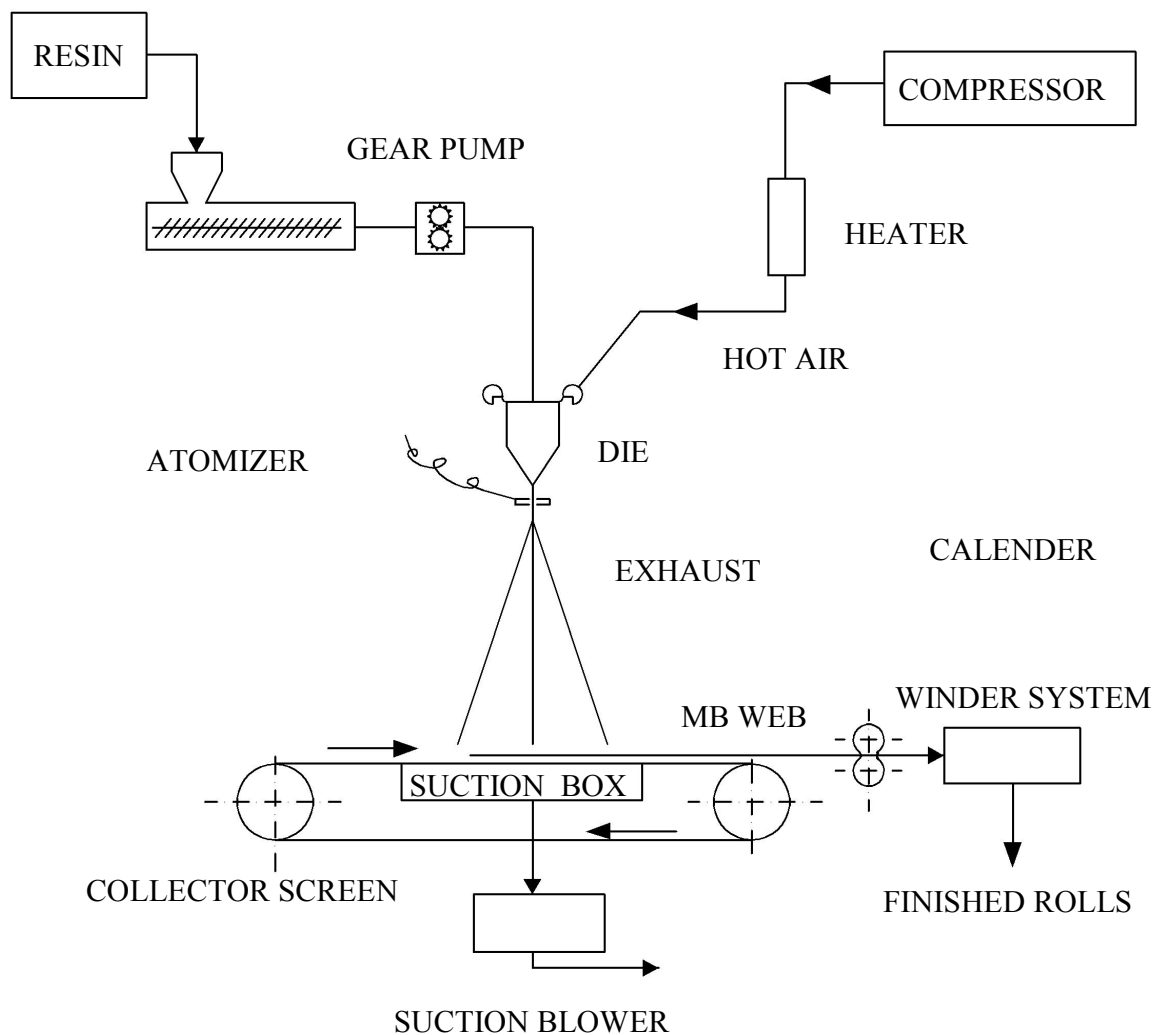
Fig. 3. Melt blown line [11]

Meltblown is one of the fastest growing processes for nonwoven production [9]. The concept of the melt blown (MB) process was first introduced in 1956 through a Naval Research Laboratory project initiated by Wente to produce filters composed of microfibers for collect radioactive particles from the atmosphere during the early years of cold war [12]. In the melt blowing process, high velocity hot air streams impact upon a stream of molten polymer as the polymer issues from a fine capillary (see Figure 3). The result of this impact is that the polymer is rapidly (in about 50 µs) attenuated into fiber as fine as 1 µm in diameter. The fiber diameter of melt blown nonwovens, therefore, is strongly affected by the air jet flow field developed from the dual slot die [13]. Meltblown nonwoven fabrics are produced directly from granules or pellets of thermoplastics [14]. Solid polymer

in the form of pellets is added into a hopper, and due to the movement of the screw in the heated barrel, the polymer pellets are melted and pushed into the melt blown die, which consists of number of very small capillaries [15].

2.2 Melt blown die design

MANIFOLD   RESTRICTOR   RELAXATION CHAMBER
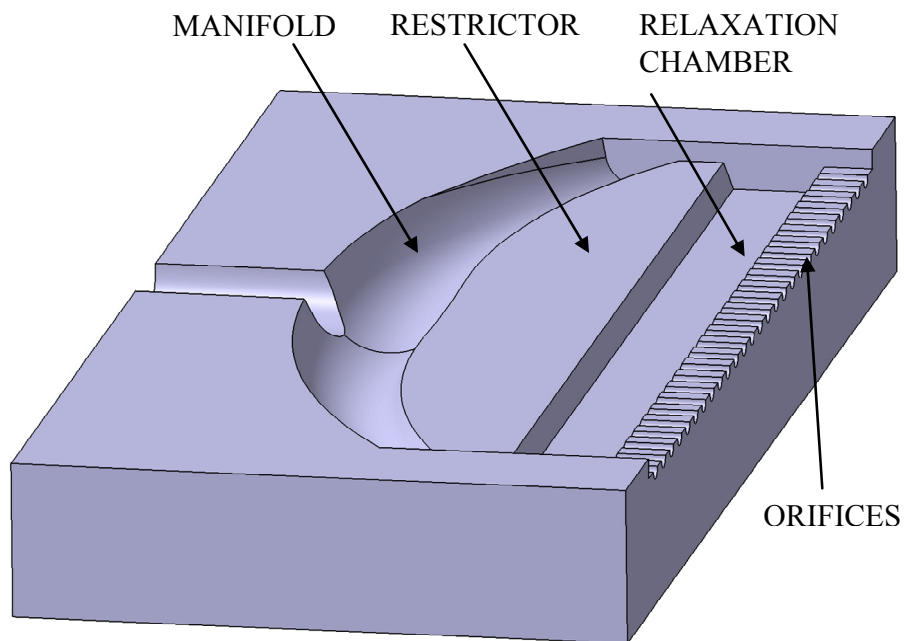
ORIFICES

Fig. 4. Flat die [16]

The design of the coat-hanger geometry of a die is very important for meltblown technology [9]. The meltblown die tip is a very wide but thin piece of metal with each orifice typically measuring about 0.4 mm. However, the orifice can vary in size to allow anywhere from 1 - 4 orifices per millimeter (see Figure 4) [6].

2.2.1   Flat die
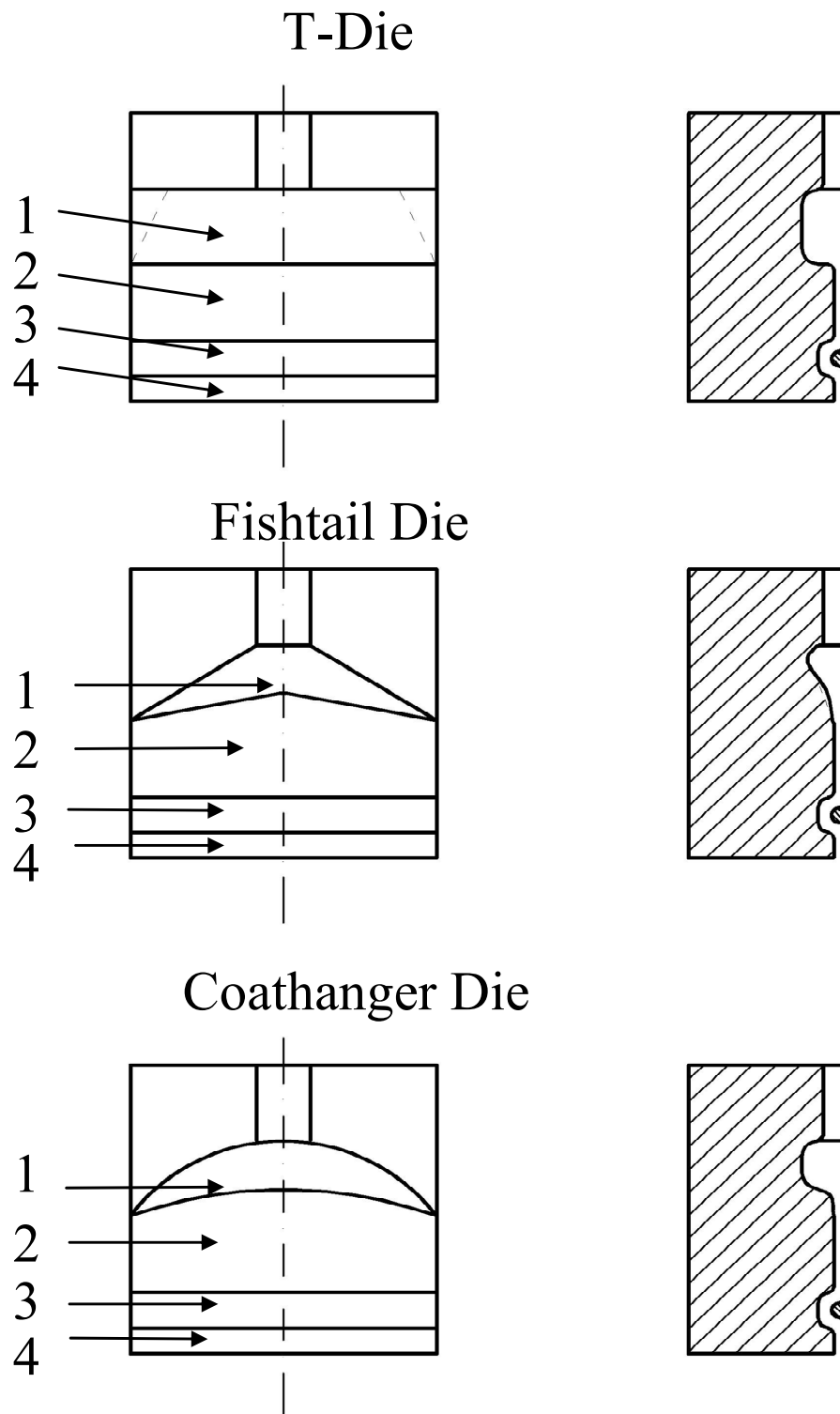
Fig. 5. Different flat die types [16] where 1 is the manifold, 2 is the restrictor, 3 is the relaxation chamber, 4 is the die land.

2.3 Die exit

6a) DIE NOSE TIP

POLYMER FEED

6b)

SLOT

6c)

6d) DIE NOSE TIP

POLYMER FEED

SLOT

6e)
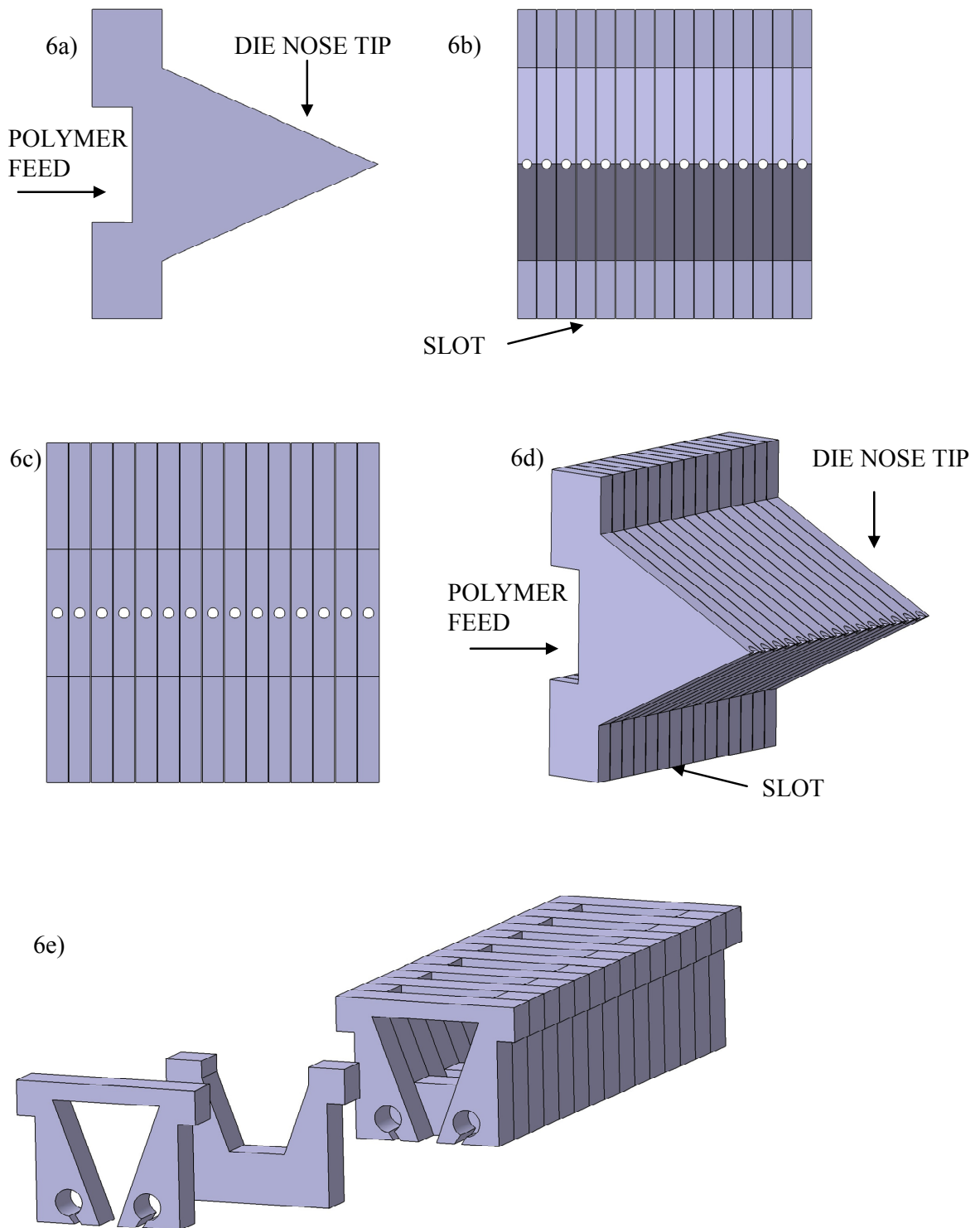
Fig. 6. Die assembly capillary types [6,17]; 6a) Left view, 6b) Front view, 6c) Rear view, 6d) Isometric view, 6e) 3D assembly.

7a)   7b)

DIE NOSE TIP

POLYMER
FEED

DRILLED
HOLES

7c)   7d)

DIE NOSE TIP

POLYMER
FEED
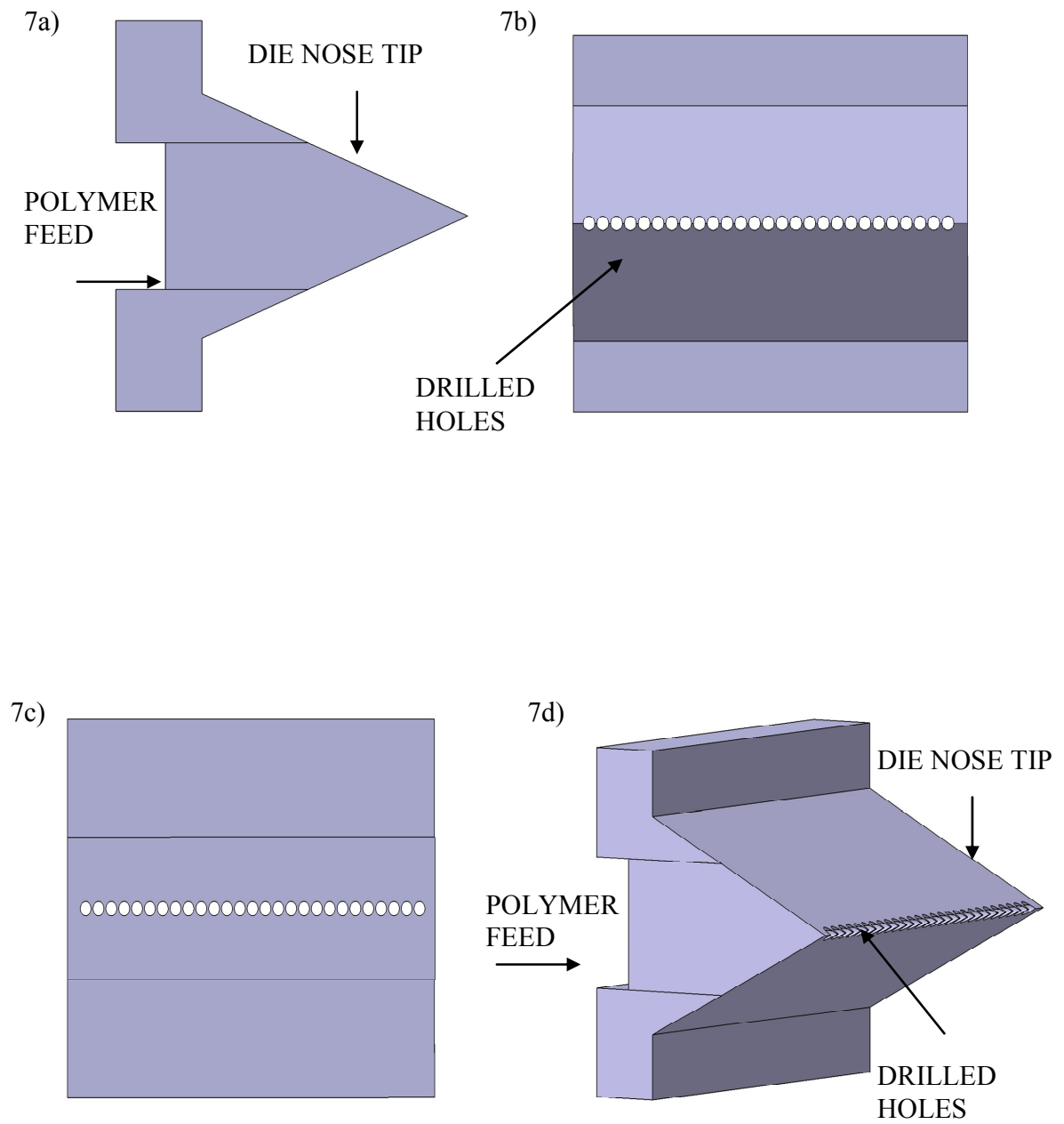
DRILLED
HOLES

Fig. 7. Die assembly drilled hole types [6]; 7a) Left view, 7b) Front view, 7c) Rear view, 7d) Isometric view
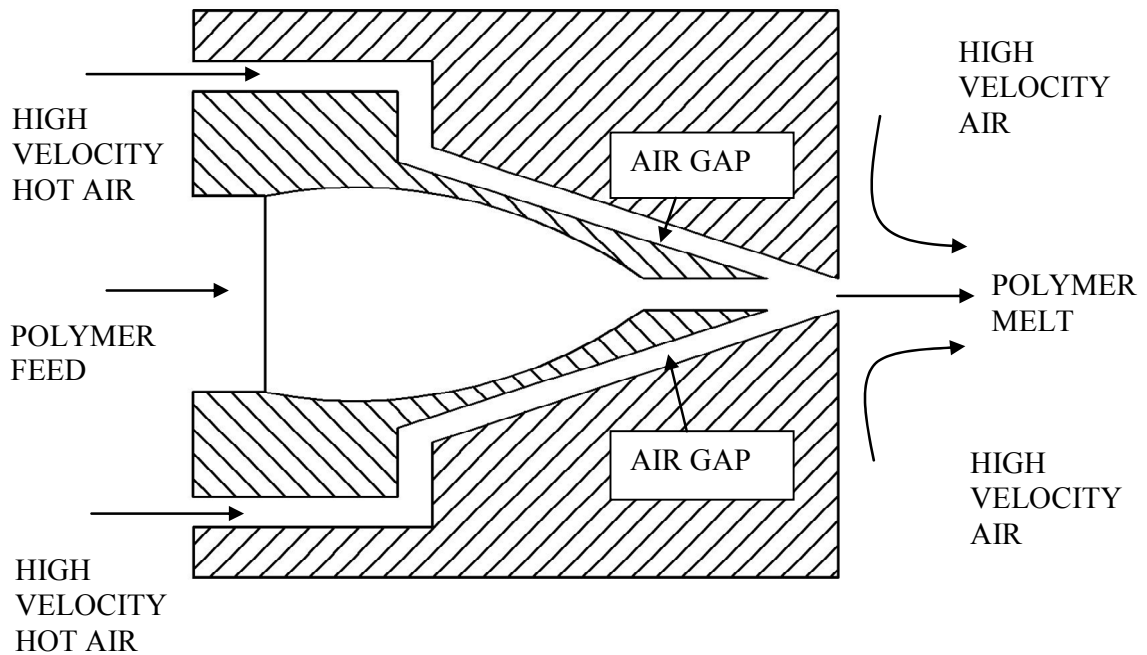
Fig. 8. Schematic view of the air flow in the die assembly [6]

The manifold is located on the sides of the die nosepiece and hits the polymer with hot, high-velocity air when it exits the die tip (see Figure 8). An air compressor is used to generate the high-velocity air, typically $0.5 - 0.8$ the speed of sound, which is passed through a heating unit to obtain the optimum air temperature, typically $230\,^{\circ}C$ to $360\,^{\circ}C$,which decreases polymer melt viscosity considerably (melt index > 1600 g/10 min). The air-gap and set-back determine the angle and length of time the air hits the polymer stream. The air is hotter than the polymer in order to hold the polymer in a liquid state [6, 15].

2.3.1 Post die area
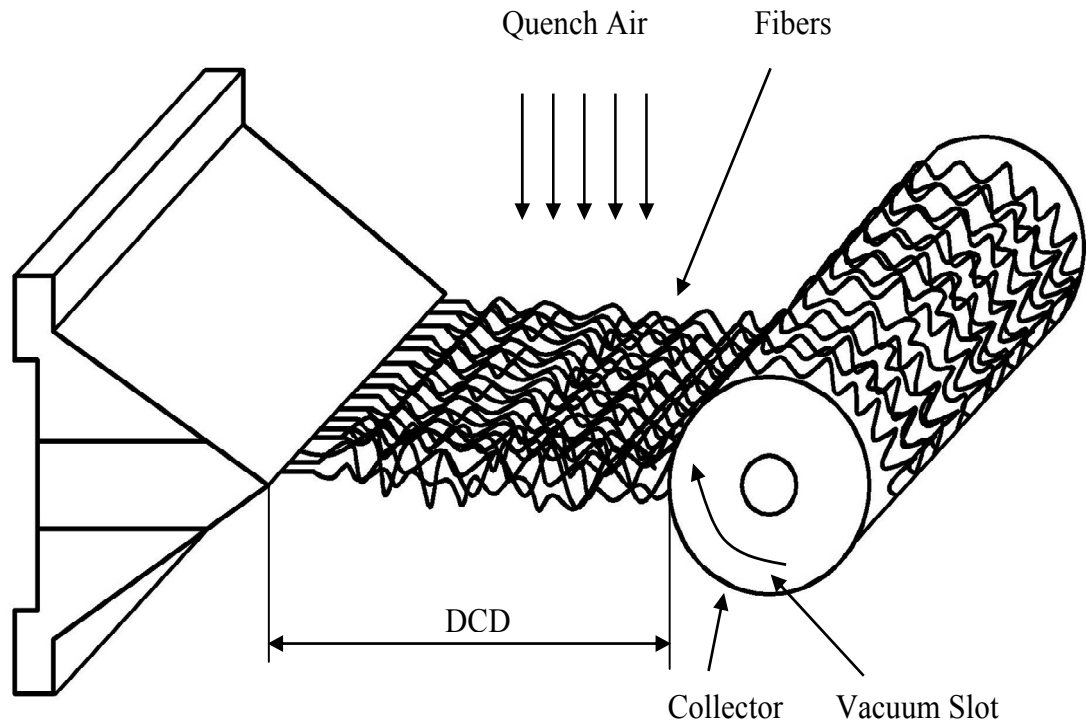
Fig. 9. Schematic of melt blown process [11]

The most commonly accepted and current definition for the MB process is following: MB process is a one-step process in which high-velocity air blows a molten thermoplastic resin from an extruder die tip onto a conveyor or take up screen to form a fine fiberous and self-bonding web. The MB process is similar to the spunbond process which converts resins to nonwoven fabrics in a single integrated process. The schematic of the process is shown MB in Figure 9 [11]. SEM image of the polymeric nanofiber nonwoven prepared by the MB technology is provided in Figure 10.
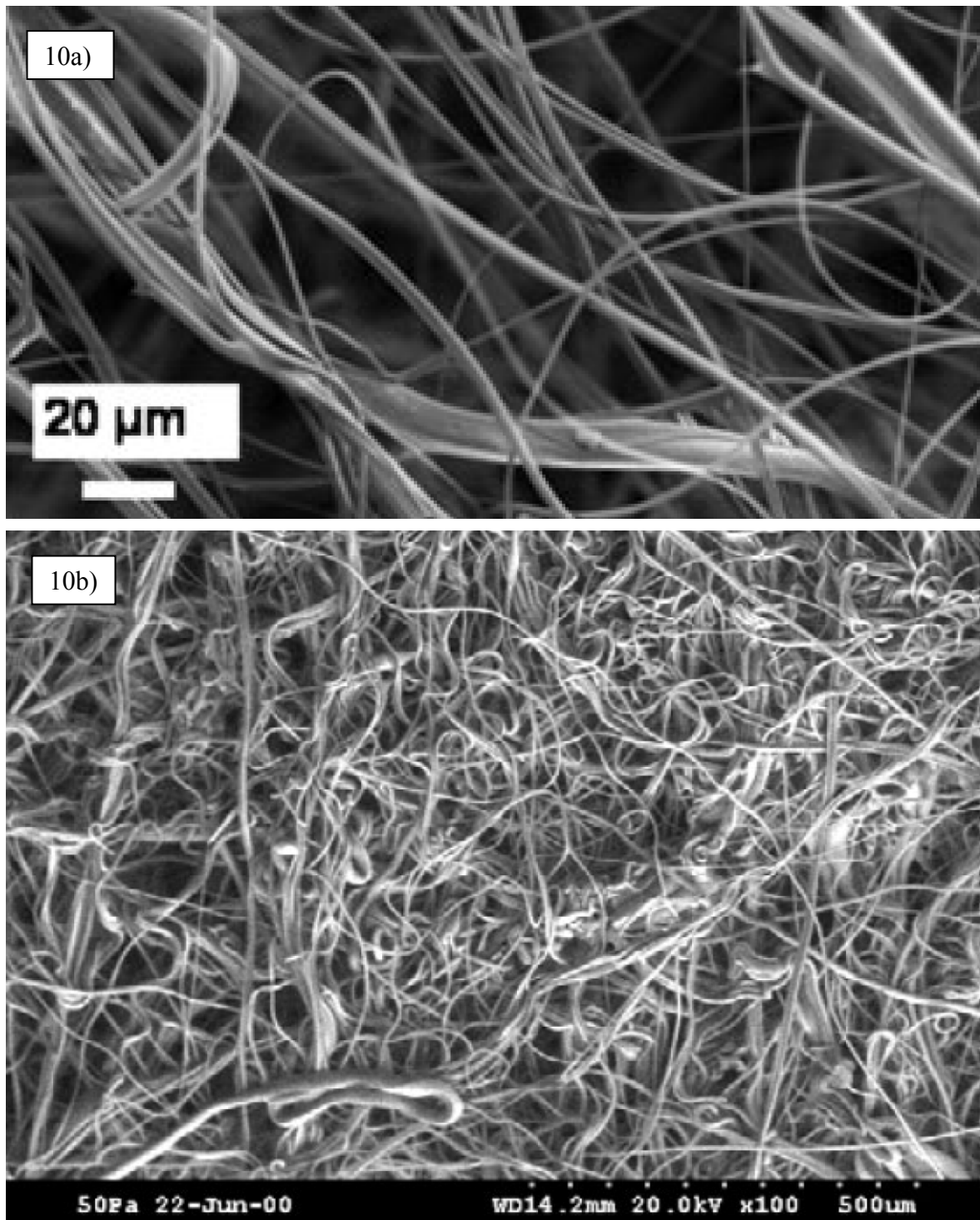
Fig. 10. SEM image of nanofiber mat produced by the melt blown process [8,18]; 10a) PP, 10b) PP+PET.

2.4 Materials

Variety of polymer samples can be used to produce nanofibers by using melt blown technology as one can see in Tables 1-2.

Tab. 1. Range of polymers which can be used in the melt blown technology [6]

Common	Others
Polypropylene (PP)	EVA,EMA,EVOH
Polystyrene	Fusibles of copolymers
Polyesters	Polybutylene terephthalate
Polyurethane (PUR)	Polyphenylene sulfide
Nylon 6, 66, 11, 12	Polymethyl pentene
Polyethylene	Polyvinyl alcohol
Low and high density polyethylene	Polytrifluorochloroethene (PCTFE)
(LLDPE, LDPE, HDPE)	Polyethylene terephthalate
Polycarbonate (PC)	Poly (4-methylpenten-1)
	Poly (tetramethylene terephthalate)

Tab. 2. Range of co-polymers which can be used in the melt blown technology [6]

Co-polymers
Ethylene/chlorotrifluoro-ethylene
Copolyesters
Polyurethane
Ethylene vinyl acetates
Polyamide polyethers

Typical nanofiber based products made by using melt blown technology are summarized in Tab. 3.

Tab. 3. Products which are distributed by the melt blown [6] and adapted from [19]

Filtration	Sorbents and Wipes	Industrial
Air	Household wipes	Protective apparel
Clean rooms	Industrial clean up wipes	Face masks
Heating	Oil clean up (oil booms)	Chemical suit
Ventilation	Food fat absorption	Protective overalls
Air conditioning (HVAC)		Vapour permeable sheets
Face masks		for roof construction
Respirators		heat and sound insula-
Gas masks		protective material for
Vacuum cleaner		performance of outdoor
Room air cleaners		work
Liquid		
Water		
Food and beverage		
Chemicals and solvents		
Blood		
Medical	**Hygiene**	**Other**
Surgical gowns	Feminine hygiene products	**Electronics**
Surgical face masks	Diapers (cover stock, waist	Battery separators
Surgical drapes	and leg reinforcement)	Cable wraps
Head covers	Incontinence products	**Adhesives**
Shoes covers	Single - use baby nappies	Hot-melt adhesives
	Nappies and towels for people	**Insulators**
	suffering from incontinency	Apparel thermal insinsu-
	Ladies hygienic towels	insulator
	and ladies slip towels	(3M Thinsulate)
		Acoustic insulation
		(appliances, automotive)

2.5 Parameters influencing melt blowing process

2.5.1 Materials

It has been found that the MB thermoplastic polyurethane (TPU) was more complicated than the MB polypropylene process because the web structures and properties of MB TPU were very sensitive to MB process conditions, especially the die/air temperature and die to collector distance (DCD) [12]. Moreover, it has been reported that the fiber diameters of the MB TPU fibers increased with increasing DCD and that the MB TPU fibers were less entangled at shorter DCDs, however, the orientation of fibers was more highly oriented with increasing DCD instead of being randomly distributed (see Figure 11).

15 cm   74 cm
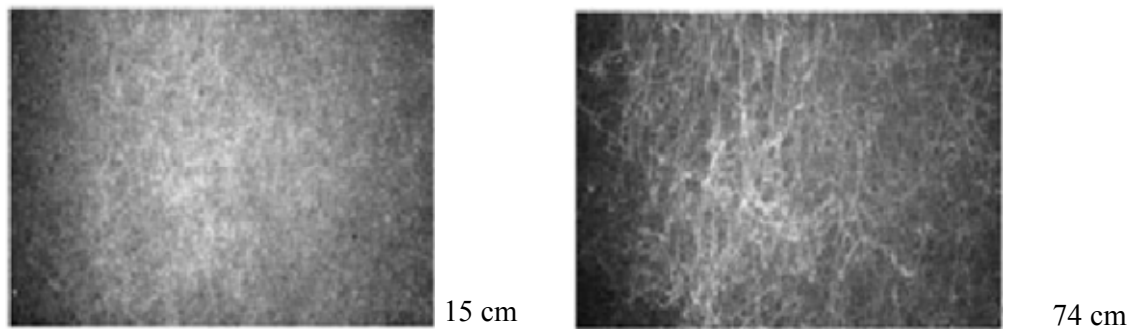
Fig. 11. TPU nanofiber based nonwovens prepared at two different DCDs [12]

It has also been revealed that Boltzmann fitting model can describe air velocity profile between die and collector very well (see Eq. 1).

$$y = \frac{A_1 - A_2}{1 + e^{(x-x_0)/dx}} + A_2 \tag{1}$$

where y is the air velocity, x is distance from the die and A_1, A_2, x_0 and d_x are adjustable parameters [12].

Effect of nanoparticles on the structure and properties of polypropylene meltblown webs have been investigated in [8]. It has been found that clay additive did not offer any benefit as far as the mechanical properties of the meltblown web are concerned. Meltblown web samples with nanoclay had higher variability in web structure, high air permeability, high stiffness, and lower mechanical properties.

The evolution of the surface nanostructures of meltblown polypropylene (PP) fibers during the process of plasma treatment followed by copper (Cu) sputter coating has been analyzed in [20]. It has been clearly demonstrated that the evolution of the surface nanostructures and chemistry has resulted in the change in surface nanomechanical properties and conductivity.

The processing-structure-property behavior of multilayer melt blown webs has been discussed in [10]. In this work, the melt blown webs have been made with a layered structure within the microfibers. In more detail, using two different polymers, alternating layer ranging from 2 up to 27 have been introduced within each microfiber, which allows to vary and control interfiber bonding and hence, obtain a wide range of web properties using the following variables: (i) polymer combination, (ii) polymer ratio, (iii) number of layers within the microfibers and (iv) layer arrangement for 3 or more layers. Compared to polymer blends this is more versatile due to features (iii) and (iv).

2.5.2 Processing conditions

Structure and filtration properties of melt blown polypropylen webs have been described in [14]. It has been found that increasing processing temperature and increasing attenuation air flow rate influenced the web structure in a similar way: increasing both variables caused a decrease in pore size, a decrease in air permeability, and an increase in filtration efficiency. This is considered to be due to a decrease in the fiber diameter and to an increase in the degree of fiber – entanglements. At medium to low polymer throughput rates, webs with smaller diameter fibers are usually produced at higher air flow rates. It has been revealed that the major energy cost in melt blowing was in providing compressed air for

the die. The ratio of mean to maximum pore size slightly increases with increasing die temperature, suggesting that the pore size distribution becomes narrow with increasing die temperature [14].

Effect of processing parameters on the uniformity of adhesive meltblown web has been analyzed in [21]. It has been determined that there are similar variation trends for the effects of the process parameters on the web weight unevenness and the web thickness unevenness, so both the weight unevenness and the thickness unevenness can be used to express the web unevenness. The web unevenness increases with increases in melt throughput rate. The web unevenness decreases firstly and increases later with the increasing primary air pressure. The web unevenness increases with the increasing accessory air pressure. The web unevenness decreases firstly and then increases later with the increasing DCD [21].

Experimental investigation of adhesive meltblown web production using accessory air has been discussed in [7]. It has been revealed that the relatively large measurement counts for fiber diameter shows that fiber diameters in the produced webs follow a log-normal distribution, not normal distribution. Therefore, the fiber diameter should be represented by the geometric mean instead of the number mean. Fiber diameters decrease with increases in primary air pressures and accessory air pressures and reductions in melt throughput rate. DCD in the range studied from 850-1200 mm do not exhibit obvious effects on fiber diameter [7].

Fiber diameter of polybutene terephthalate (PBT) meltblown nonwovens has been revealed in [22]. A polymer air-drawing model of PBT melt blown nonwovens has been established. The effects of processing parameters on the fiber diameter have been investigated. A lower polymer flow rate, a higher initial air velocity, and a larger DCD can all produce finer fibers, whereas too high an initial air velocity an too large a DCD contribute little to the polymer drawing of PBT melt blown nonwovens [22].

Properties of PP/PET bicomponent melt blown microfiber nonwovens after heat treatment have been analyzed in [18]. It has been stated that the PET MB webs shrink significantly under heat treatment, from 90°C to 155°C, which leads to increased fiber diameter and lowered air permeability. The PP/PET bico MB webs exhibit excellent thermal dimensional stability. Due to this stability, these bico MB webs keep their original properties, unaffected up to 155°C [18].

3D modeling of filtration process via polyurethane nanofiber based nonwoven filters prepared by electrospinning process has been explained in [2]. It has been found that the effect of different factors such as air velocity, viscosity, temperature, pressure and particle-fiber friction coefficient has been theoretically investigated for the produced polyurethane nanofiber based filter. It has been revealed that the change of the particle-fiber friction coefficient (which can be done by particle – surface modification for example) has one of the highest effects on the filtration efficiency (within the range of all tested parameters and their values), especially for nanoparticles having diameter less than about 200 nm for the studied conditions and filter structure [2].

2.5.3   Equipment design

Analysis and simulation of non-Newtonian flow in the coat-hanger die of a melt blown process have been investigated in [9]. It has been revealed that the design of the coat-hanger geometry of a die is very important for melt blown technology. The coat-hanger die has a good operation feasibility for different resins and various operation conditions from the view of web uniformity. The pressure drop through the orifices is the major contribution to the pressure drop in the die [9].

Numerical computation of the fiber diameter of melt blown nonwovens produced by inset die has been explained in [13]. It has been found that the dual slot inset die is often used to produce polymeric fibers in the melt blowing process. The air jet flow field model for the dual slot inset die has also been established. In this theoretical work, the flow field model has been solved by using the finite difference method. Computer simulation showed that

large inset distance will yield higher air velocity in the flow field. The air drawing model of polymers in the melt blowing process has been solved with the aid of simulation results of the air jet flow field [13].

2.5.4 Nanofiber structure morphology

Melt blown fiber diameter distributions and onset of fiber breakup has been discussed in [23]. It has been revealed that comparing the width/shape of the size distribution for nanofiber mats and mats with average fiber diameters in excess of 1 μm reveals that the diameter dependence of the distribution widths are nonuniversal. Fibers made at the highest temperatures and air flow rates revealed the onset of fiber breakup instabilities (driven by surface tension) leads to spherical particles dispersed among the fiber mat. It has been concluded that this phenomenon may represent a fundamental limit on the smallest fibers achievable by melt blowing for given materials and processing conditions [23].

An influence of viscosity and elasticity on diameter distribution of melt blown nanofibers has been explained in [3]. It has been revealed that increasing the melt viscosity led to an increasing in average fiber diameter (d_{av}) with almost no effect on coefficient of variation (CV). On the other hand increasing the elasticity appeared to decrease CV and increase d_{av}. Furthermore, there seems to be a threshold for elasticity that must be exceeded to obtain a significant decrease in CV [3].

Development and characterization of poly(trimethylene terephthalate) - based bicomponent meltblown nonwovens has been discussed in [24]. It this work, the surface response methodology was applied for the web development with melt throughput from 0.3 to 1.5 g/hole/min, melt temperature from 270 to 305°C, air temperature from 230 to 310°C, air flow rate from 12.5 to 29.2 SCFM/in, and die DCD from 11 to 19 inches. The fiber diameter obtained was in the range of 1.71 to 4.76 μm. Poly trimethylene terephthalate (PTT) and bico PTT/PP exhibited excellent meltblown processability and web quality. Compared with conventional (mono) round and smooth meltblown fibers, the bico PTT/PP webs showed the structure of nonround cross-section and twisted fibers [24].

Adsorption filtration characteristics of melt blown polypropylene fiber in purification of reclaimed water have been discussed in [25]. It has been revealed that due to the 3-dimensional network structure with multilayers, wide ranged pore size distribution, and large specific surface area, melt blown polypropylene fiber were successfully used as the filter to remove particles and some organic compounds from reclaimed water. After filtration with melt blown polypropylene fiber filter, NH_3-N in the reclaimed water is reduced over 95 % [25].

3 EXPERIMENTAL RHEOLOGY

Rheological measurements allow determining material properties with respect to flow and deformation. Fundamental rheological theories then can be utilized i.e. how to treat results of measurements of these properties and how to use them in solving applied problems. In more detail, several main directions of application of rheology in practice exists: Rheology is a physical method of characterization of the structure of matter. Rheology gives unambiguous, physically meaningful, quantitative parameters of materials. Results of rheological characterization of various similar materials give a basis for comparison of these materials. Rheology does not answer questions as to whether materials under test are "good" or "bad". The answer depends on expert estimation and previous experiences in the application of similar materials. Description (and modeling) of the flow behavior of different materials during their processing, including their flow in technological equipment, is based on solving field of flow equations where rheological (material) properties enter these equations as coefficients and/or functions [26].

The summarization of the most common experimental techniques to measure basic rheological data is provided bellow.

3.1 Disk rheometers

A disk rheometer can be presented as a rheometer in which both conical surfaces degenerate into the parallel plates (disk-disk) separated by a clearance of height, h (see Figure 12). In this case, the liquid being investigated is placed into a clearance between the disks, and one of the disks revolves relative to another around the common axis. This instrument is called the disk rheometer. Range of measurable shear rates is 10^{-4}-10^1 1/s [26]. The Table 4 summarizes utility and possible errors if disk rheometers are utilized for the rheological evaluation of polymer melts.

Tab. 4. Errors and utility of parallel disks method [16]

Errors	Utility
Inertia and secondary flow	Sample preparation and loading is simpler for very viscous materials and soft solids
Edge failure (same as cone and plate)	Can vary shear rate (and shear strain) independently by rotation rate Ω or by changing the gap h, permits
Shear heating	increased range with a given experimental set up
Nonhomogeneous strain field (correctable)	Determine wall slip by taking measurements at two gaps
	Delay edge failure to higher shear rate by decreasing gap during an experiment (requires change of cone angle in cone and plane)
	Measure N_2 when used with cone and plane thrust data
	Preferred geometry for viscous melts for small strain material functions
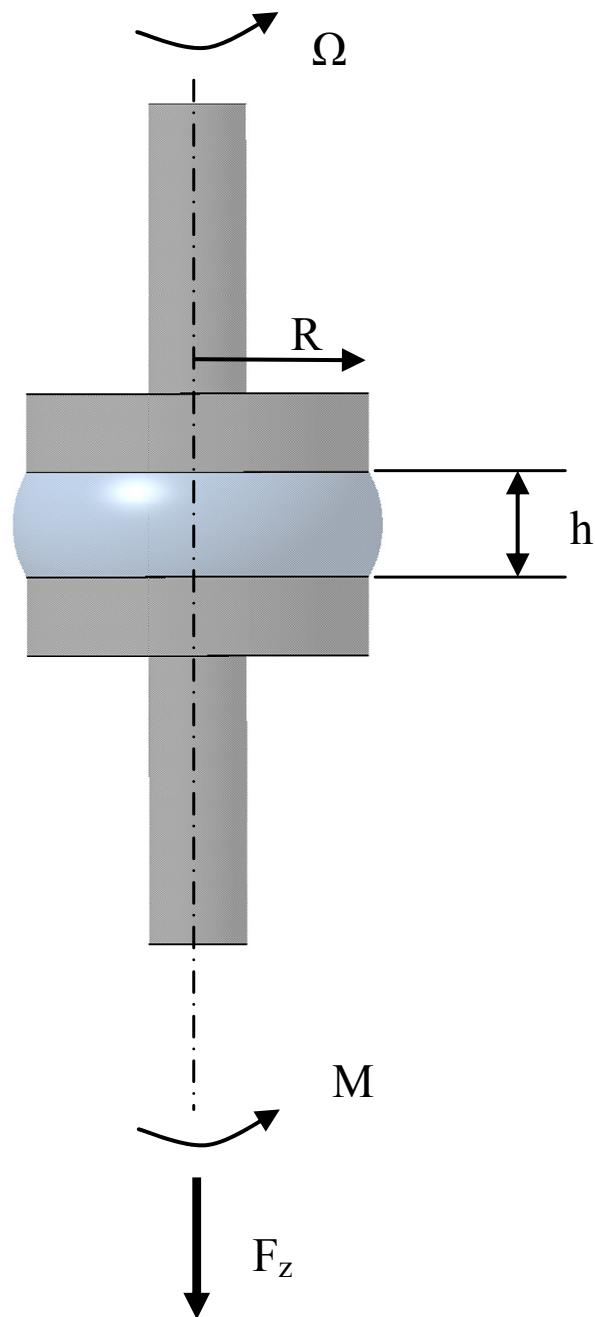
Fig. 12. Scheme of parallel disks rheometer [16] where Ω is the rotation rate, R is the

plate radius, h is the gap size, M is the torque and Fz is the normal force.

3.2 Capillary rheometer

A capillary was the first rheometer, and this device remains the most common method for measuring viscosity. The basic features of the instrument are shown in Figures 13-14. Gravity, compressed gas, or a piston is used to generate pressure on the test fluid in a reservoir. A capillary tube of radius R and length L is connected to the bottom of the reservoir. Pressure drop and flow rate through this tube are used to determine viscosity. Range of measurable shear rates is $1\text{-}10^4$ 1/s [16]. The Table 5 summarizes utility and possible errors if capillary rheometers are utilized for the rheological evaluation of polymer melts.

Tab. 5. Errors and utility of capillary rheometer [16]

Errors		Utility
Wall slip with concentrated dispersions		Simplest rheometer, yet most accurate for steady viscosity
Melt fracture at $\tau_c \approx 10^5\ Pa$		High $\dot{\gamma}$
Reservoir pressure drop		Sealed system: pressurize, prevent evaporation
Entrance pressure drop:		Process simulator
	Bagley plot	Quality control: melt index
	Single die $L/R \cong 60$	Nonhomogeneous flow, only steady shear material functions
	Kinetic energy for low η, high $\dot{\gamma}$	Entrance corrections entail more data collection
Viscous heating - $Na \geq 1$		
Material compressibility		
Pressure dependence of viscosity		
Shear history, degradation in reservoir		

Capillary rheometry is the oldest and most widely used method of qualitative estimation and viscosity measurement. Its ubiquity is due to obviousness of experiment, simplicity of experimental units, relative inexpense, and it is easy to standardize test procedure.

The essence of method consists in measuring the resistance to flow of liquid through a calibrated channel. The central task of capillary rheometry is establishing the correspondence between volumetric flux (output), Q, and pressure drop in capillary, Δp, which induces flow. The term ''capillary'' usually means any tube (channel) with arbitrary length and cross section, though, as a general rule, cylindrical tubes (capillaries) with large length to radius, L/R, (or diameter, D) ratio are used [26].
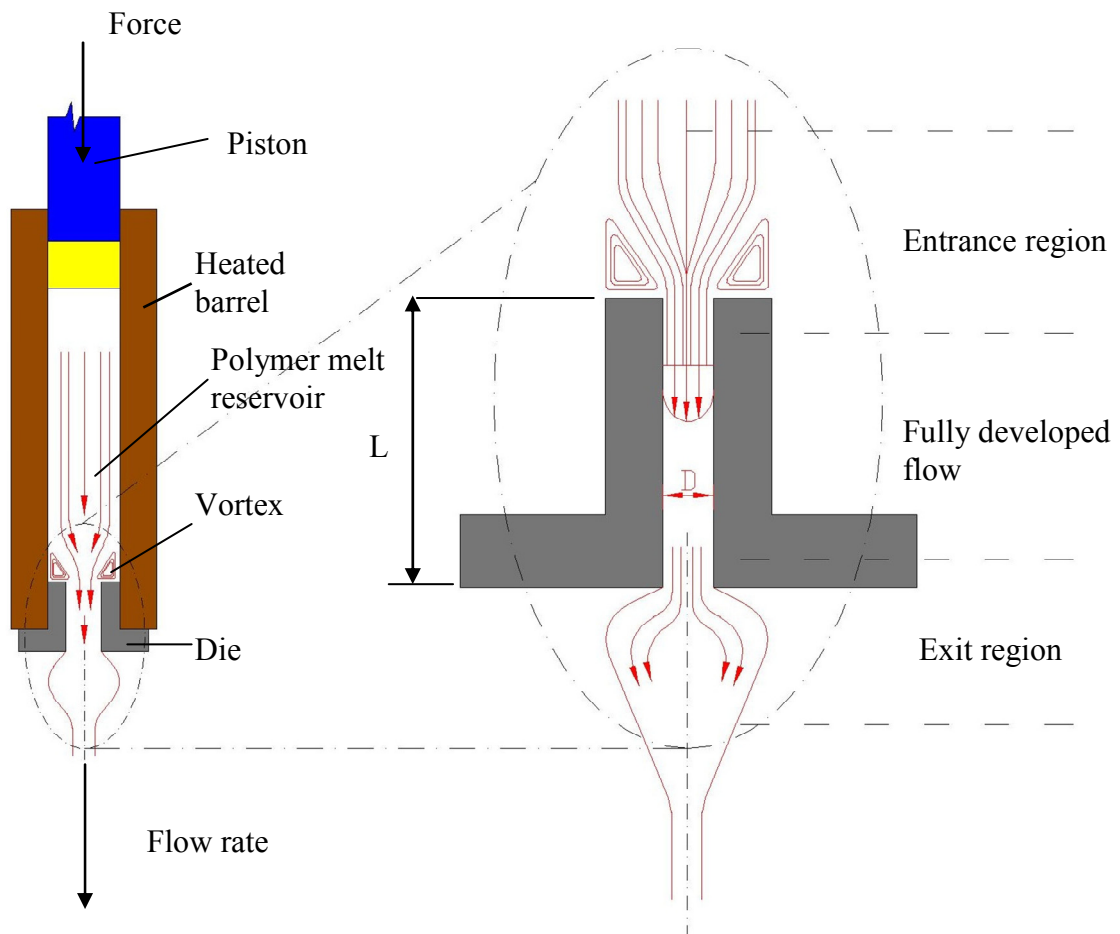
Fig. 13. Scheme of capillary rheometer [27]
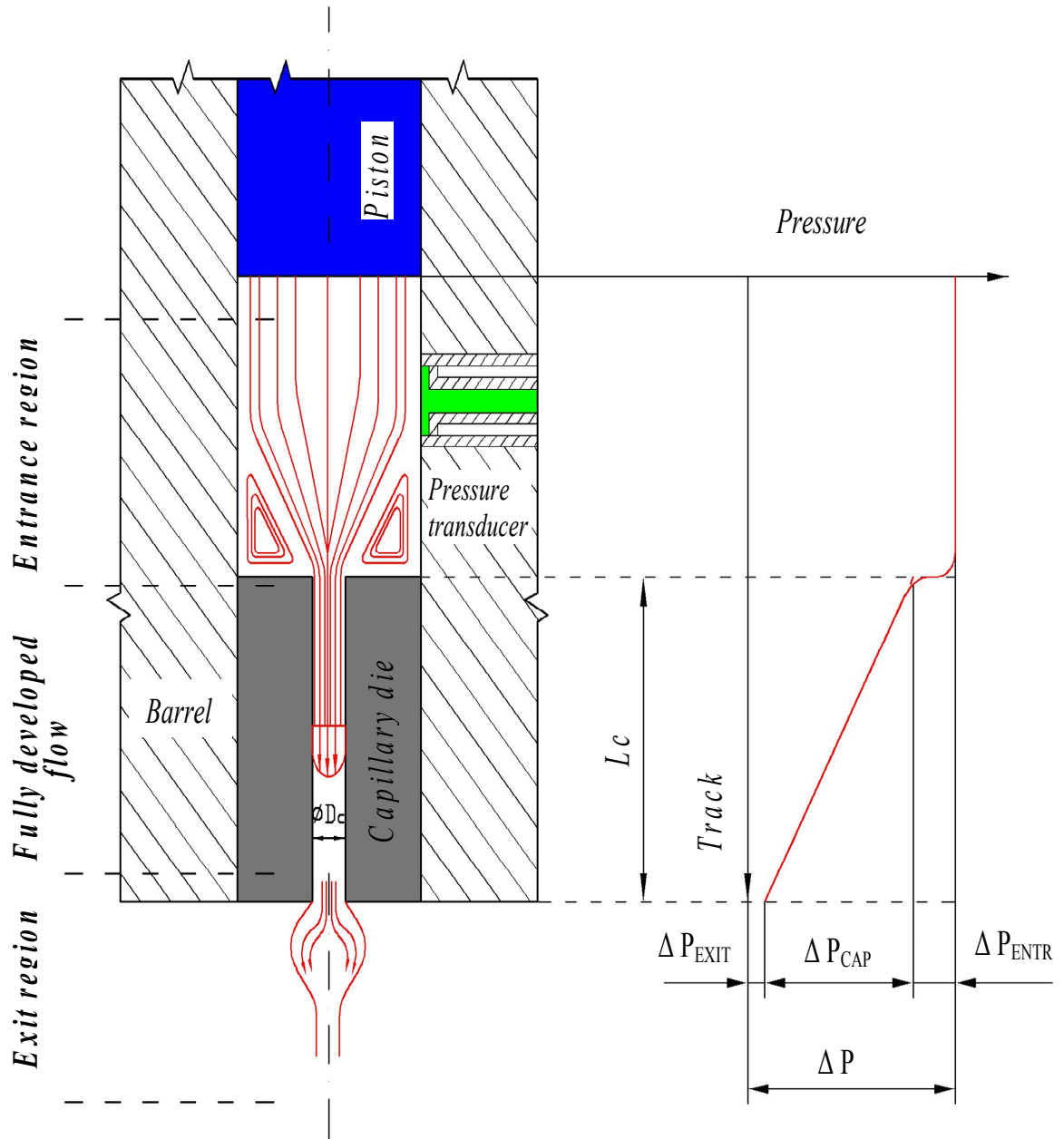
Fig. 14. The pressure profile along the capillary [28]

4 CONSTITUTIVE EQUATIONS FOR POLYMER MELTS

Constitutive equations for polymer melts can be viewed as theoretical tools for mathematical representation of measured rheological data. In this work, two of them are considered: Generalized Newtonian model and modified White-Metzner model which are describe bellow in more details.

4.1 Generalized Newtonian model

Generalized Newtonian model is derived from the simple Newtonian model, whose form is following [16]:

$$\underline{\underline{\tau}} = 2\eta_0 \underline{\underline{D}} \tag{2}$$

where $\underline{\underline{\tau}}$ represent the extra stress tensor, η_0 is the Newtonian viscosity, and $\underline{\underline{D}}$ stand for the deformation rate tensor. The Newtonian law is valid for the Newtonian liquids only. This Newtonian law can be generalized for the non-Newtonian fluids by considering that the viscosity is defined as the function of the strain rate tensor rather than the constant value. In the open literature, the different viscosity functions have been suggested. W.N. Song, Z.M. Xia [29] suggested the following formula for the viscosity function:

$$\eta = \frac{\left[\eta_0 a_t - \eta_\infty Tr_1\left(\mathrm{III}_D\right)\right] + \left[\eta_\infty Tr_1\left(\mathrm{III}_D\right)\right]}{a_t\left[1 + \left(\lambda a_t 2\sqrt{\mathrm{II}_D}\right)^a\right]^{(1-n)/a}} \tag{3}$$

where II_d and III_d stands for the second and third invariants of deformation rate tensor, η_∞ is the limiting shear viscosity at infinite shear rate, η_0, λ, a, n are adjustable parameters, Tr_1 is Trouton ratio function defined according to Eq. 4 and a_t is the temperature function (Arrhenius equation) defined by Eq. (5) or (6) [16]:

$$Tr_1 = Tr_{1\infty} + (1 - Tr_{1\infty})(1 + \mu^3 |III_D|)^{(l-1)/3} \tag{4}$$

$$a_t = \exp\left[\frac{E_a}{R}\left(\frac{1}{273.15 + T} - \frac{1}{273.15 + T_r}\right)\right] \tag{5}$$

or

$$a_t = \exp^{-b(T - T_r)} \tag{6}$$

where $Tr_{1\infty}$, μ and l are adjustable parameters, E_a stands for the activation energy, R represents the universal gas constant, T is the actual temperature, T_r is the reference temperature and b is the temperature sensitivity parameter.

Macosko suggested the following viscosity function for the generalized Newtonian law [16]:

$$\eta = \eta_0 \frac{(1 + m|II_D|)^{(n-1)/2}}{\left[1 + 3m(3III_D / II_D)^2\right]^{(n-1)/2}} \tag{7}$$

where m, n and η_0 are adjustable model parameters, II_D and III_D represent second and third invariant of deformation rate tensor.

Recently, Zatloukal has proposed the specific viscosity function in generalized Newtonian law allowing properly represent flow behavior of the polymer melts in extensional flows [30, 31] in the following form:

$$\eta(I_{|D|}, II_D, III_D, |III_D|) = A^{1 - f(I_{|D|}, II_D, III_D, |III_D|)} \eta(II_D)^{f(I_{|D|}, II_D, III_D, |III_D|)} \tag{8}$$

where $\eta\left(\mathrm{II}_{\mathrm{D}}\right)$ is given by the well known Carreau-Yasuda model presented in Eq. (9), and exponent $f\left(\mathrm{I}_{|D|},\mathrm{II}_{D},\mathrm{III}_{D},\left|\mathrm{III}_{D}\right|\right)$ is given by Eq. (10). The first, second and third invariant of the deformation rate tensor are defined as $\mathrm{I}_{\mathrm{D}}=\mathrm{tr}(\mathrm{D})$, $\mathrm{II}_{\mathrm{D}}=2\mathrm{tr}\left(\mathrm{D}^{2}\right)$ and $\mathrm{III}_{\mathrm{D}}=\det(\mathrm{D})$.

$$\eta\left(\mathrm{II}_{D}\right)=\frac{\eta_{0}a_{t}}{\left[1+\left(\lambda a_{t}\sqrt{\mathrm{II}_{D}}\right)^{a}\right]^{(1-n)/a}} \tag{9}$$

$$f\left(\mathrm{I}_{|D|},\mathrm{II}_{D},\mathrm{III}_{D},\left|\mathrm{III}_{D}\right|\right)=\left\{\tanh\left[\alpha\,a_{t}\left(1+\frac{1}{4\left(\sqrt{3}\right)^{3}}\right)^{-\psi}\left(\left|1+\frac{\mathrm{III}_{D}}{\mathrm{II}_{D}^{3/2}}\right|\right)^{\psi}\frac{\sqrt[3]{4\left|\mathrm{III}_{D}\right|+\mathrm{I}_{|D|}}}{3}+\beta\right]\frac{1}{\tanh(\beta)}\right\}^{\zeta} \tag{10}$$

where $\eta_{0},\lambda,a,n,\alpha,\psi,\beta,\zeta$ are adjustable parameters and a_{t} is the temperature shift factor defined by Eq. 5-6.

4.2 Modified White-Metzner model

The White-Metzner constitutive equation [32, 33, 34] is a simple Maxwell model for which the viscosity and relaxation time are allowed to vary with the second invariant of the deformation rate tensor:

$$\underline{\underline{\tau}}+\overline{\lambda}\left(\mathrm{II}_{D},T\right)\overset{\nabla}{\underline{\underline{\tau}}}=2\eta\left(\mathrm{II}_{D},T\right)\underline{\underline{D}} \tag{11}$$

$$\overset{\nabla}{\underline{\underline{\tau}}}=\frac{\delta\tau^{(i)}}{\delta t}=\frac{D\,\tau^{(i)}}{Dt}-L\,.\,\tau^{(i)}-\tau^{(i)}\,.\,L^{T} \tag{12}$$

$$\frac{D\tau^{(i)}}{Dt}=\frac{\partial\tau^{(i)}}{\partial t}=\frac{d\tau^{(i)}}{dt} \tag{13}$$

$$L=\nabla v \tag{14}$$

$$(\nabla v)_{ij} = \frac{\partial v_i}{\partial x_j} \tag{15}$$

$$d = \frac{1}{2} \cdot (\nabla v + \nabla v^T) \tag{16}$$

where $\underline{\underline{\tau}}$ is stress tensor, $\underline{\underline{D}}$ is deformation rate tensor, $\overset{\nabla}{\underline{\underline{\tau}}}$ expresses upper convected stress tensor derivate, $\frac{D}{Dt}$ is substantial derivate, L is the velocity gradient, v is velocity vector, II_D is the second invariant of the deformation rate tensor, $\overline{\lambda}(\mathrm{II}_D, T)$ stands for the deformation rate-dependent relaxation time and $\eta(\mathrm{II}_D, T)$ is the deformation rate-dependent viscosity.

Although this modification improves the behavior in steady shear flows, in elongation flows the model predicts unrealistic infinitive elongation viscosity. In order to overcome this problem, Barnes [33] has proposed specific functions for the relaxation time and viscosity (see Eq. 12 and 13) with $\lambda_0/K_2 < (\sqrt{3/2})$.

$$\eta(\mathrm{II}_D, T) = \frac{\eta_0 a_t}{\left[1 + \left(\lambda a_t \sqrt{\mathrm{II}_D}\right)^a\right]^{(1-n)/a}} \tag{17}$$

$$\overline{\lambda}(\mathrm{II}_D, T) = \frac{\lambda_0 . a_t}{1 + K_2 a_t \mathrm{II}_D} \tag{18}$$

where η_0 is the Newtonian viscosity, and $\lambda_0, \lambda, K_2, n$ and a are constants.

It should be pointed out that use for the phenomenological modified White-Metzner model is only reasonable in steady flows because in this model the relaxation time depends on II_d [33]. On the other hand, an existence of analytical expressions for the basic rheological variables such as first normal stress difference (Eq. 19) and uniaxial extensional viscosity (Eq. 20) can be considered as the significant advantage of the model.

$$N_1 = 2 \frac{\eta_0 a_t}{1 + (K_1 a_t \dot{\gamma})^n} \frac{\lambda_0 a_t}{1 + (K_2 a_t \dot{\gamma})} \dot{\gamma}^2 \tag{19}$$

$$\eta_E = \frac{2\eta(T, \mathrm{II}_D)}{1 - \frac{2}{\sqrt{3}} \lambda a_t(T, \mathrm{II}_D) \mathrm{II}_D} + \frac{\eta(T, \mathrm{II}_D)}{1 + \frac{1}{\sqrt{3}} \lambda a_t(T, \mathrm{II}_D) \mathrm{II}_D} \tag{20}$$

where $\dot{\gamma}$ is the shear rate.

II. ANALYSIS

5 MATERIALS

In this work, the following materials have been used:

– PP, Borflow HL504 FB B2-70006: Melt Flow Rate (230˚C/ 2,16 kg) = 450 g/10min, Melting temperature (DSC) = 161˚C, Molecular weight distribution - very narrow

– PP, Borflow HL512 FB B2-90367: Melt Flow Rate (230˚C/ 2,16 kg) = 1200 g/10min, Melting temperature (DSC) = 158˚C, Molecular weight distribution - very narrow

6   EQUIPMENT AND METHODS

In order to determine basic rheological characteristics of selected melt blown polymer samples, twin bore capillary rheometer RH7-2 (Rosand Precision, Ltd., Great Britain) has been used. Detailed description of the experimental set-up is provided in the next chapter.

6.1   Capillary rheometer Rosand RH7-2

The twin bore capillary rheometer Rosand RH7-2, which allows performing two measurements at the same time, is visualized in Figure 15-18. It is equipped with two (orifice and long) capillary dies. Due to twin-bore technology, shear and extensional viscosity data can directly be measured without using a set of various capillary dies.

Detailed view of
two pistons and
the entry barrel
area

Detailed view of
heated barrel
with three heated
belts and two
pressure
transducers
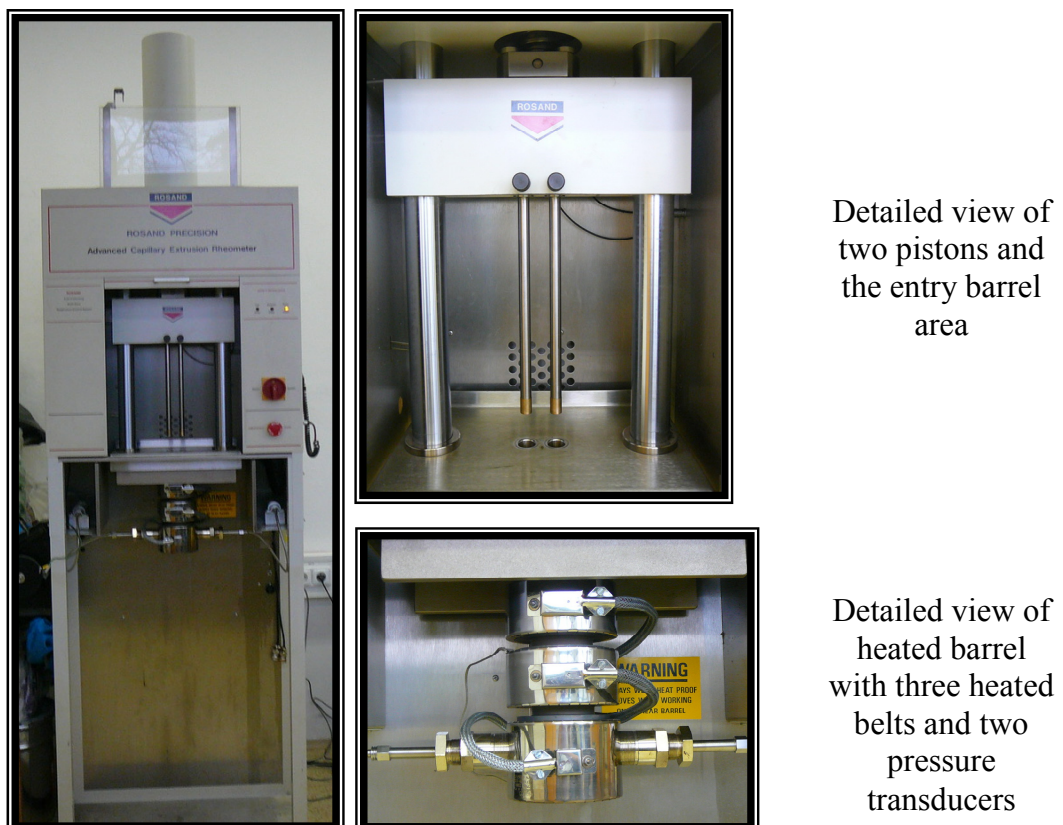
Fig. 15. Photo of Rosand RH7-2 twin-bore capillary rheometer

Due to the fact that the melt index of both chosen melt blown samples is extremely high, polyether ether ketone (PEEK) piston tips rather than copper ones have been used. The PEEK piston tips have been used in order to prevent any possible polymer melt leakage flow between the piston tips and the barrel due to very low shear viscosity of the melt blown samples. The comparison between the PEEK and copper piston tips for the capillary rheometer is provided in Figure 16.

Detail of tip from copper and PEEK

Piston with two different tips

Fig. 16. Comparison between the PEEK (grey color piston tip) and copper piston tips for the capillary rheometer

The measurements were performed in a constant piston speed mode at the shear rate range of (20-80000) 1/s. In our measurements we used pressure transducers (Dynisco, USA) in ranges of (10000) PSI (68.9476 MPa), (1500) PSI (10.3421 Mpa), (500) PSI (3.4473 MPa). In order to obtain the most accurate data of extensional viscosity for low extensional strain rates range, the highly sensitive pressure transducer (250) PSI (1.7237 MPa) calibrated into its down resolution limit was used for pressure recording at the entrance to the orifice capillary die (right-hand capillary in Figs. 18 - 25).
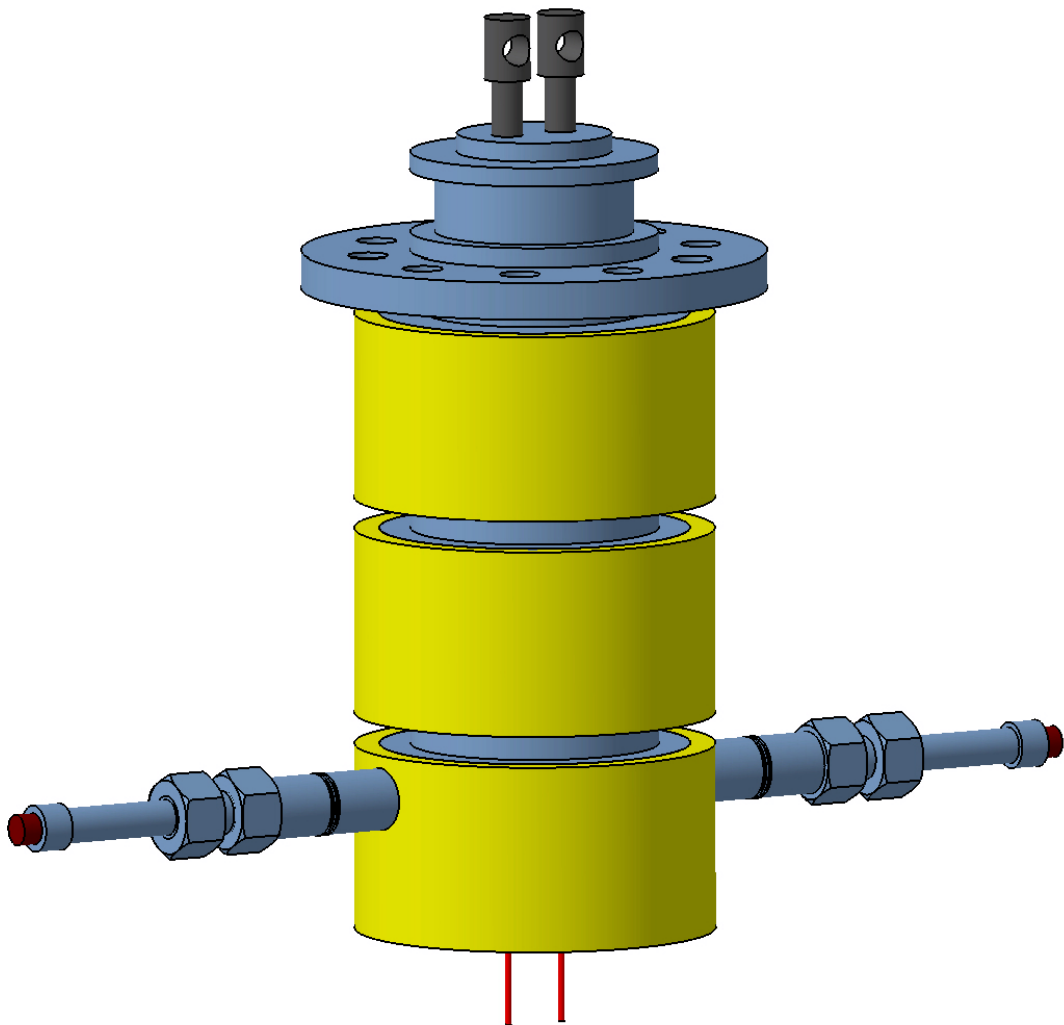
Fig. 17. Scheme of twin-bore capillary rheometer
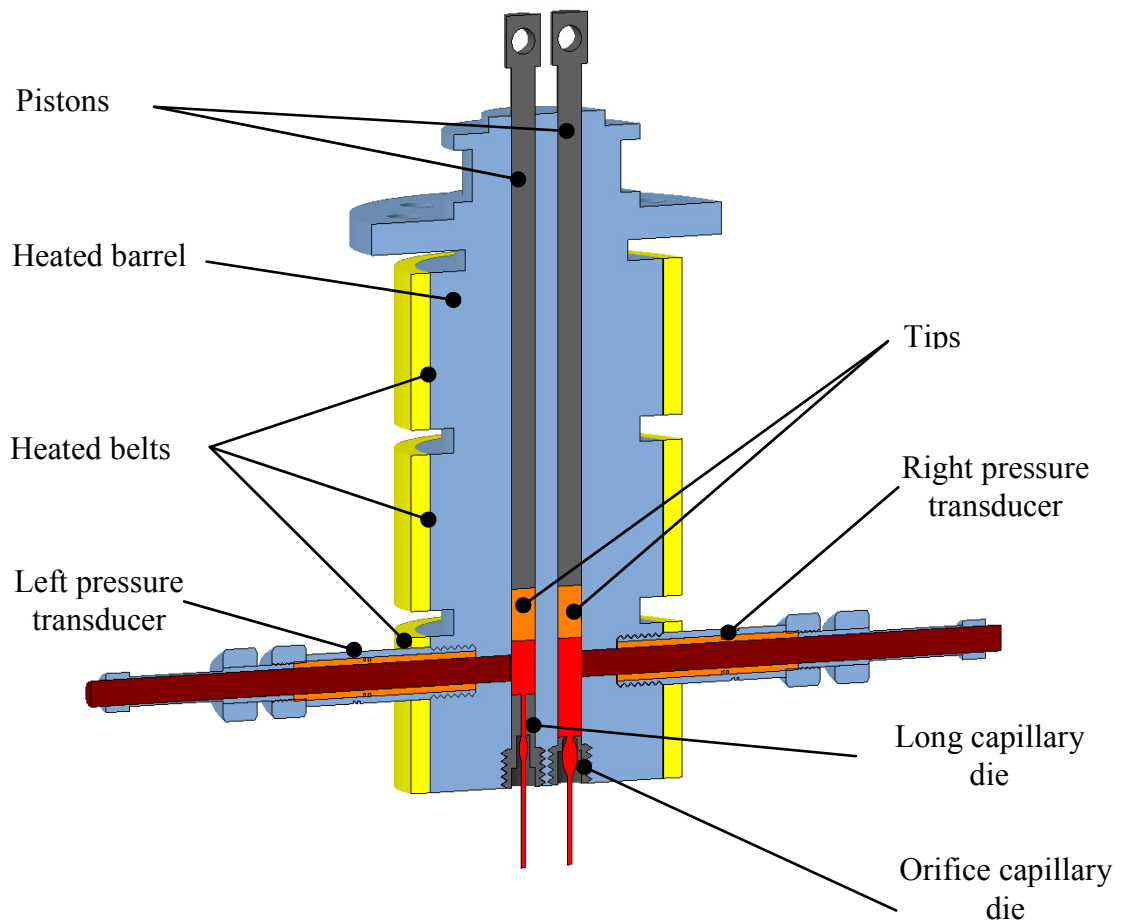
Fig. 18. Section of twin-bore capillary rheometer

Two sets of capillaries were used for the measurements. Their dimensions were following:

orifice (short) capillary die new design [35]: $L_{OC} = 0\ mm,\ D_{OC} = 1\ mm$

$$L_{OC} = 0\ mm,\ D_{OC} = 0.5\ mm$$

orifice (short) capillary die old design: $\quad L_{OC} = 0\ mm,\ D_{OC} = 1\ mm$

$$L_{OC} = 0\ mm,\ D_{OC} = 0.5\ mm$$

long capillary die: $\quad L_{LC} = 16\ mm,\ D_{LC} = 1\ mm$

$$L_{LC} = 8\ mm,\ D_{LC} = 0.5\ mm$$

The scheme of capillary dies is shown in Figures 19-25. The diameter of barrel was $D_B = 15\ mm$.
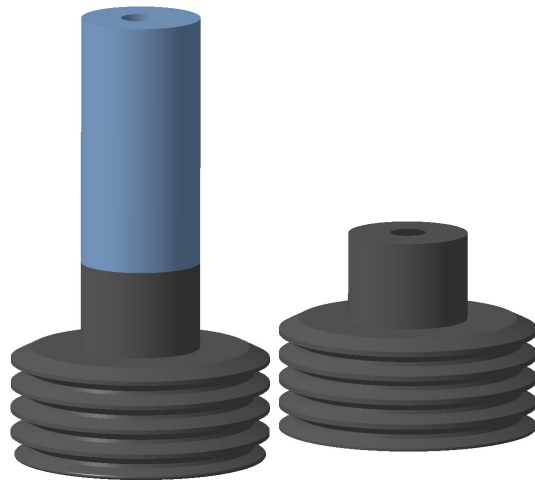
Fig. 19. Detail view of long (left) and orifice (right) capillary dies
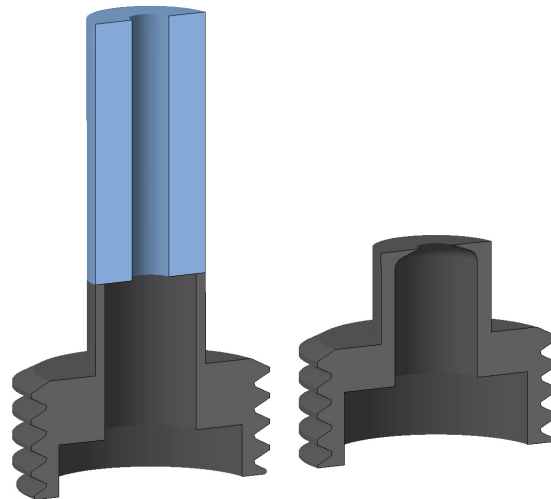
Fig. 20. Section view of long (left) and orifice (right) capillary dies
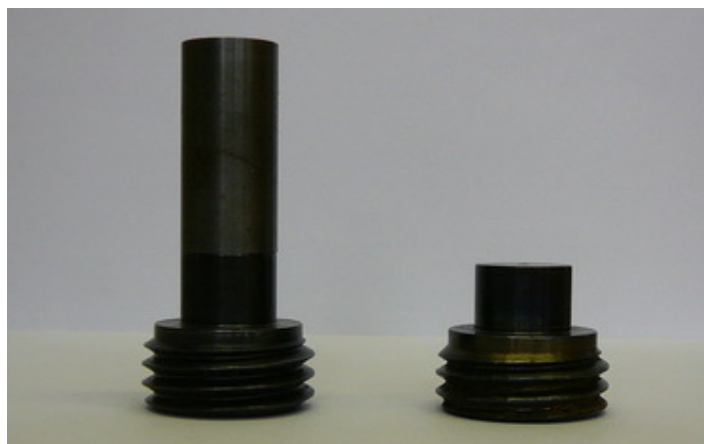
Fig. 21. Photo of long (left) and orifice (right) capillary dies
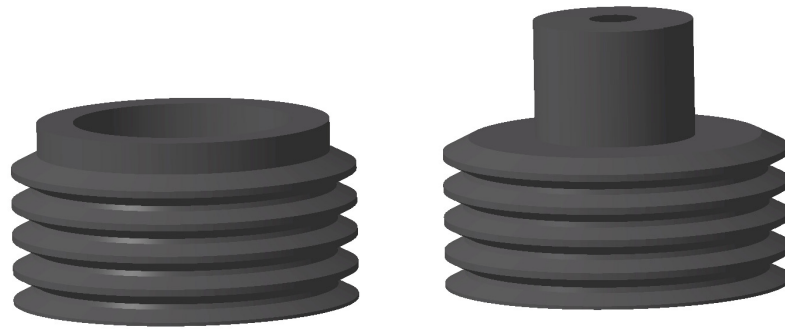
Fig. 22. New (left [35]) and old (right) orifice die design
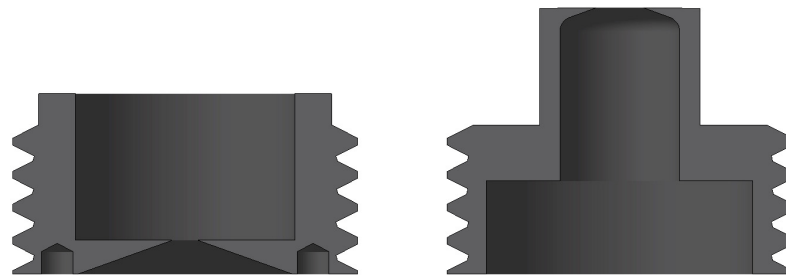
23a)   23b)

Fig. 23. Section view of new (23a) [35]) and old (23b) orifice die design

Fig. 24. Photo of new (left [35]) and old (right) orifice die design
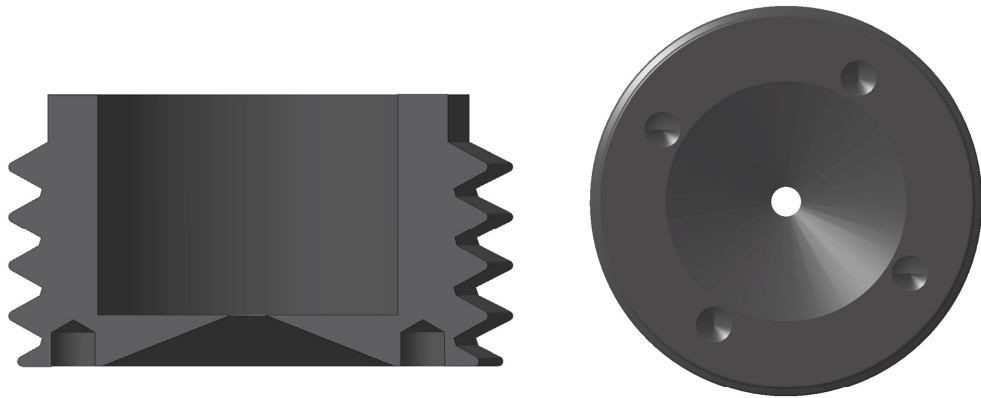
Fig. 25. Section (left) and bottom (right) view of the new orifice die design [35].

The rheological properties of both melt blown samples (PP Borflow HL504FB B2-70006 and PP Borflow HL512FB B2-90367) were investigated at three different temperatures (190˚C, 210˚C, and 230˚C). In order to perfectly compact the sample granules and eliminate air bubbles in the polymer melt, two preheating steps (for 4 and 6 minutes) and two compression steps (to 0.1 MPa) were applied before each experimental cycle.

6.1.1 Shear viscosity determination determination

With the aid of suitable software, the Rosand rheometer is able to analyze the measured data automatically including Bagley correction for the wall shear stress as well as Rabinowitsch correction for the shear rate. In more detail, the shear viscosity can be determined from below provided relationships [36]. The corrected shear stress is calculated according to following equation:

$$\tau_{xy} = \frac{(P_{LC} - P_{OC})}{2L_{LC}} R_C \tag{21}$$

where P_{LC} stands for pressure drop measured on the long capillary, P_{OC} on the orifice capillary, L_{LC} is the length of the long capillary, and R_C represents capillary die radius.

Apparent shear rate, $\dot{\gamma}_{APP}$, can be determined from equation:

$$\dot{\gamma}_{APP} = \frac{4Q}{\pi R_C^3} \tag{22}$$

where Q is volume flow rate and R_C represents capillary radius.

In order to obtain the realistic wall shear rate, Rabinowitsch correction has to be applied on the apparent shear rate:

$$\dot{\gamma} = \frac{4Q}{\pi R_C^3} \frac{3N+1}{4N} \tag{23}$$

where N expresses power-law index (index of non-Newtonian behavior) and can be obtained from the following expression:

$$N = \frac{d(\log \tau_{xy})}{d(\log \dot{\gamma}_{APP})} \tag{24}$$

Finally, shear viscosity is simply:

$$\eta = \frac{\tau_{xy}}{\dot{\gamma}} \tag{25}$$

6.1.2 Uniaxial extensional viscosity determination

In this work, uniaxil extensional viscosity has been determined according to Cogswell methodology. Definition sketch of flow geometry which was used by the Cogswell is depicted in Fig.26 (adapted from [28]). It is clear that the extensional character of flow along the centerline takes place. For many fluids, recirculation vortices in the corners are created. In these cases, the main flow is through a funnel-shape section near the center of the flow field.
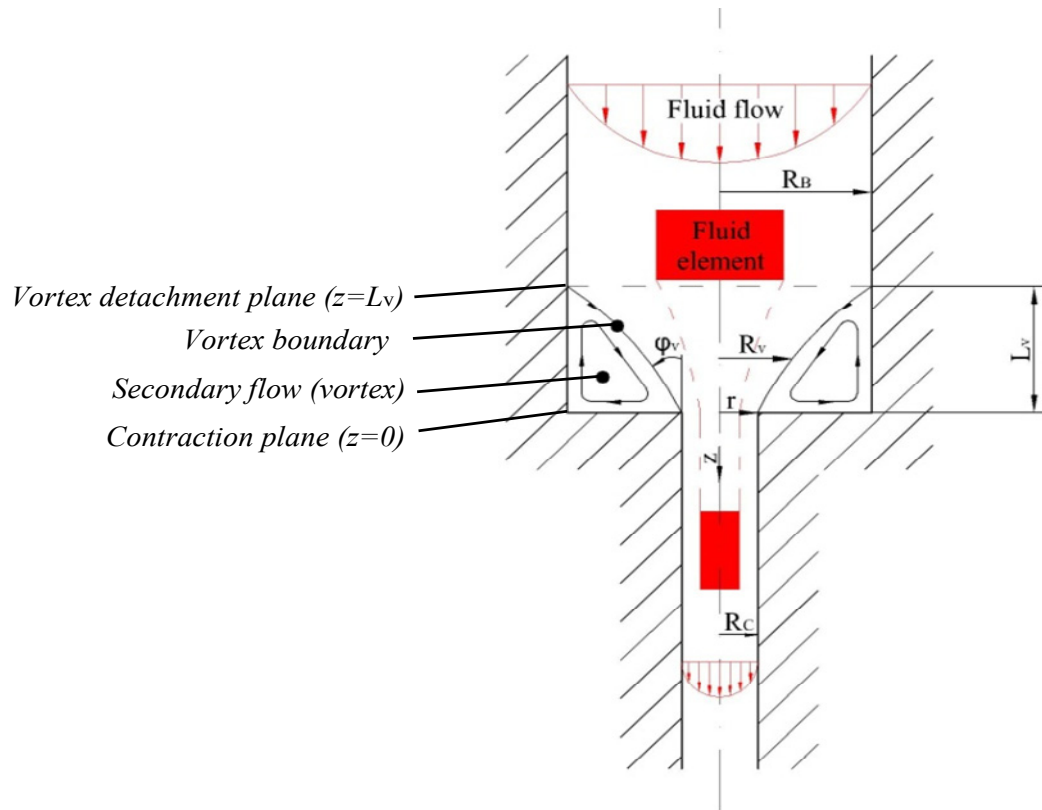
Fig. 26. Definition sketch of entry flow [29]

On the boundary between vortices and the funnel-shaped flow region the velocity is not equal zero but its value is small and in comparison with centerline velocity it can be neglected.

Equation and extensional flow parameters in Cogswell method are obtained through minimizing local pressure gradient in the converging region. This analysis is based on the following assumptions in the converging region [28]:

1. Incompressible fluid;

2. Funnel-shape flow; no slip ($v_z = 0$) on funnel surface;

3. Unidirectional flow in funnel region;

4. Fully developed flow upstream and downstream;

5. Axis symmetry;

6. Pressure drops due to shear and elongation may be calculated separately and summed to given total entrance pressure loss;

7. Neglected Weissenberg-Rabinowitsch correction, $\dot{\gamma} = \dot{\gamma}_{APP} = \dfrac{4Q}{\pi R_C^3}$;

8. Shear stress is related to shear rate through a power law, $\tau_{xy} = m\dot{\gamma}_{APP}^{n}$;

9. Elongational viscosity is constant;

10. Shape of funnel is determined by the minimum generated pressure drop;

11. No effect of elasticity (shear normal stresses neglected);

12. Inertia neglected

In order to determine extensional viscosity data, the Cogswell [37] has derived particular set of equations which are provided bellow:

Uniaxial extensional stress is given by Eq. 26

$$\sigma_E = \frac{3}{8}(N+1)P_{OC} \tag{26}$$

where N expresses the power-law index and P_{OC} is the entrance pressure drop.

The extensional rate is express as:

$$\dot{\varepsilon} = \frac{4}{3(N+1)}\frac{\tau_{xy}\dot{\gamma}_{APP}}{P_{OC}} \tag{27}$$

The extensional viscosity is simply given by Eq. 28

$$\eta_E = \frac{\sigma_E}{\dot{\varepsilon}} \tag{28}$$

RESULTS AND DISCUSSION

The role of the capillary rheometer set-up in rheological evaluation of melt blown samples

As it has been mentioned, the melt flow index of both tested melt blown PP samples is extremely high (450 and 1200 g/10min determined at 230°C/ 2,16 kg) which indicates that the shear as well as extensional viscosities of both samples can be expected to be very low. Thus, the selection of suitable pressure transducer as well as zero length die to properly capture rheological responses of such fluids is called for. Two different pressure transducers (1500 PSI and 500 PSI for pressure drop measurements on the long die) as well as two different orifice dies (with old and new designs described in Chapter 6 in more detail) have been investigated in order to find out the optimal testing conditions for precise determination of shear and extensional viscosities of these two extremely low viscosity melt blown PP samples.

The Figure 28 shows comparison between strain rate dependent shear viscosities determined on capillary rheometer equipped with two different pressure transducers having different sensitivity: 10000 PSI (long capillary)/1500 PSI (short capillary) and 500 PSI (long capillary)/250 PSI (short capillary). It is clearly visible that utilization of the low sensitive pressure transducer leads to overestimation of the shear viscosity especially at low share rate in comparison with high sensitive pressure transducer by using which the Newtonian plateau in shear viscosity has been reached as expected. Thus it can be concluded that the 500 PSI (long capillary)/250 PSI (short capillary) pressure transducer set-up should be preferred to measure the basic rheological characteristic on the twin bore capillary rheometer for melt blown polymer samples.

The role of the zero length die design on the measured entrance pressure drop (or entrance viscosity which is defined as the ratio of entrance pressure drop and apparent shear rate) has been investigated for one polymer sample (PP HL 512) and one temperature (210°C) in Figure 29. It is clearly visible that entrance viscosity measured by using so called 'old' orifice die design (see Figure 23b) is higher than in the case of 'new' orifice die design (see Figure 23a). This can be explained by the fact that during the flow of polymer melt in downstream old orifice die region the melt fills that region which artificially increases the entrance viscosity, which is not the case of the new orifice die design see (Figure 27). Due to the fact that the entrance viscosity is a key rheological characteristic for extensional vis-

cosity calculation, the new orifice die design should be prefer during rheological testing. This is conclusion is consistent with previous rheological studies for high viscosity polymer samples [35].

<div align="center">27a)   27b)</div>

Fig. 27.Orifice downstream region during melt extrusion; 27a) Old orifice die design 27b) New design orifice die design

Effect of approximation function type selection on the index of non-Newtonian behavior determination

The key problem to properly determine the index of non-Newtonian behavior defined by Eq. 24 in chapter 6.1.1. is the proper evaluation of the term $d(\log \tau_{xy})/d(\log \dot{\gamma}_{APP})$ from discontinues set of τ_{xy} and $\dot{\gamma}_{APP}$ pairs measured experimentally. In fact, there is number of possible ways to determine this term which is widely utilized in the practice. One possibility is to find out the 'proper' approximation function to fit the measured data and then to calculate the particular derivatives for given apparent shear rates by using that function. In this chapter, the following four approximation functions are selected, tested and evaluated for the index of non-Newtonian behavior determination for both melt blown polymer samples:

$$\log(\tau_{xy}) = A \log(\dot{\gamma}_{APP}) + B \qquad (29)$$

$$\log(\tau_{xy}) = A[\log(\dot{\gamma}_{APP})]^2 + B \log(\dot{\gamma}_{APP}) + C \qquad (30)$$

$$\log(\tau_{xy}) = A[\log(\dot{\gamma}_{APP})]^3 + B[\log(\dot{\gamma}_{APP})]^2 + C\log(\dot{\gamma}_{APP}) + D \tag{31}$$

$$\log(\tau_{xy}) = \frac{A}{\left\{1 + \left[B10^{\log(\dot{\gamma}_{APP})}\right]C\right\}^{\frac{1-D}{C}}} \tag{32}$$

Just note, that Eqs. 29-31 represent unphysical polynomial functions widely used in the engineering practice whereas Eq. 32 represents well known Carreau-Yasadu physical model widely used for the flow curve modeling.

In the first step, the measured τ_{xy} and $\dot{\gamma}_{APP}$ dependences have been fitted by all above mentioned equations and the parameters A, B, C and D have been estimated for both polymer samples at three different temperatures, which are summarized in Tables 6-11. In the second step, the index of non-Newtonian behavior has been determined according to Eq. 24 in the chapter 6.1.1. utilizing particular approximation function defined by Eqs. 29-32. The effect of approximation function type selection on the index of non-Newtonian behavior determination for both tested polymer melt blown samples is visualized in Figures 30-35. It is clearly visible that the type of the utilized approximation function has significant effect on the index of non-Newtonian behavior determination within whole range of shear rates. Clearly, the utilization of the Carreau-Yasuda model for determination of shear rate dependent index of non-Newtonian behavior is the most realistic because it gives physically correct values at low and high shear rates, which is not the case of an another utilized models. Therefore it can be concluded that the specific care has to be paid during approximation function selection for the index of non-Newtonian behavior determination and physical rather than unphysical polynomial functions should be preferred.

The Figures 36-41 shows the effect of approximation function type selection utilized during the index of non-Newtonian behavior determination on the deformation rate dependent shear and extensional viscosities for both tested melt blown samples at three different temperatures. It is clearly visible that the way in which the index of non-Newtonian behavior

is determined influences both shear as well as extensional viscosities, especially at low deformation rates.

Rheological behavior modeling of deformation rate dependent melt blown polymer melts

In this chapter, the capability of two different rheological models to describe the strain rate dependent shear and extensional viscosities of melt blown polymer samples will be tested. For that purpose, modified White-Metzner model proposed by Barnes [33] and recently proposed Zatloukal model [30,31] are considered. Full mathematical formulations of both models are provided in Chapter 4.1 and 4.2.

The comparison between the measured deformation rate dependent shear and extensional viscosities and both considered model fits are provided in Figures 42 - 55. All model fitting parameters are provided in Tables 12, 13. In order to quantify the fitting model efficiency, the sum of squared residuals (defined as logarithmic difference between the measured viscosity and predicted viscosity) for shear as well as extensional viscosities have been calculated for both materials and summarized in Table 14. Note that in the pure shear flow, both constitutive equations lead to the same expression for the strain rate dependent shear viscosity (well known Carreau-Yasuda model) which results in the identical fitting capabilities for both models in that case.

Based on the performed analysis it can be concluded that both models can describe the measured shear as well as uniaxial extensional viscosity data of both melt blown polymer samples at different temperatures very well.

Flow behavior evaluation of melt blown polymer samples with respect to nanofiber production by melt blown technology

The comparison between the strain rate dependent shear viscosities for both tested samples is provided in Figures 50-52. It can be clearly seen that Newtonian viscosity for PP HL 504 (which varies between 62.8 Pa.s and 24.5 Pa.s for 190-230°C temperature range) is much higher than for PP HL 512 sample having Newtonian viscosity between 18.9 Pa.s and 7.8 Pa.s for 190-230°C temperature range. This indicates that PP HL 504 sample has higher molecular weight than sample PP HL 512. Thus, it can be expected that sample PP

HL 504 will cause higher pressure drop though the melt blown die in comparison with PP HL 512 sample during melt blown process.

According to Tables 12-13, it can be concluded that sample PP HL 504 is more elastic (relaxation time varies between 0.0021s and 0.0012s for 190-230°C temperature range) than sample PP HL 512 (relaxation time is equal to 0.001s for 190-230°C temperature range). Thus, based on the work of Macosko et. al. [3], it can be concluded that the diameter variation of the PP HL 504 based nanofibers can be expected to be smaller and fiber production more stable in comparison with PP HL 512 based nanofibers.

This is in good correspondence with the index of non-Newtonian behavior of PP HL 504 sample, which is higher (between 0.2870-0.3863 for 190-230°C temperature range) in comparison with PP HL 512 sample (between 0.18224-0.28128 for 190-230°C temperature range). This simply means that PP HL 512 shear viscosity is more shear rate (i.e. flow channel shape) dependent than in the case of PP HL 504 sample. Thus, the flow of PP HL 512 inside the melt blown die will be less balanced than for PP HL 504 sample i.e. there will be more polymer melt in the middle of the melt blown die (high diameter fibers will be created at that region) and less polymer melt at the die edges (low diameter fibers will be created at that region). This suggest that specific care should be paid during melt blown die designing for PP HL 512 sample due to its high flow sensitivity to flow channel shape.

The comparison between the strain rate dependent extensional viscosities for both tested samples is provided in Figures 53-55. It is clearly visible that PP HL 512 sample has lower extensional viscosity than PP HL 504 at all three tested temperatures over the whole tested extensional strain rate range. This means that PP HL 512 sample can be stretched more in post die area by the surrounding air i.e. the resulting fibers will have smaller diameter than PP HL 504 based fibers.

Tab. 6. Approximation function parameters for HL 504, T=190 ˚C

Approximation function name	A	B	C	D
Equation (29)	0.57848258	2.58117264	-	-
Equation (30)	-0.11911000	1.31716193	1.57597129	-
Equation (31)	0.01405944	-0.24998443	1.69374102	1.24760671
Equation (32)	62.90000000	0.00170000	-0.88880000	-0.30740000

Tab. 7. Approximation function parameters for HL 504, T=210 ˚C

Approximation function name	A	B	C	D
Equation (29)	0.60283682	2.40029066	-	-
Equation (30)	-0.12763221	1.41274135	1.25500120	-
Equation (31)	0.00855855	-0.20910430	1.65469331	1.03410090
Equation (32)	40.49000000	0.00100000	-0.86750000	-0.28690000

Tab. 8. Approximation function parameters for HL 504, T=230 ˚C

Approximation function name	A	B	C	D
Equation (29)	0.67252255	2.04903325	-	-
Equation (30)	-0.12669382	1.45886700	0.97747021	-
Equation (31)	0.00709665	-0.19271282	1.64866538	0.81199820
Equation (32)	24.56000000	0.00100000	-1.15800000	-0.38690000

Tab. 9. Approximation function parameters for HL 512, T=190 ˚C

Approximation function name	A	B	C	D
Equation (29)	0.67021357	2.02849073	-	-
Equation (30)	-0.12741080	1.51497453	0.74551751	-
Equation (31)	-0.00299474	-0.09758934	1.42091326	0.83866339
Equation (32)	19.63580000	0.00030931	0.75080000	1.00000000

Tab. 10. Approximation function parameters for HL 512, T=210 ˚C

Approximation function name	A	B	C	D
Equation (29)	0.67905804	1.88407784	-	-
Equation (30)	-0.14239489	1.68435648	0.20949748	-
Equation (31)	0.00440901	-0.18910588	1.84383081	0.03469315
Equation (32)	11.10880000	0.00014166	0.81315000	1.00000000

Tab. 11. Approximation function parameters for HL 512, T=230˚C

Approximation function name	A	B	C	D
Equation (29)	0.71010168	1.64974543	-	-
Equation (30)	-0.12644892	1.61999785	0.08934769	-
Equation (31)	0.00210174	-0.14919204	1.69968172	-0.00077951
Equation (32)	7.81695000	0.00012911	0.72279000	1.00000000

Tab. 12. modified White-Metzner model parameters for tested melt blown samples

Function	modified White-Metzner model					
Material	η_0 (Pa.s)	λ (s)	a (-)	n (-)	λ_0 (s)	K_2 (s)
HL504 (190˚C)	62.8100	0.002100	0.88610	0.30790	0.003344	0.006497
HL504 (210˚C)	40.5200	0.001200	0.85790	0.28700	0.000336	0.001000
HL504 (230˚C)	24.4800	0.001200	1.16800	0.38630	0.000038	0.001000
HL512 (190˚C)	19.6349	0.000382	0.74609	0.25391	1204.20000	4854.300000
HL512 (210˚C)	10.8755	0.000163	0.81776	0.18224	410.200000	2189.100000
HL512 (230˚C)	7.8170	0.000160	0.71872	0.28128	1424.70000	5681.400000

Tab. 13. Zatloukal model parameters for tested melt blown samples (α = 1s, ψ = 20)

Function	Zatloukal model						
Material	η_0 (Pa.s)	λ (s)	a (-)	n (-)	β (-)	ζ (-)	A (Pa.s)
HL504 (190˚C)	62.8100	0.002100	0.88610	0.30790	1.944670	0.282969	$1.54*10^{-16}$
HL504 (210˚C)	40.5200	0.001200	0.85790	0.28700	2.164868	0.040920	$1.72*10^{-16}$
HL504 (230˚C)	24.4800	0.001200	1.16800	0.38630	19.110593	0.000100	2.78
HL512 (190˚C)	19.6349	0.000382	0.74609	0.25391	0.841879	0.995902	8.33
HL512 (210˚C)	10.8755	0.000163	0.81776	0.18224	1.343158	0.827069	3.47
HL512 (230˚C)	7.8170	0.000160	0.71872	0.28128	0.952464	1.172837	3.77

Tab. 14. Logarithmic sum of squared residuals between measured and predicted values for both rheological models, tested samples and flow situations

Material	HL504		HL512	
Fitting model	Extensional flow	Shear flow	Extensional flow	Shear flow
mWM	0.221013	0.006191	0.321289	0.008065
Zatloukal	0.347931	0.006191	0.210780	0.008065
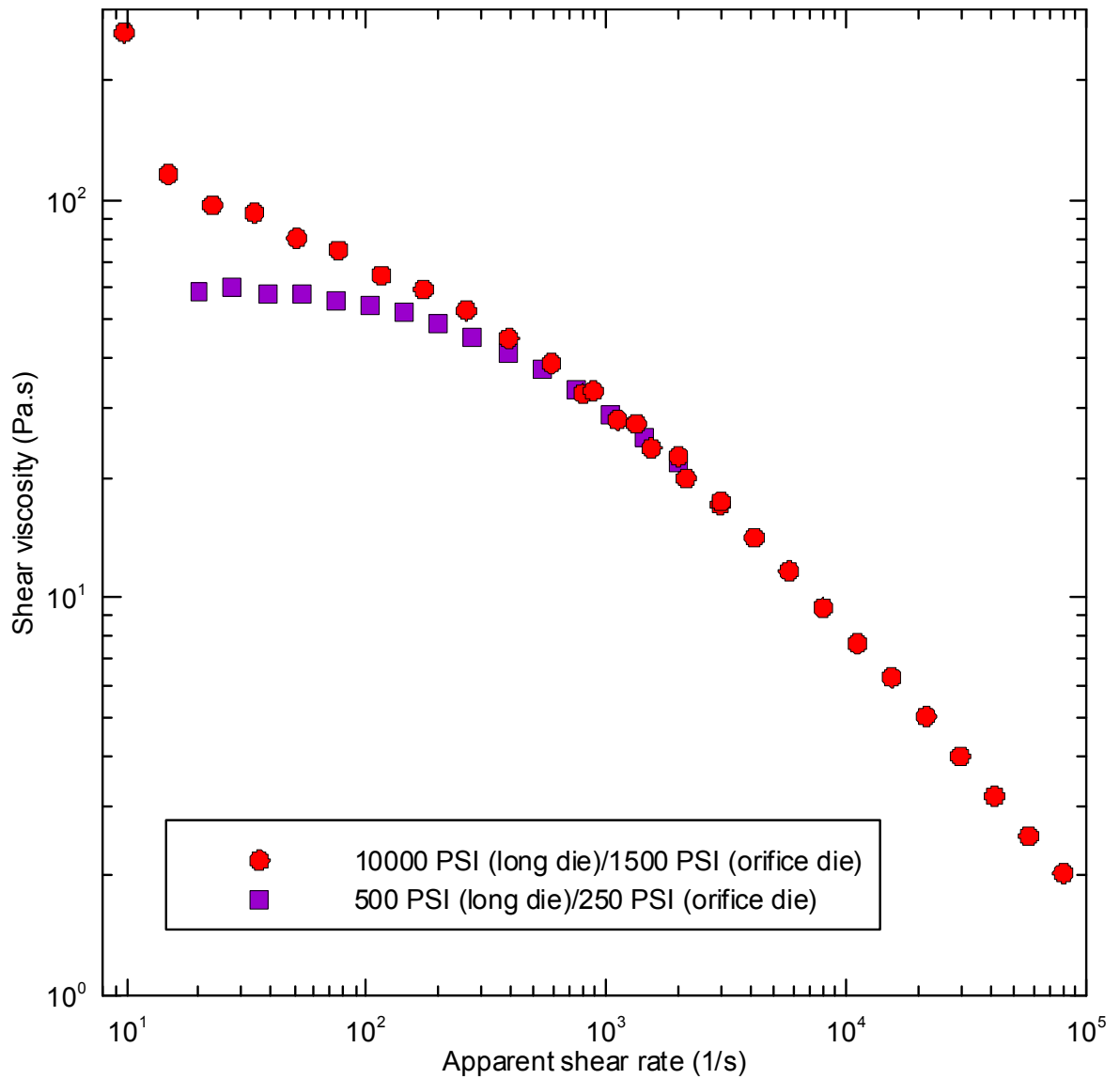
Fig. 28. Effect of pressure transducer sensitivity on the measured shear rate dependent shear viscosity for HL 504 sample at 190°C.
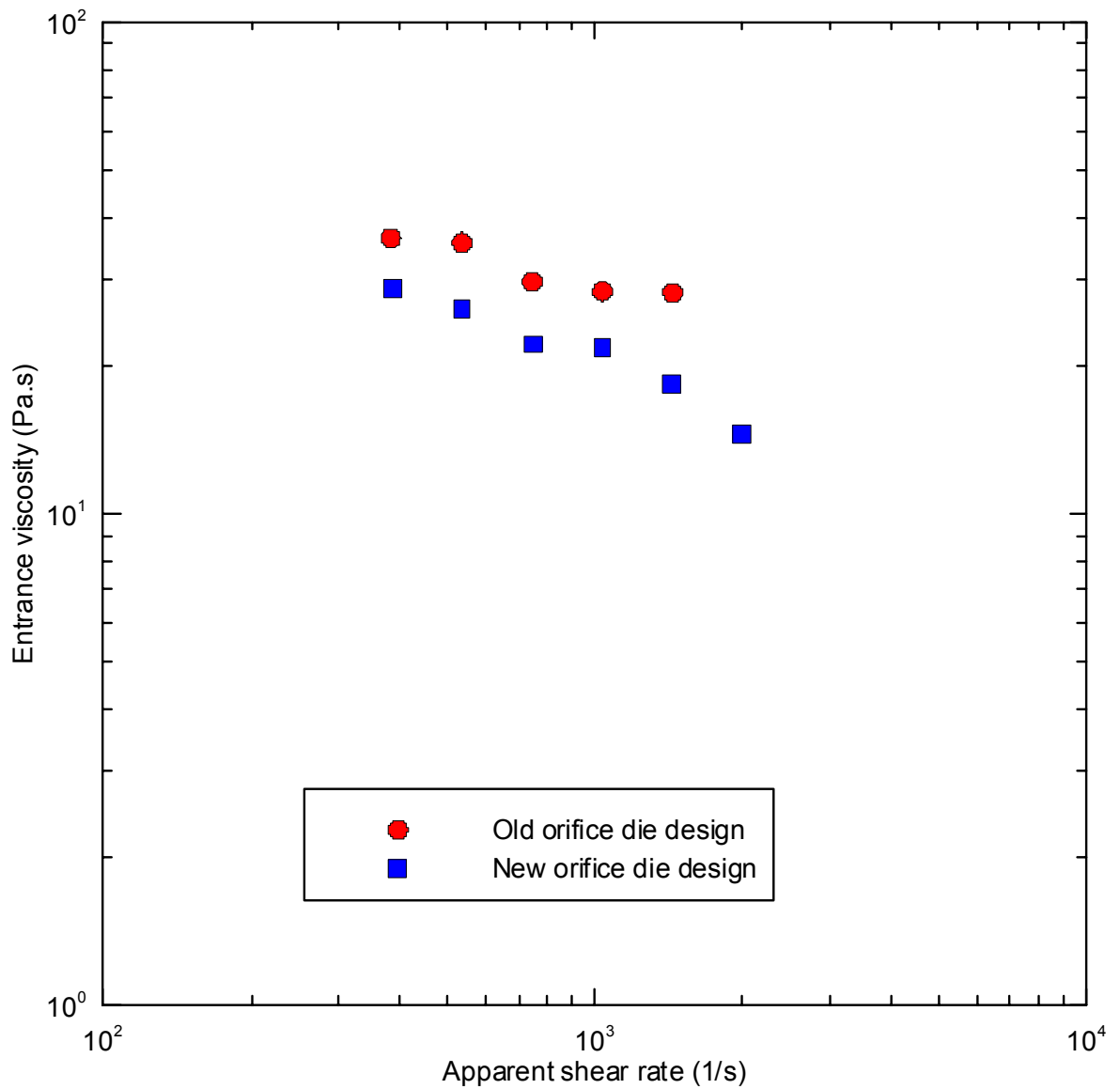
Fig. 29. Effect of orifice die design on the measured shear rate dependent entrance viscosity for HL 512 sample at 210ºC.
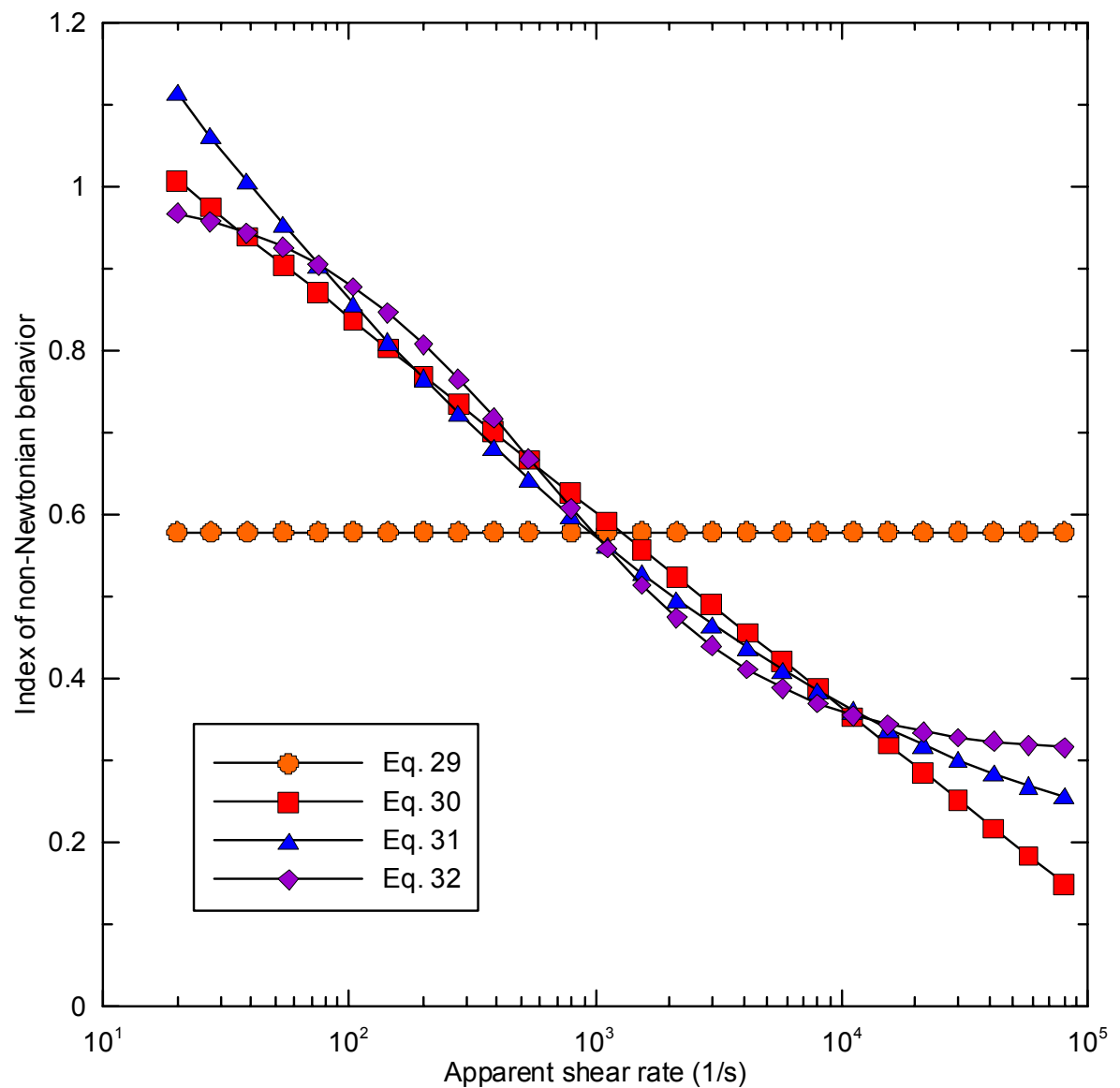
Fig. 30. Effect of approximation function type selection on the index of non-Newtonian behavior determination for HL 504 sample at 190ºC.
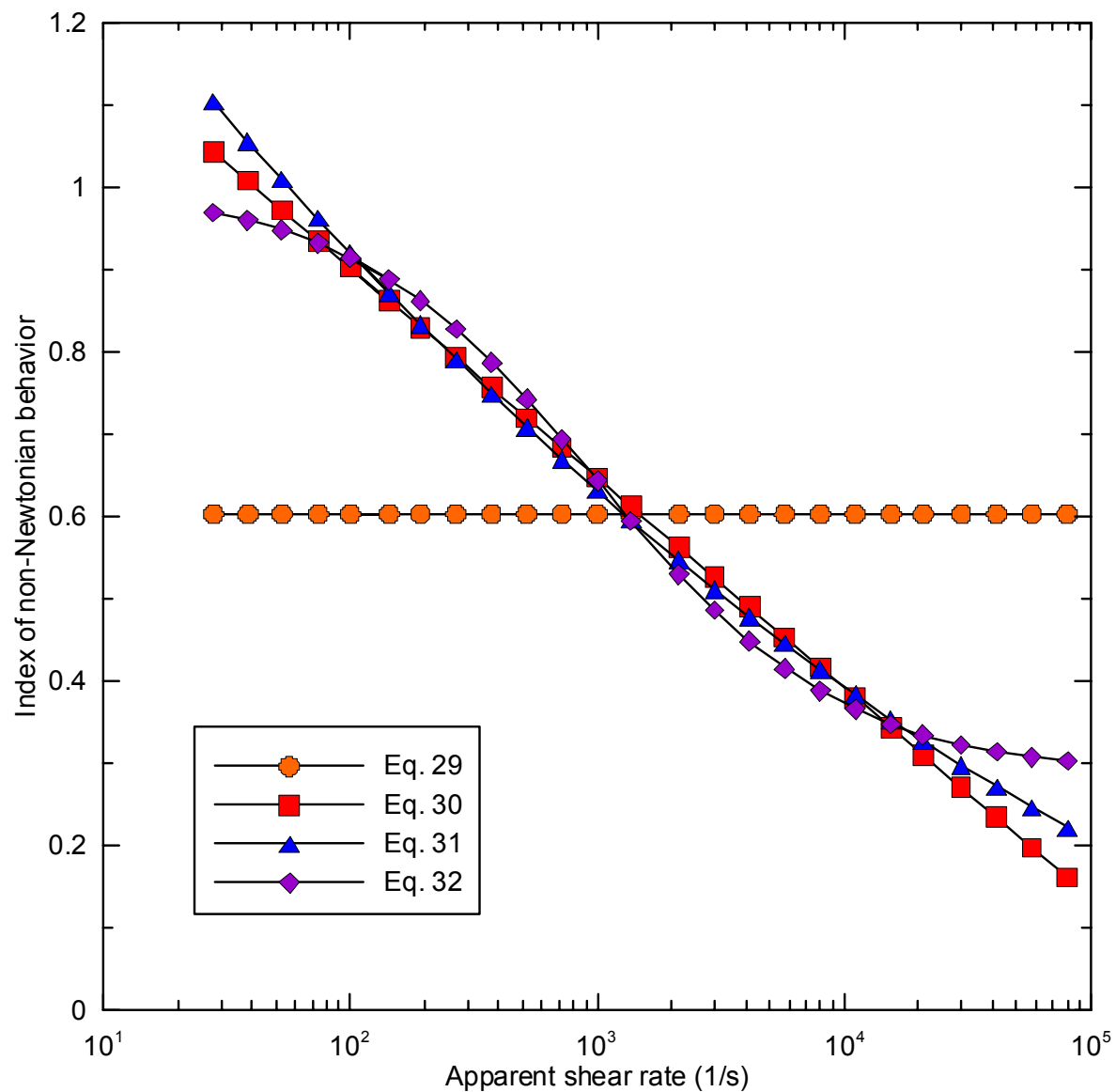
Fig. 31. Effect of approximation function type selection on the index of non-Newtonian behavior determination for HL 504 sample at 210°C.
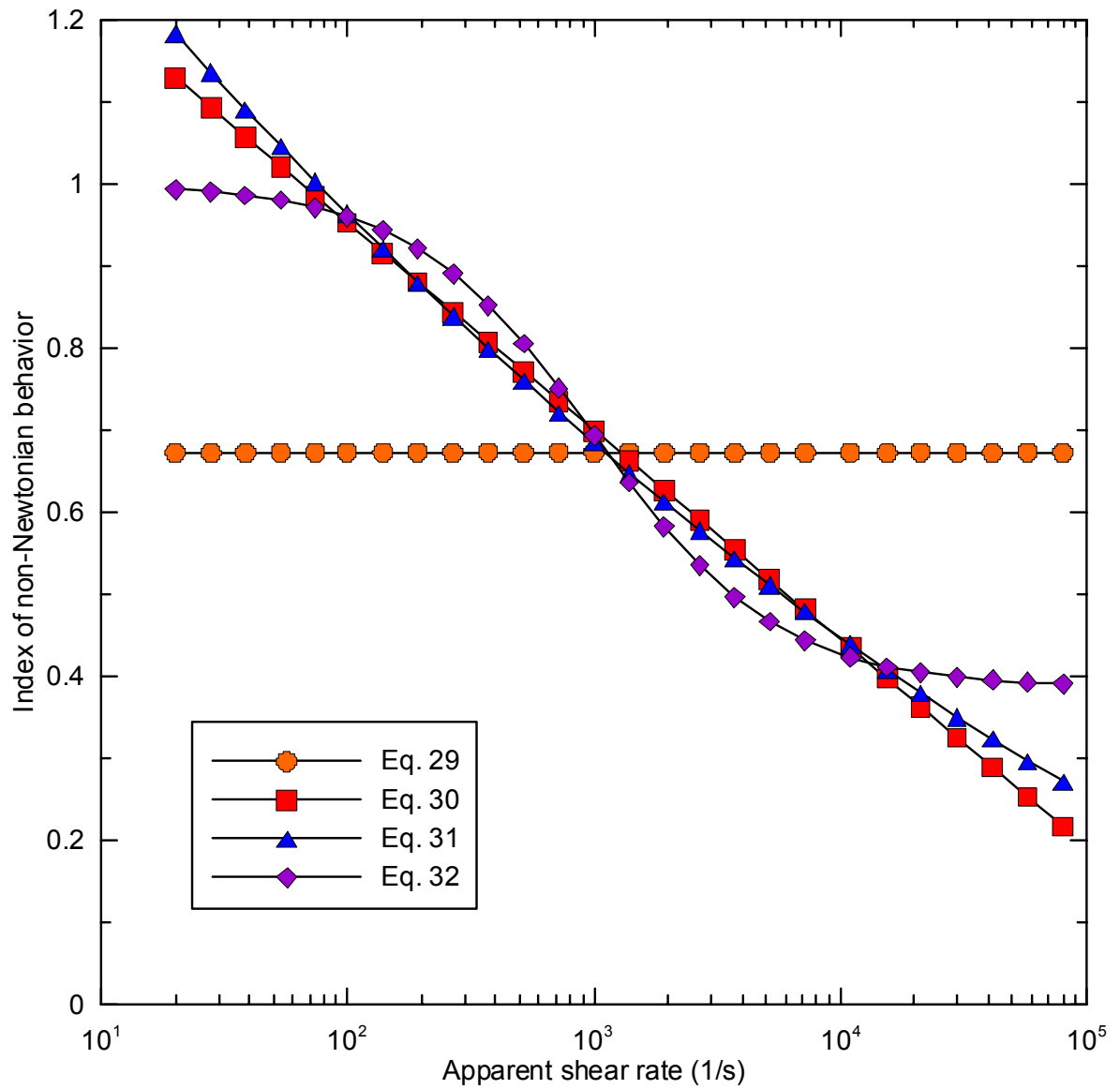
Fig. 32. Effect of approximation function type selection on the index of non-Newtonian behavior determination for HL 504 sample at 230ºC.
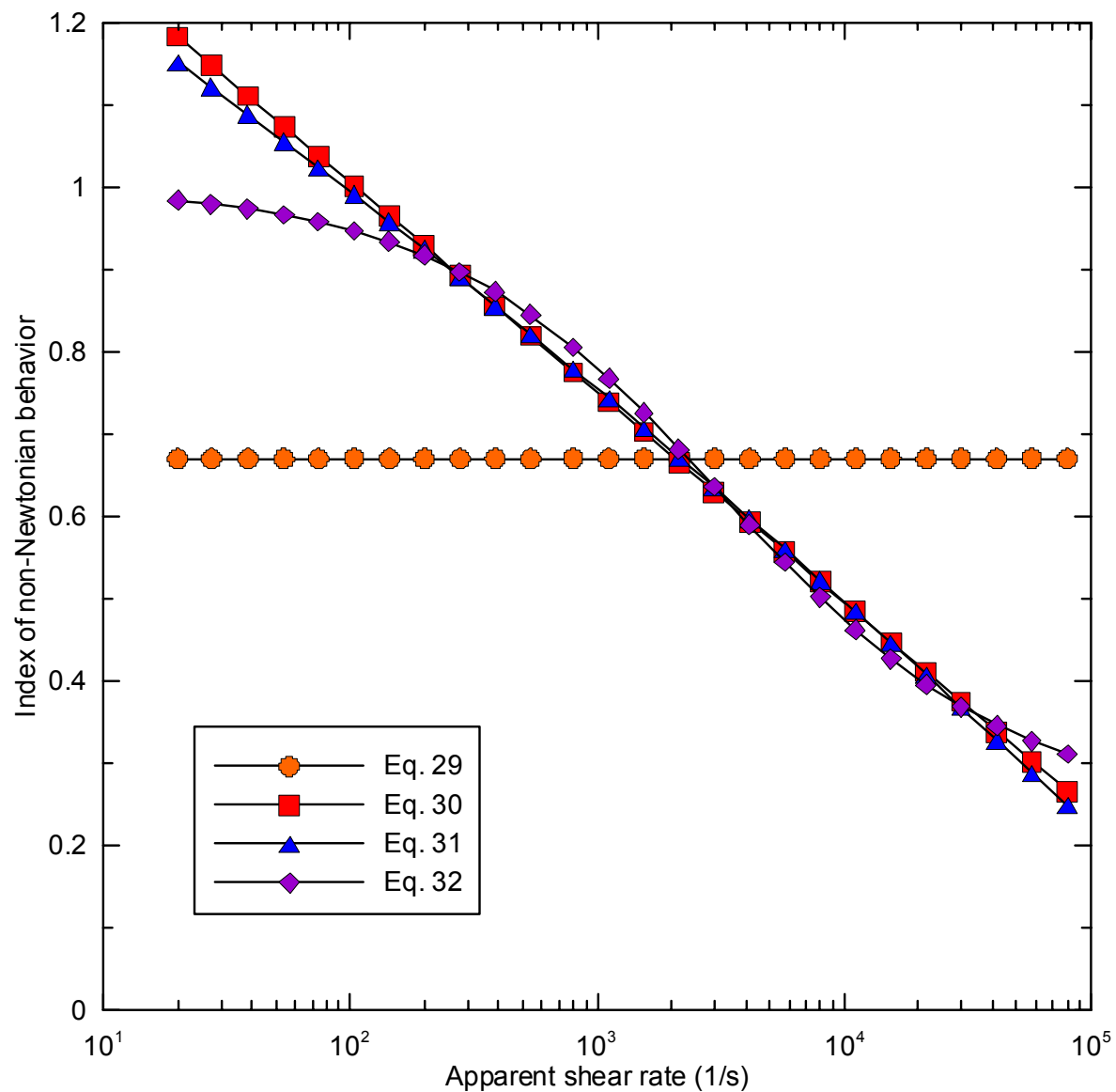
Fig. 33. Effect of approximation function type selection on the index of non-Newtonian

behavior determination for HL 512 sample at 190°C.
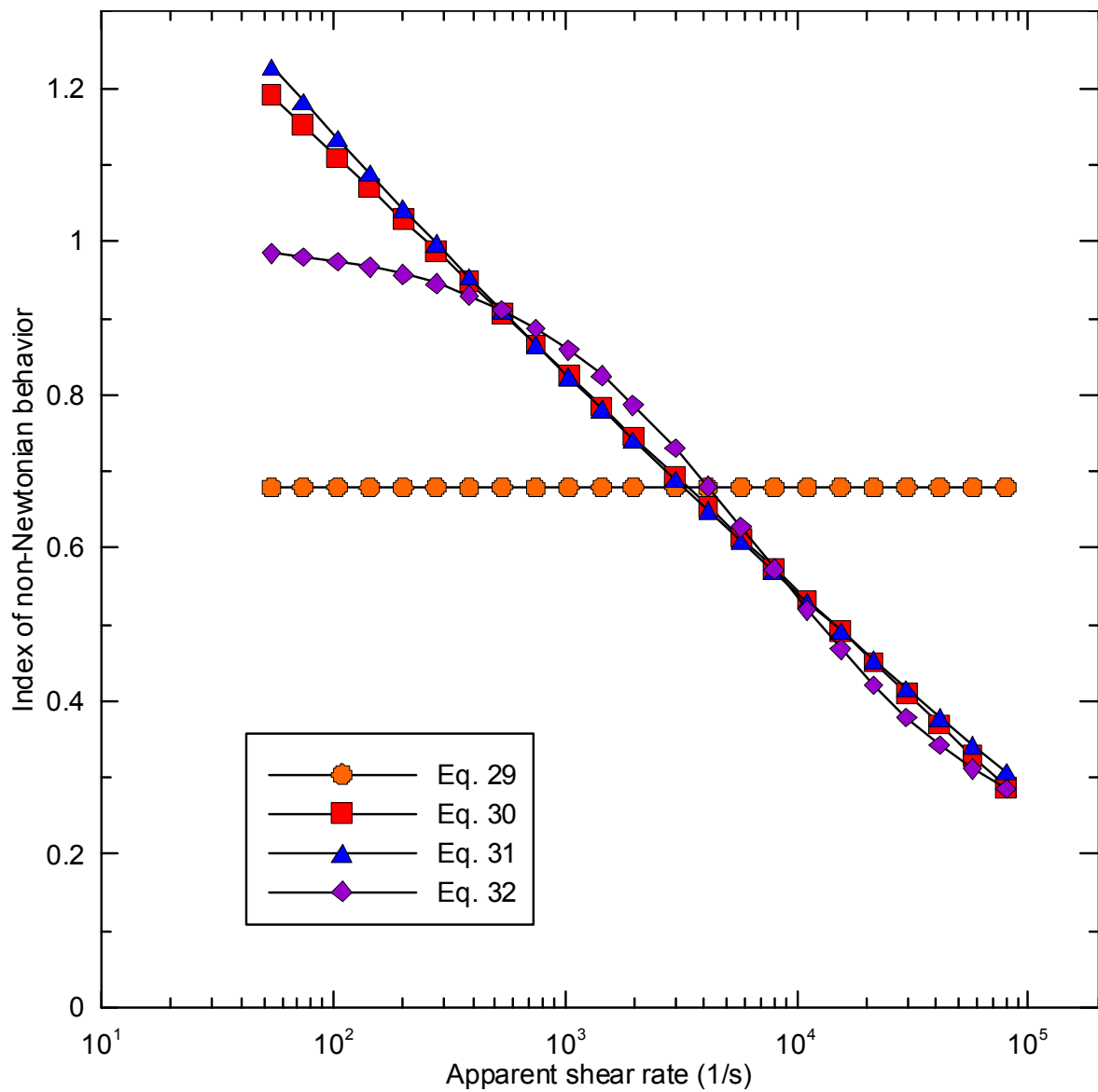
Fig. 34. Effect of approximation function type selection on the index of non-Newtonian

behavior determination for HL 512 sample at 210ºC.
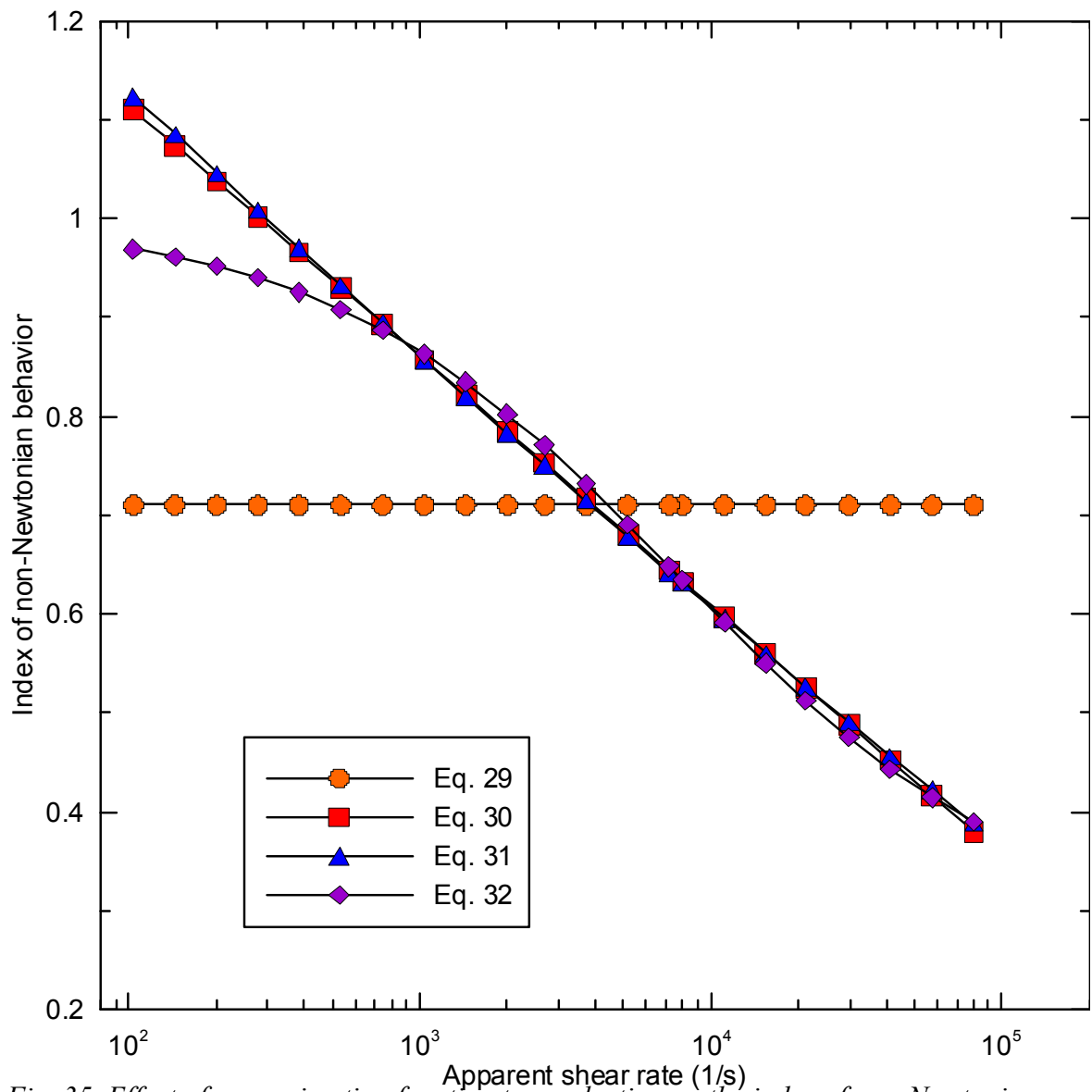
Fig. 35. Effect of approximation function type selection on the index of non-Newtonian behavior determination for HL 512 sample at 230ºC.
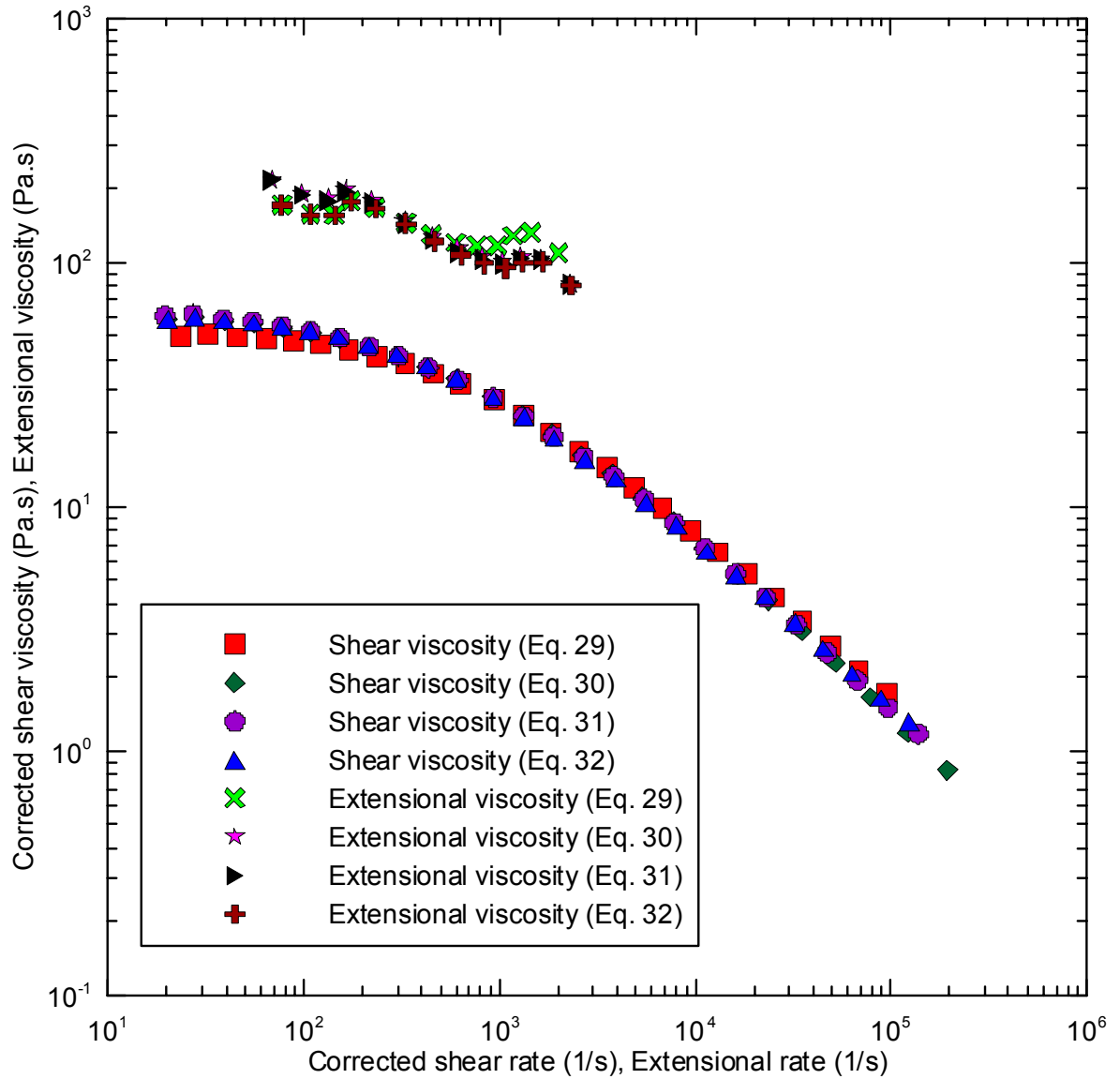
Fig. 36. Effect of approximation function type selection utilized during the index of non-Newtonian behavior determination on the deformation rate dependent shear and extensional viscosities for HL 504 sample at 190°C.
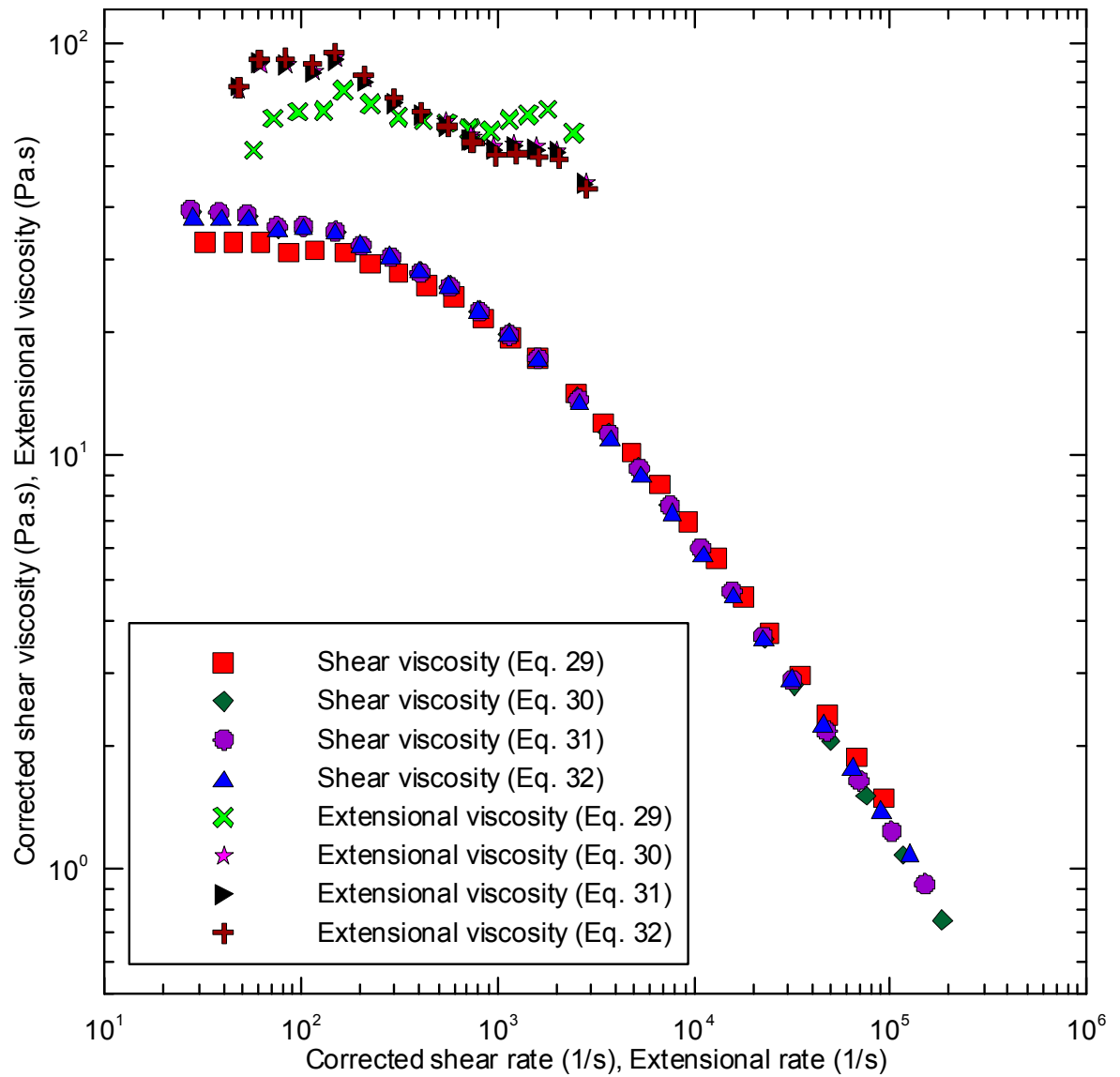
Fig. 37. Effect of approximation function type selection utilized during the index of non-Newtonian behavior determination on the deformation rate dependent shear and extensional viscosities for HL 504 sample at 210°C.
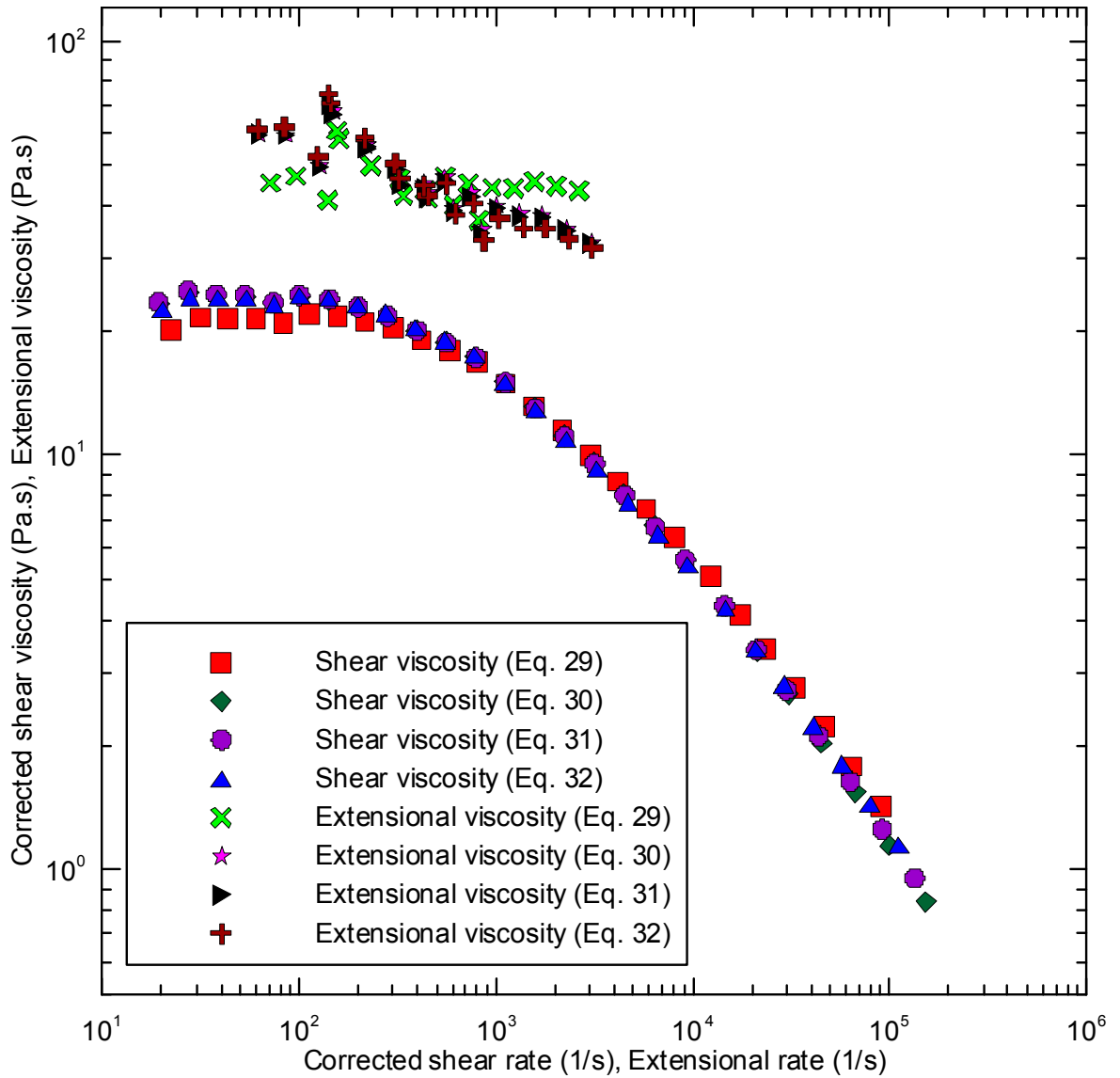
Fig. 38. Effect of approximation function type selection utilized during the index of non-Newtonian behavior determination on the deformation rate dependent shear and extensional viscosities for HL 504 sample at 230ºC.
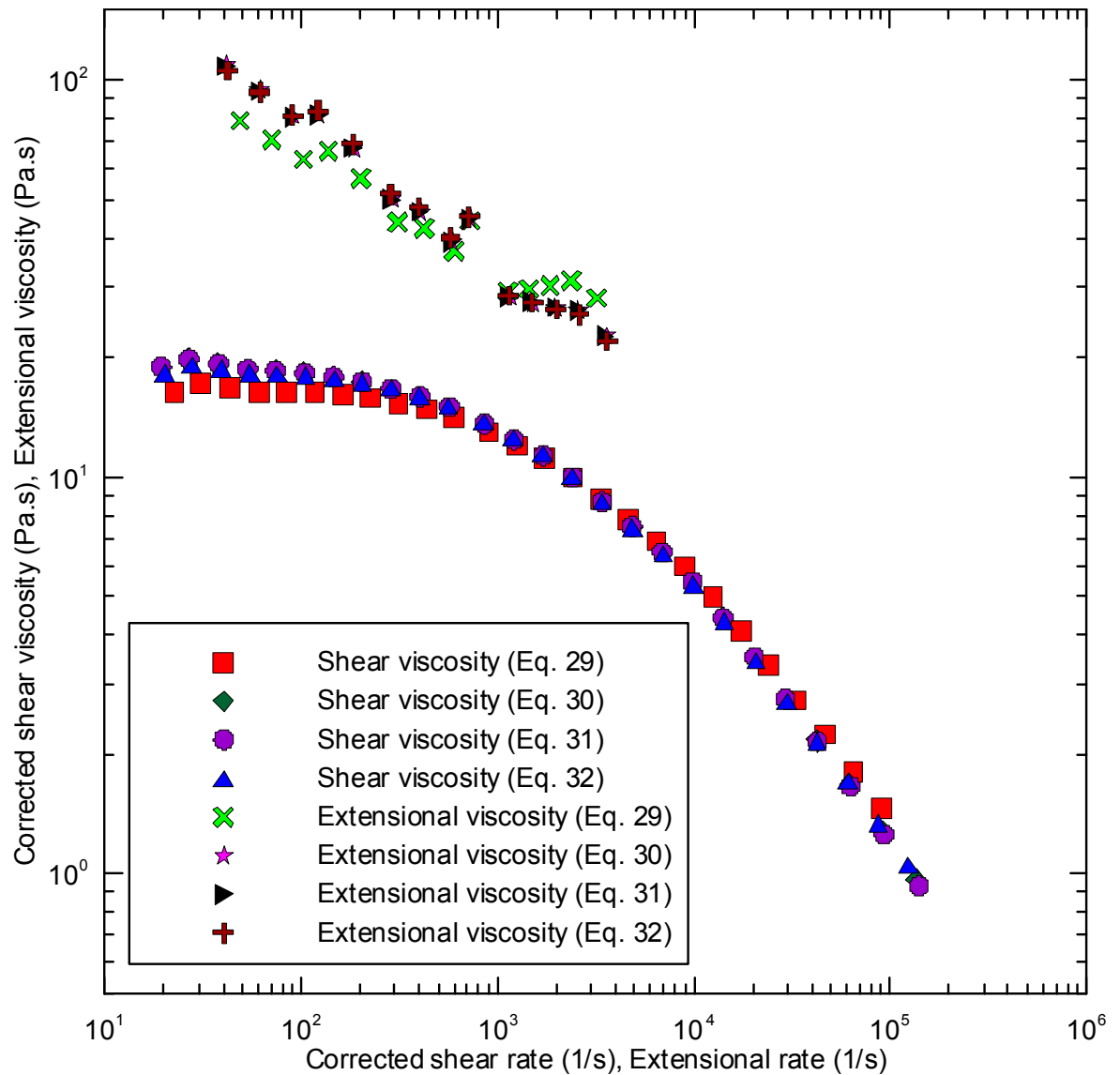
Fig. 39. Effect of approximation function type selection utilized during the index of non-Newtonian behavior determination on the deformation rate dependent shear and extensional viscosities for HL 512 sample at 190°C.
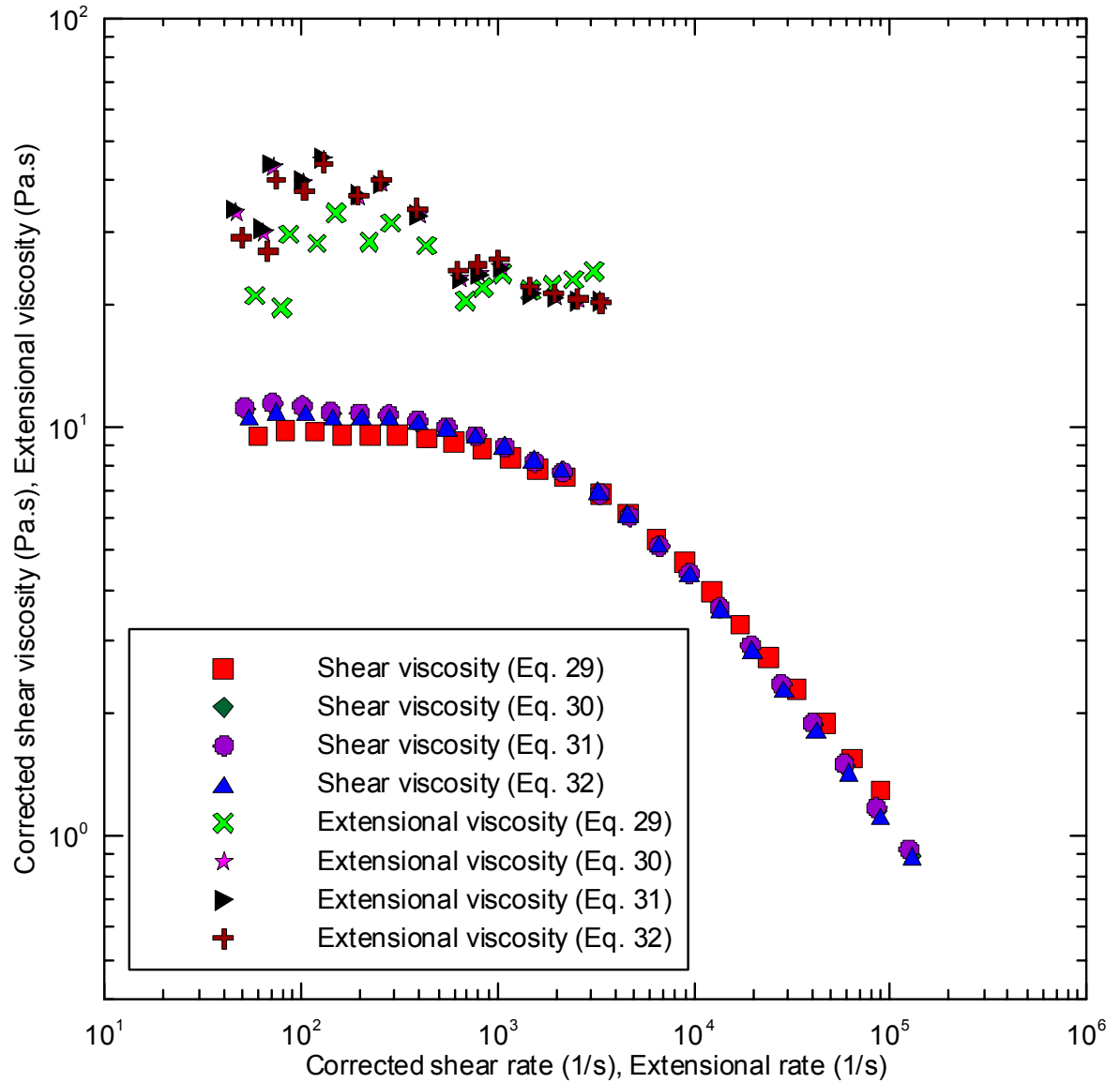
Fig. 40. Effect of approximation function type selection utilized during the index of non-Newtonian behavior determination on the deformation rate dependent shear and extensional viscosities for HL 512 sample at 210°C.
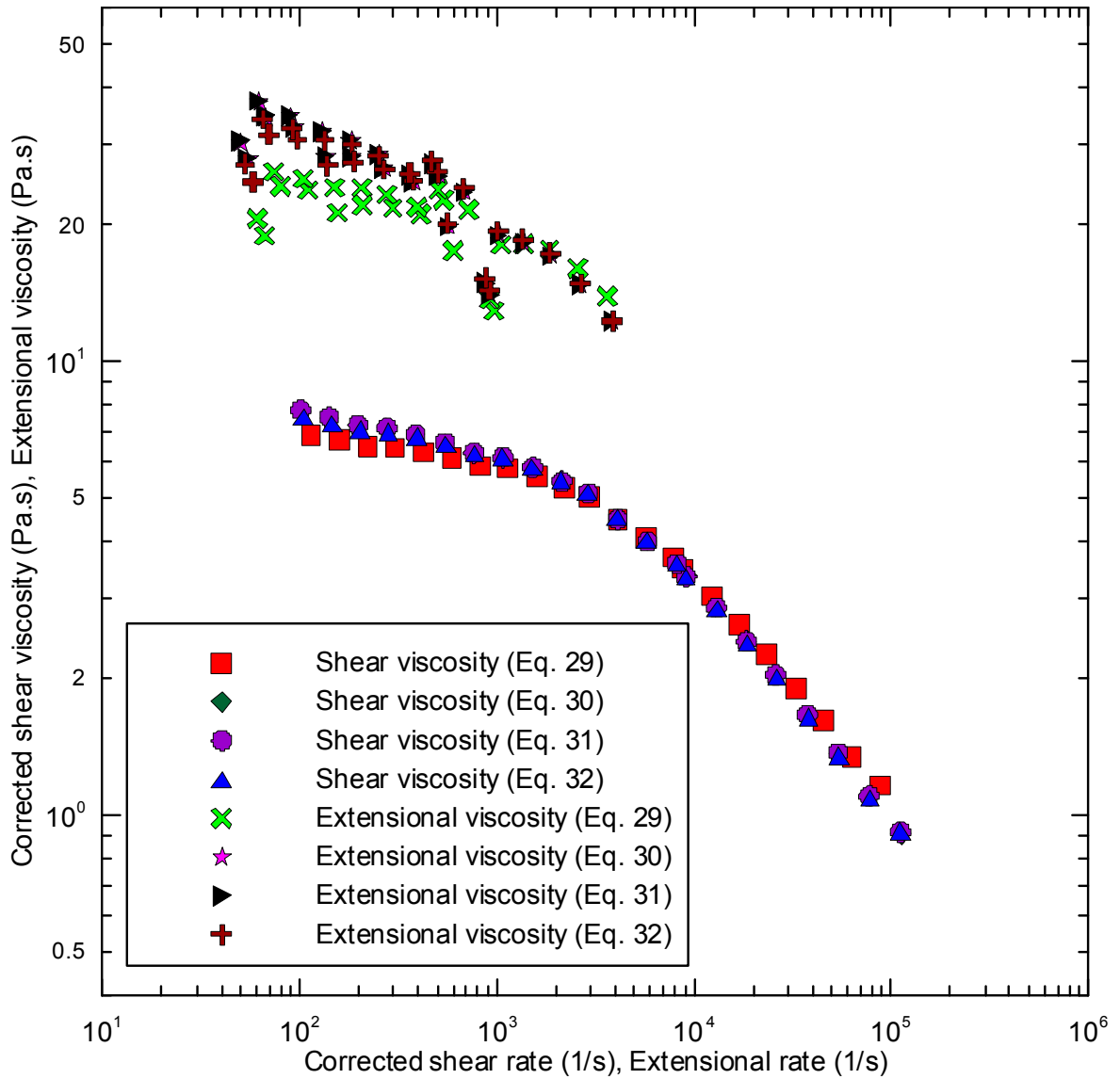
Fig. 41. Effect of approximation function type selection utilized during the index of non-Newtonian behavior determination on the deformation rate dependent shear and extensional viscosities for HL 512 sample at 230ºC.
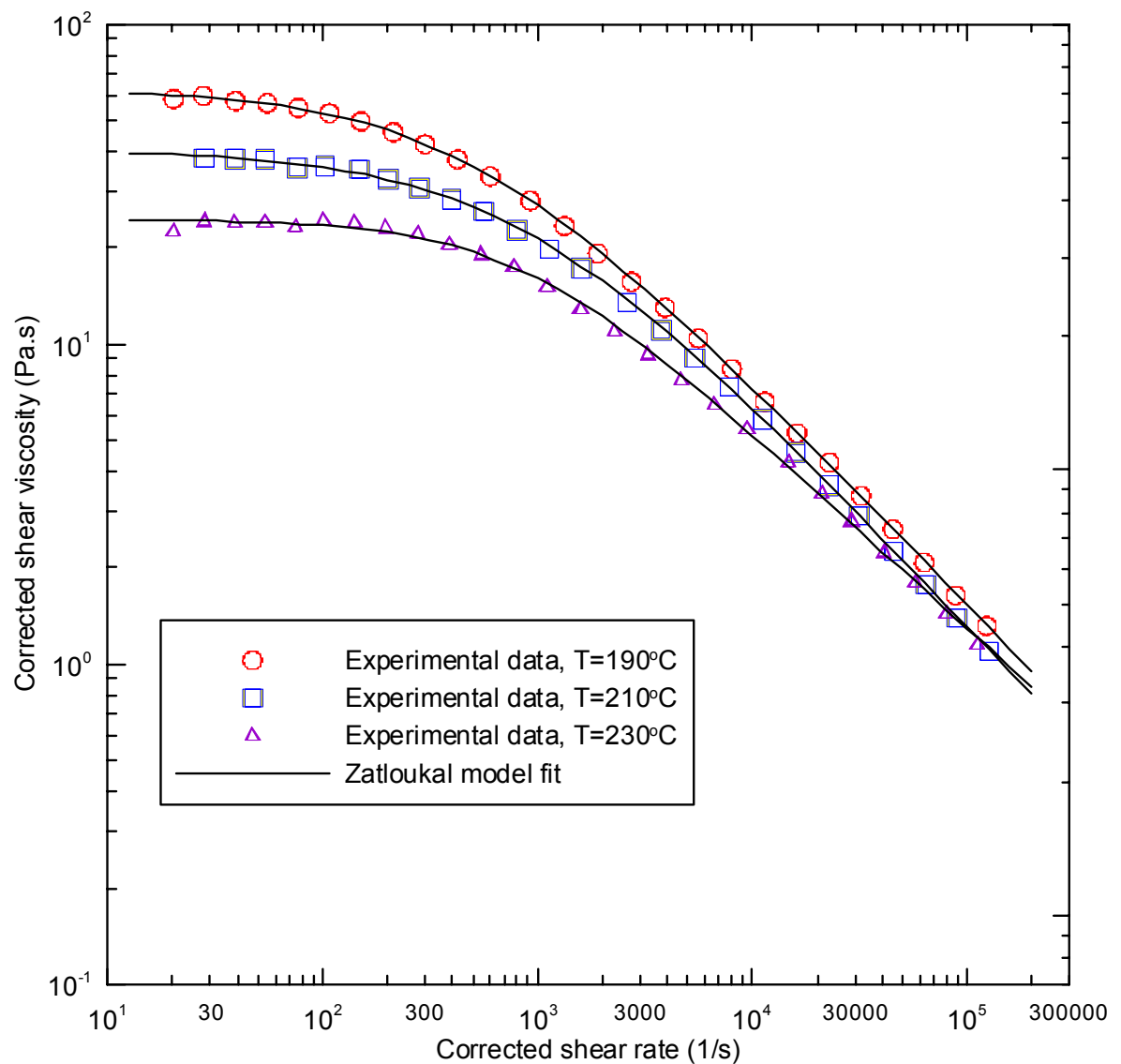
Fig. 42. Comparison between Zatloukal model fits (Eq. 8-10) and deformation rate dependent shear viscosity for HL 504 sample measured at three different temperatures.
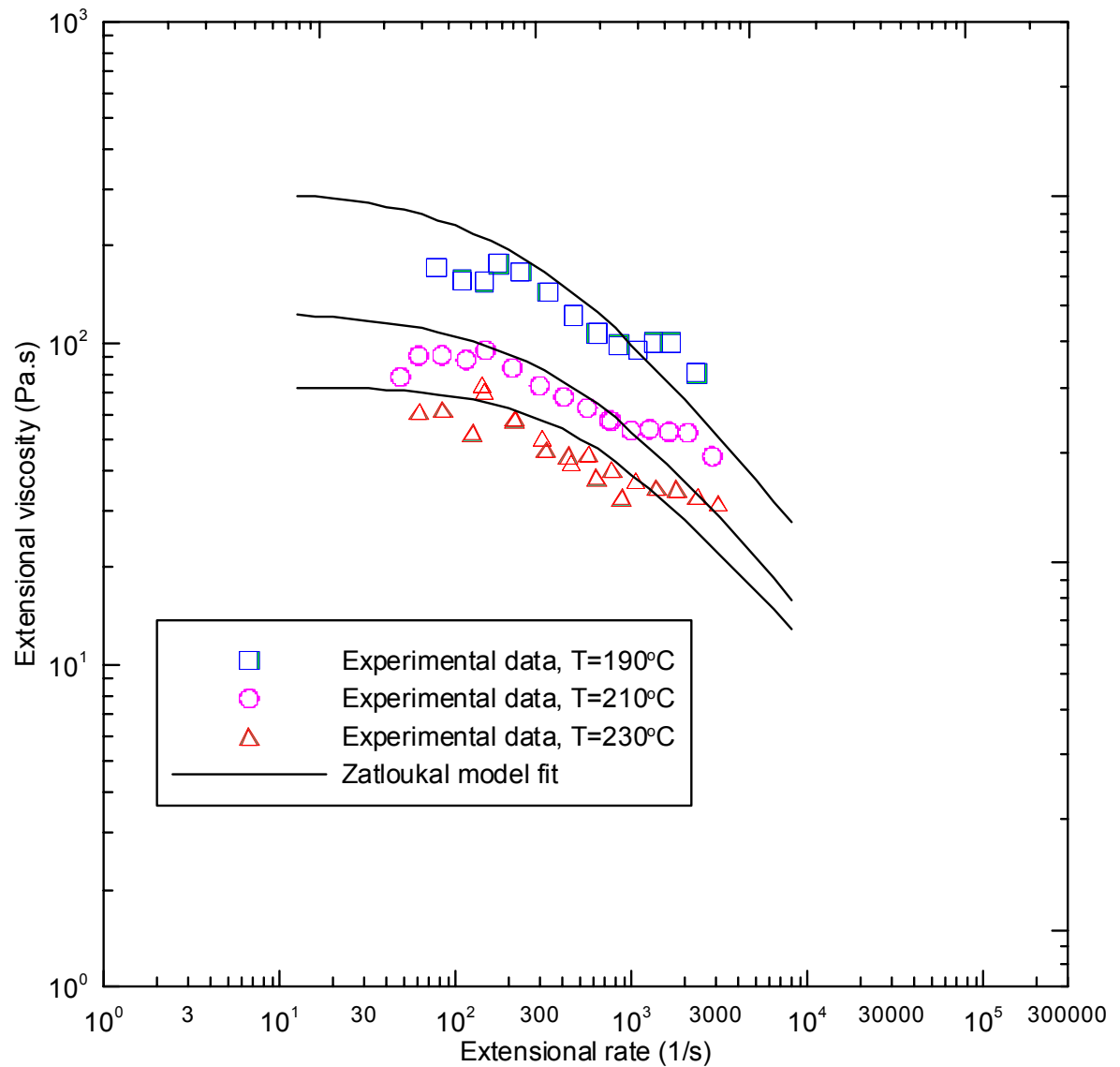
Fig. 43. Comparison between Zatloukal model fits (Eq. 8-10) and deformation rate dependent uniaxial extensional viscosity for HL 504 sample measured at three different temperatures.
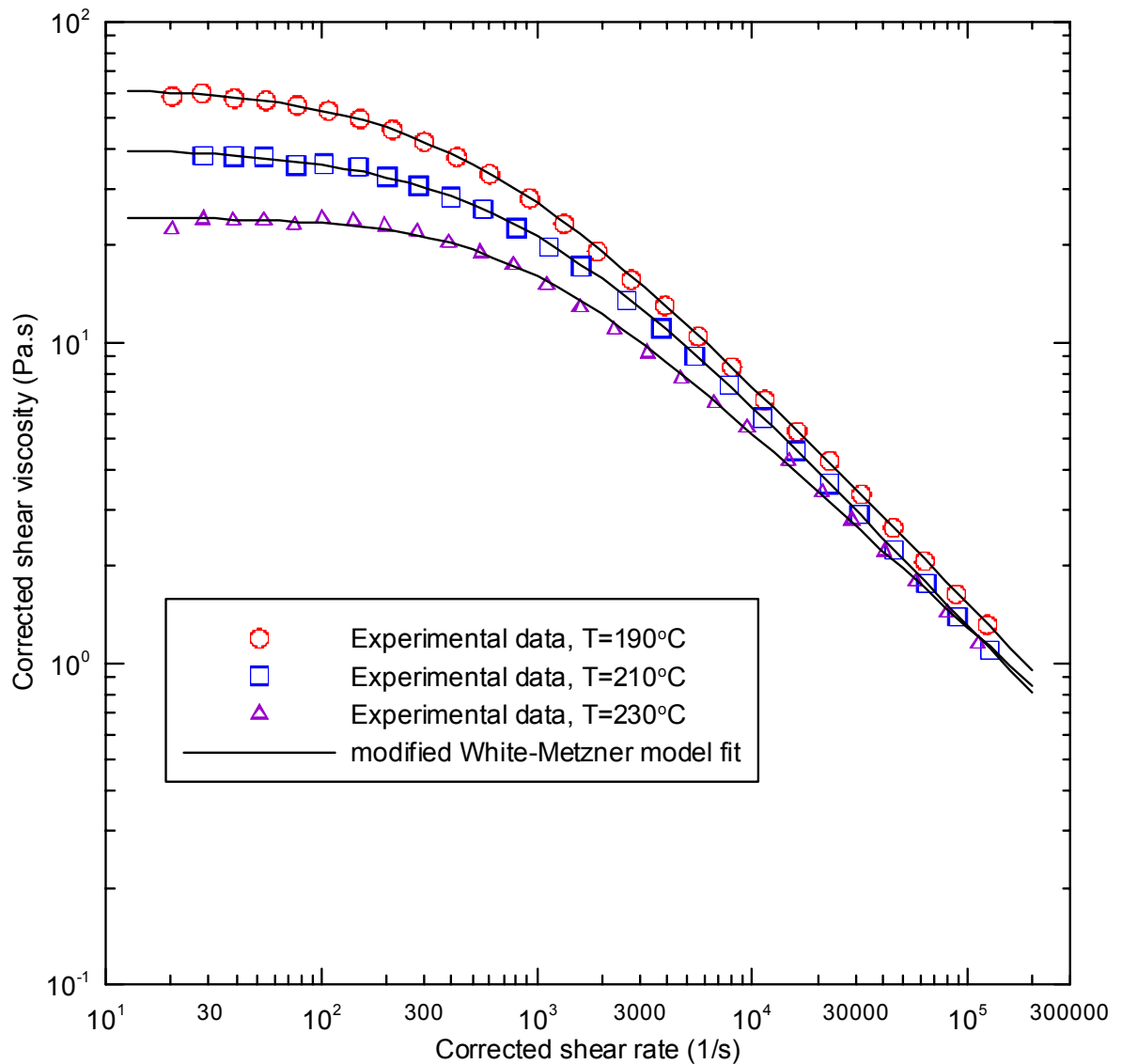
Fig. 44. Comparison between modified White-Metzner model fits (Eq. 11-18) and deformation rate dependent shear viscosity for HL 504 sample measured at three different temperatures.
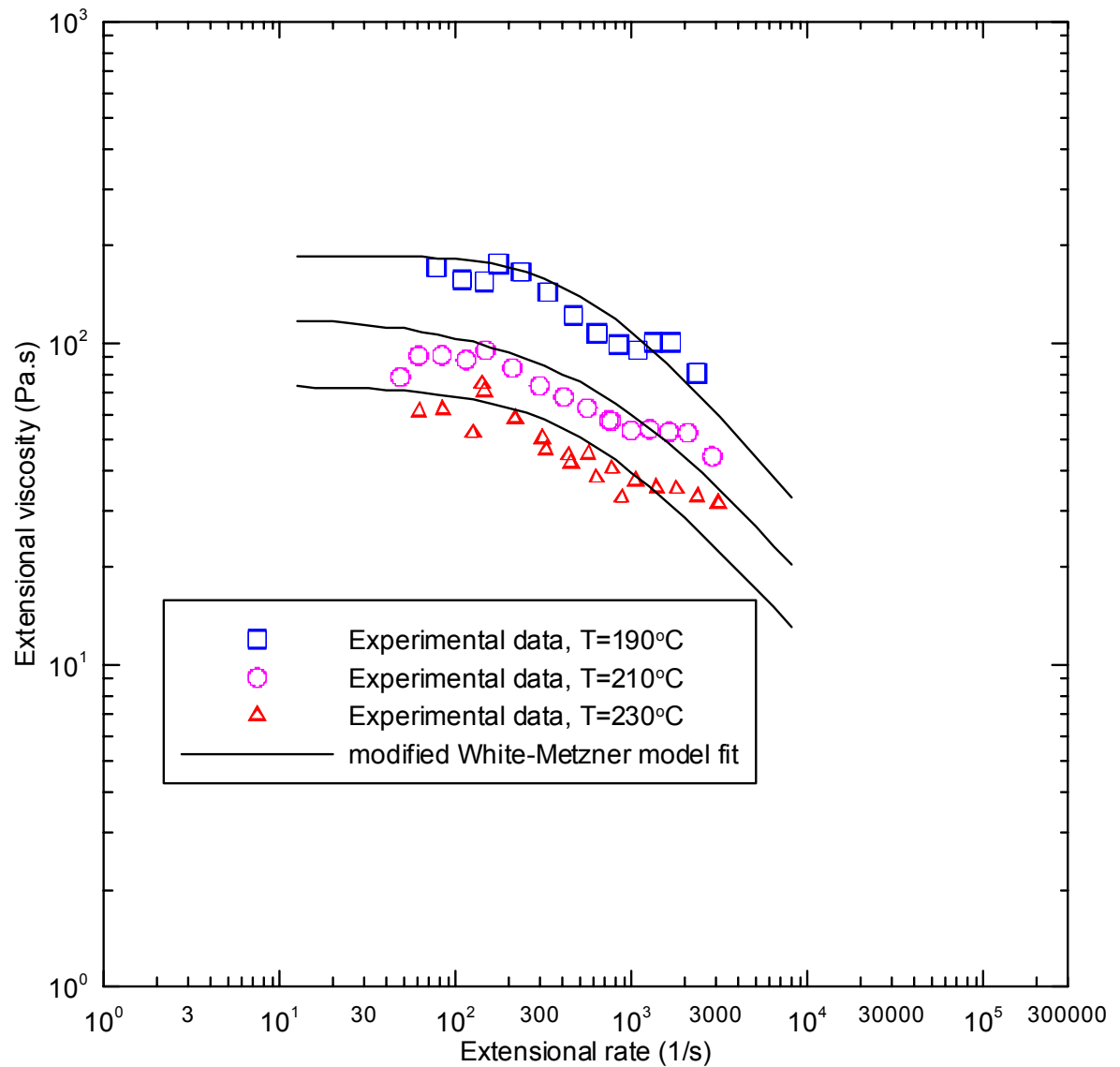
Fig. 45. Comparison between modified White-Metzner model fits (Eq. 11-18) and deformation rate dependent uniaxial extensional viscosity for HL 504 sample measured at three different temperatures.
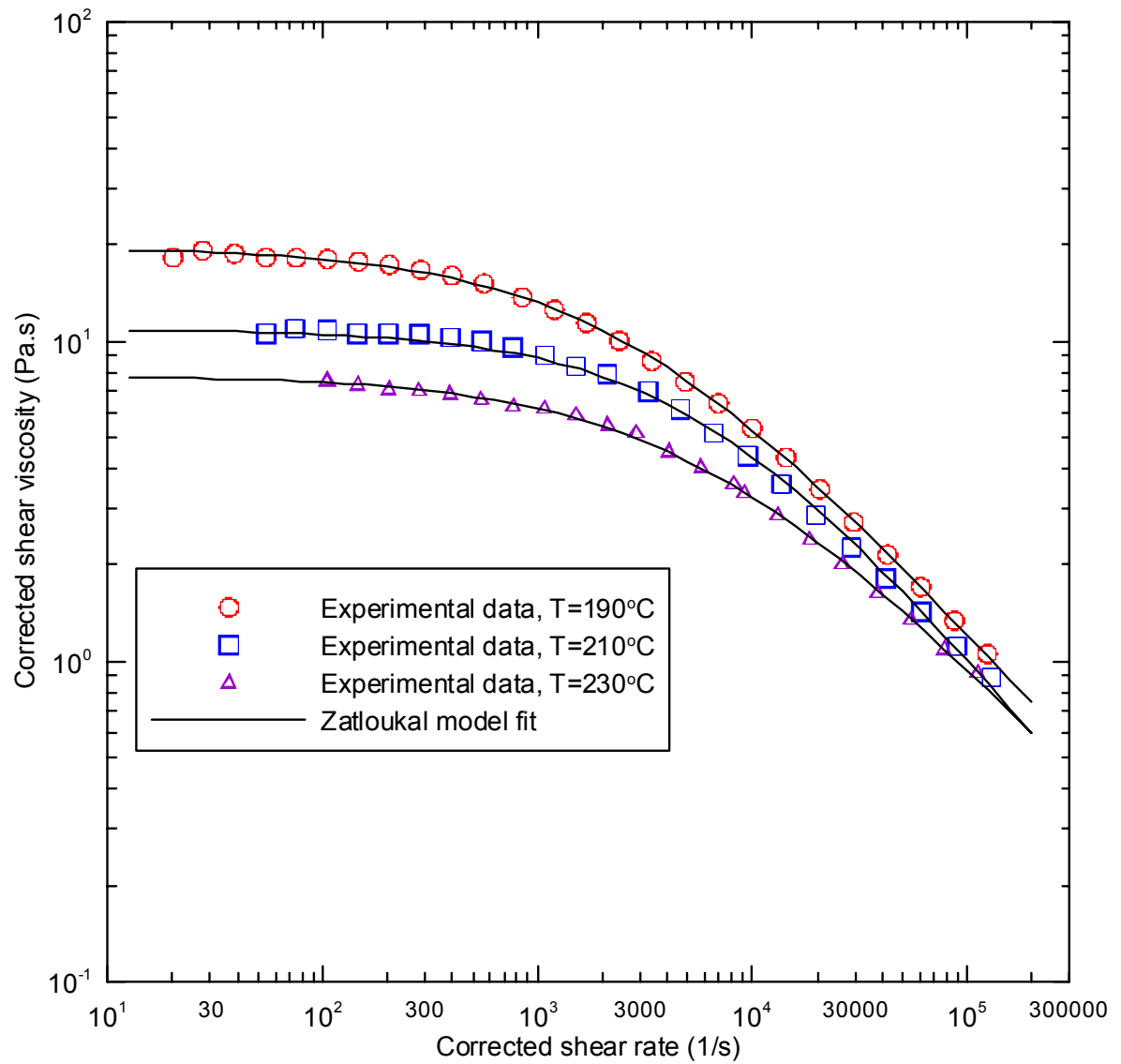
Fig. 46. Comparison between Zatloukal model fits (Eq. 8-10) and deformation rate dependent shear viscosity for HL 512 sample measured at three different temperatures.
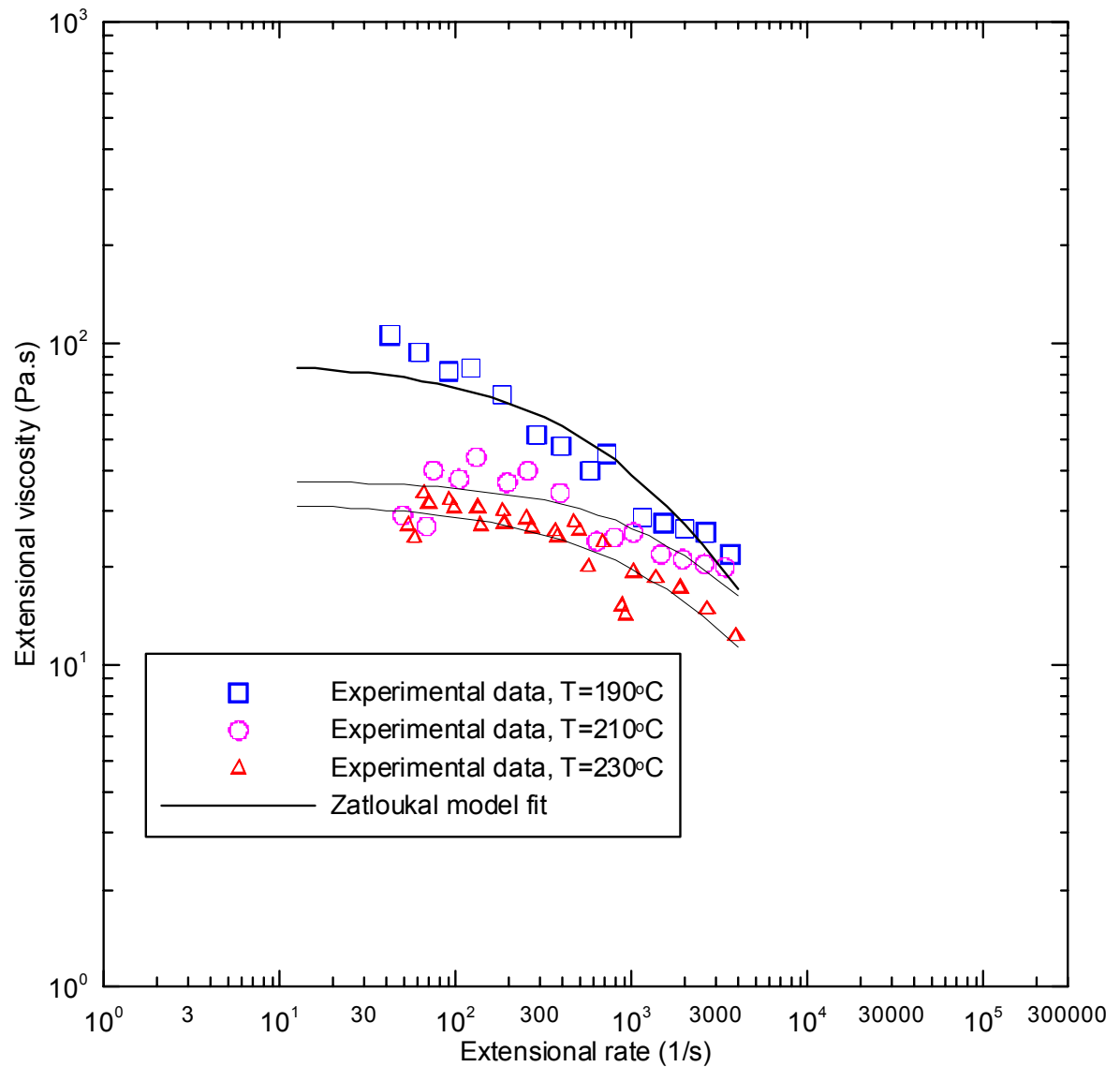
Fig. 47. Comparison between Zatloukal model fits (Eq. 8-10) and deformation rate dependent uniaxial extensional viscosity for HL 512 sample measured at three different temperatures.
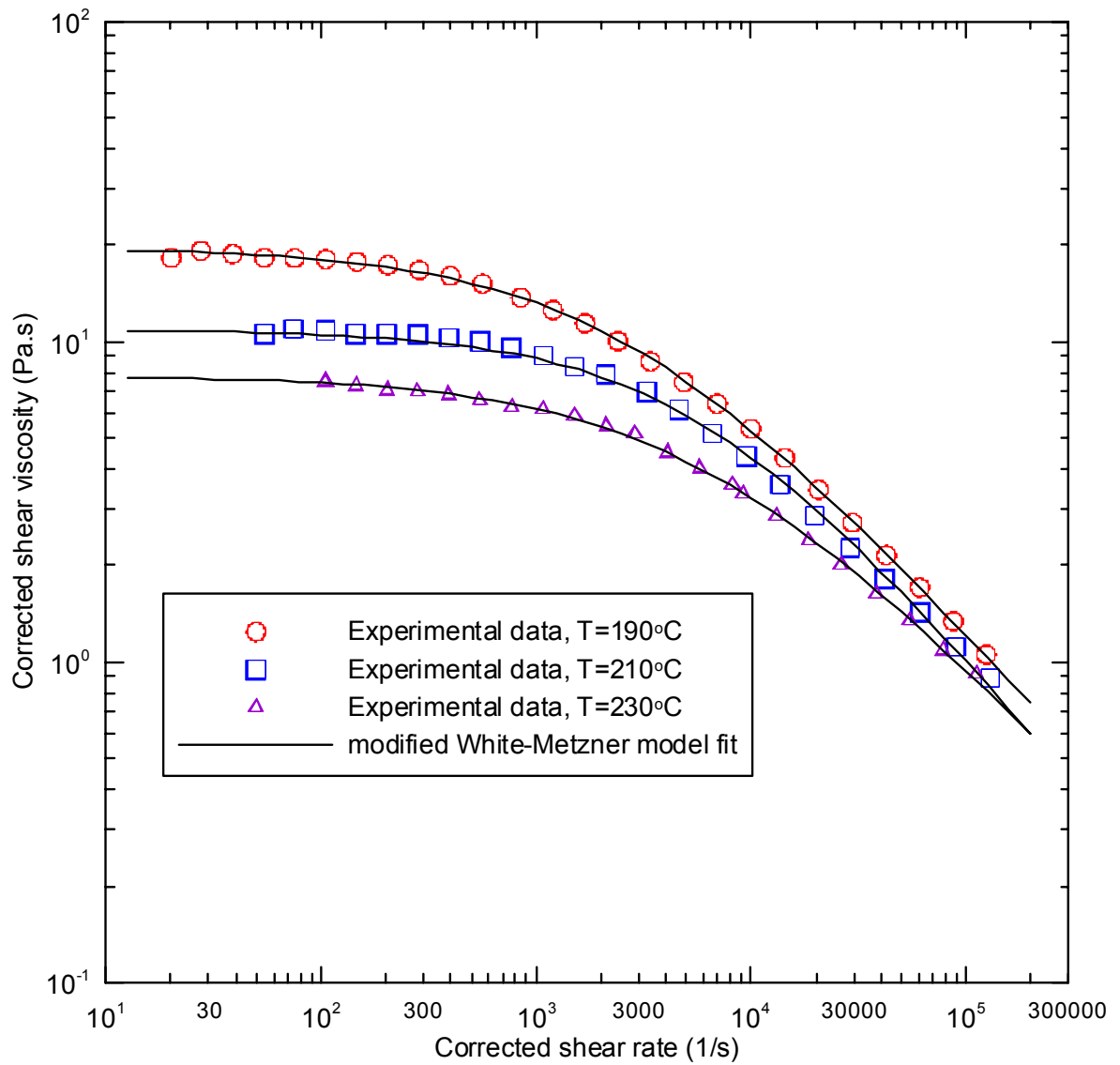
Fig. 48. Comparison between modified White-Metzner model fits (Eq. 11-18) and deformation rate dependent shear viscosity for HL 512 sample measured at three different temperatures.
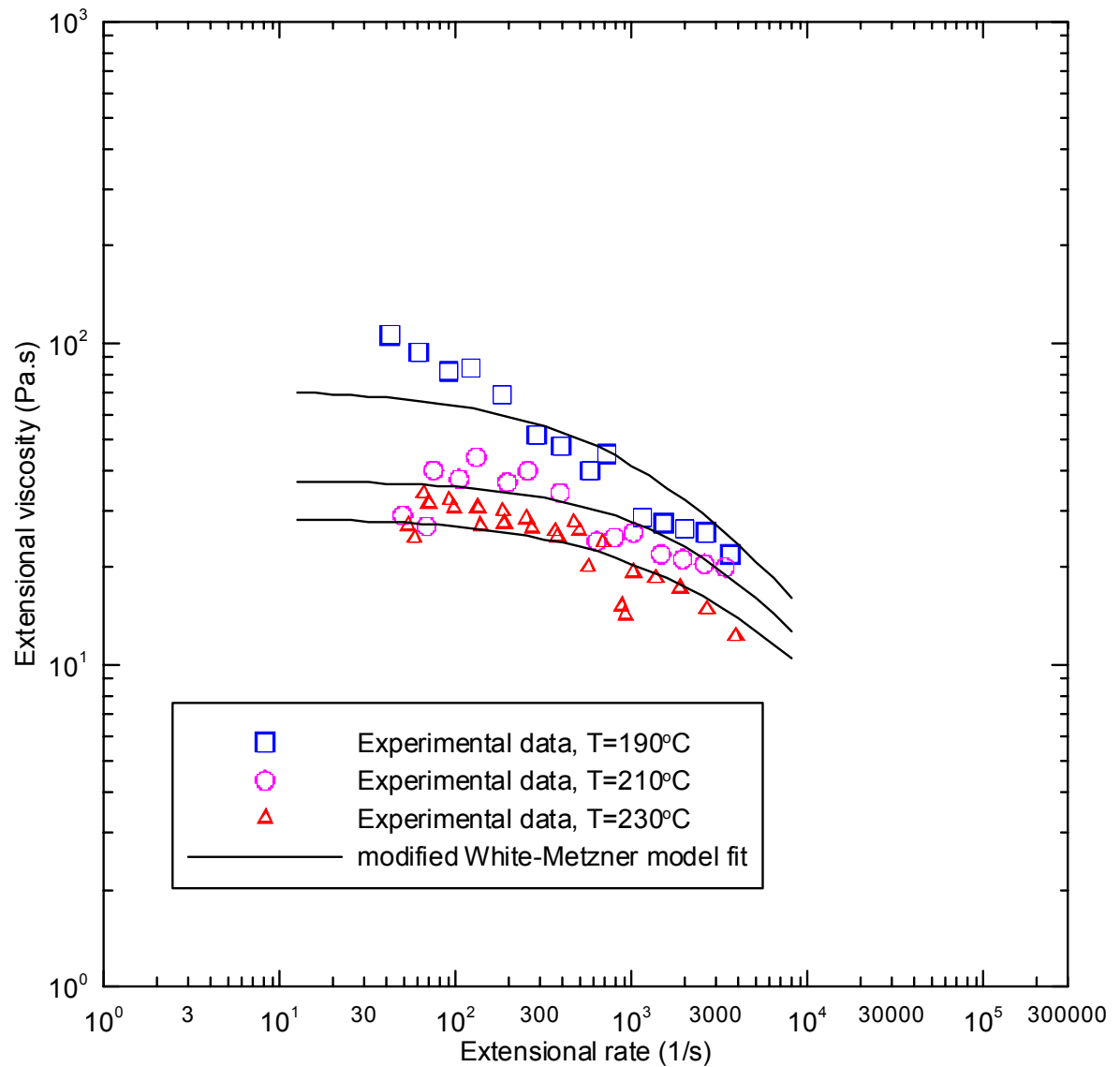
Fig. 49. Comparison between modified White-Metzner model fits (Eq. 11-18) and deformation rate dependent uniaxial extensional viscosity for HL 512 sample measured at three different temperatures.
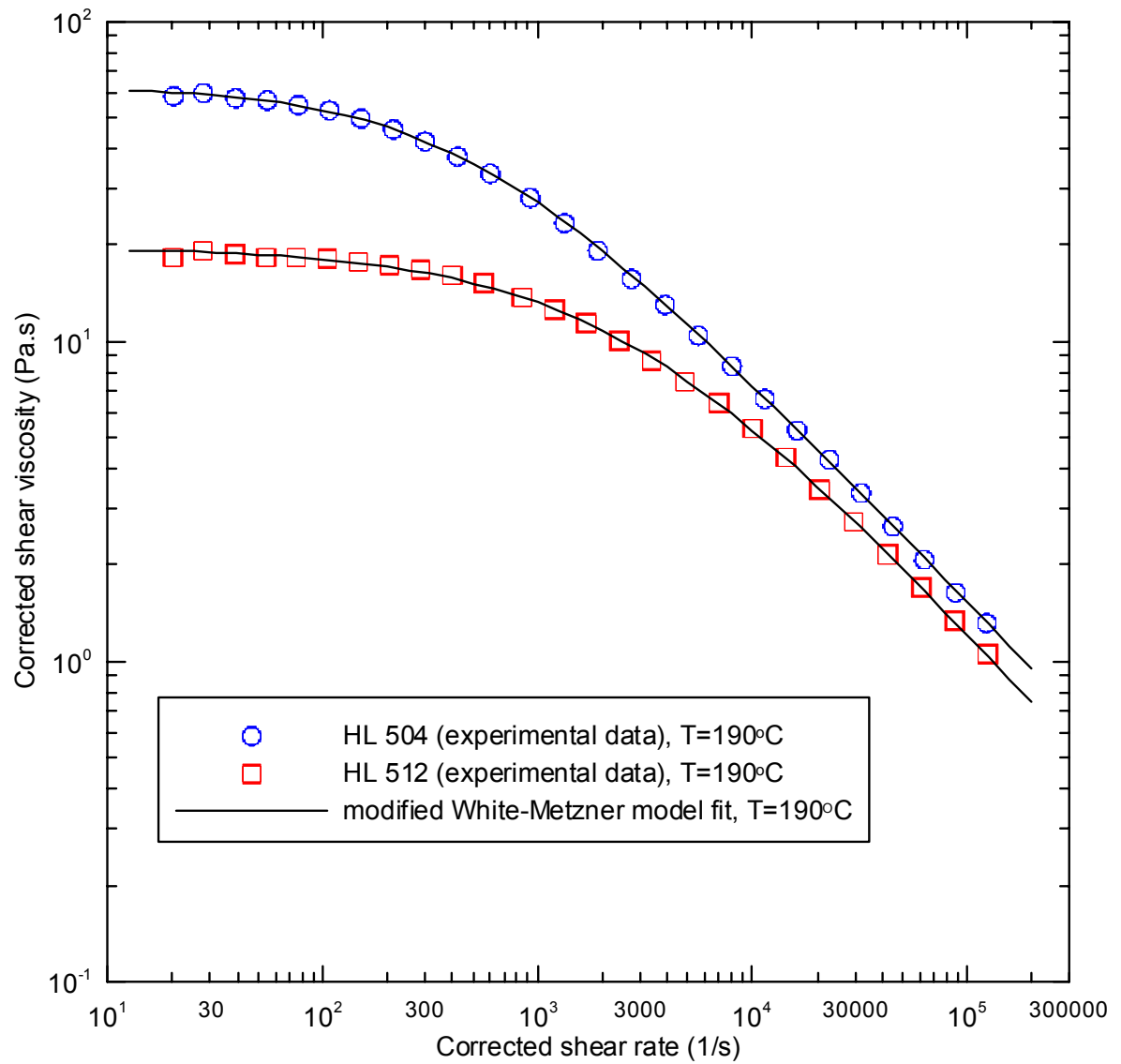
Fig. 50. Deformation rate dependent shear viscosity for HL 504 and HL 512 measured at 190°C.
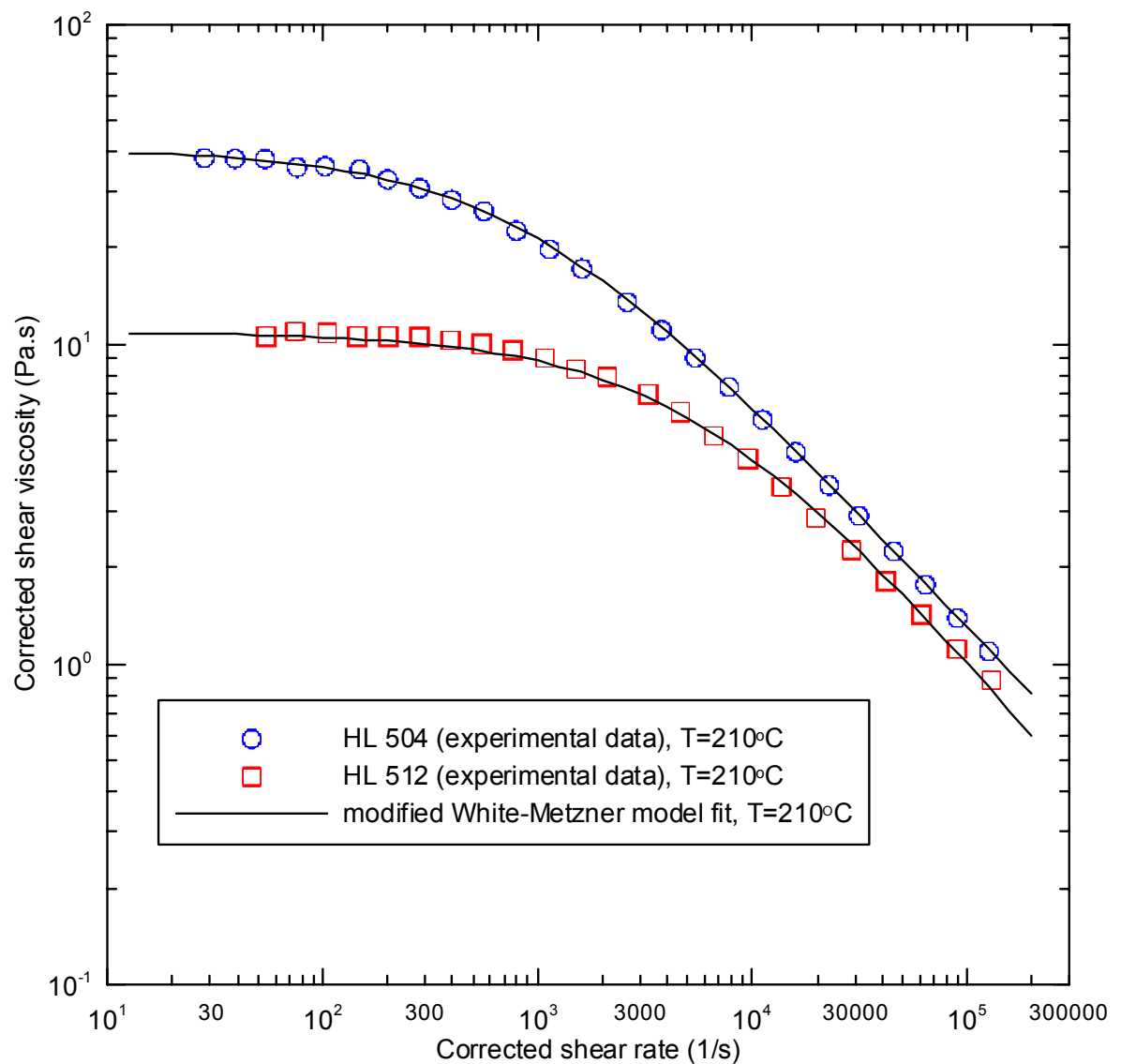
Fig. 51. Deformation rate dependent shear viscosity for HL 504 and HL 512 measured at 210ºC.
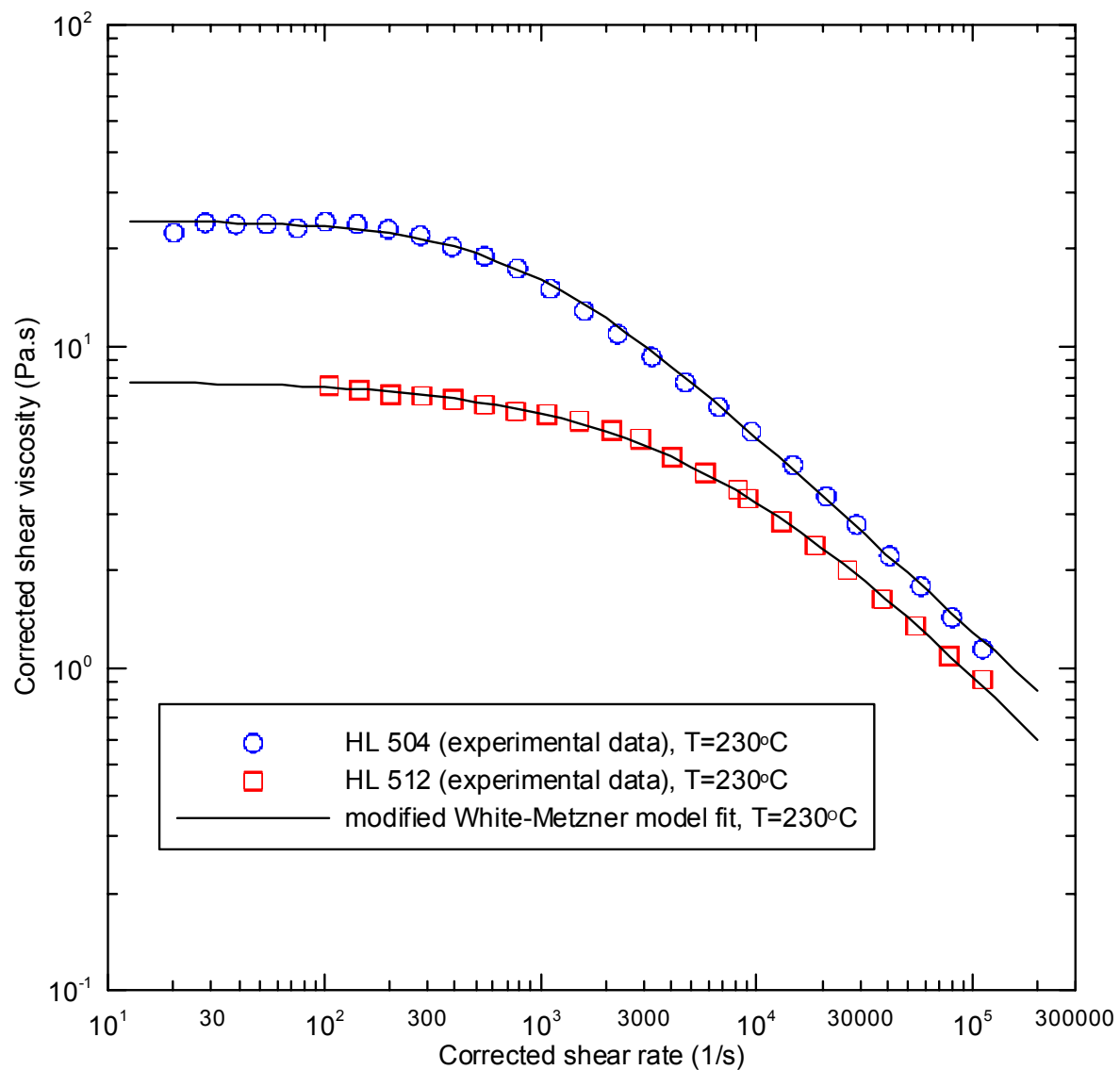
Fig. 52. Deformation rate dependent shear viscosity for HL 504 and HL 512 measured at 230ºC.
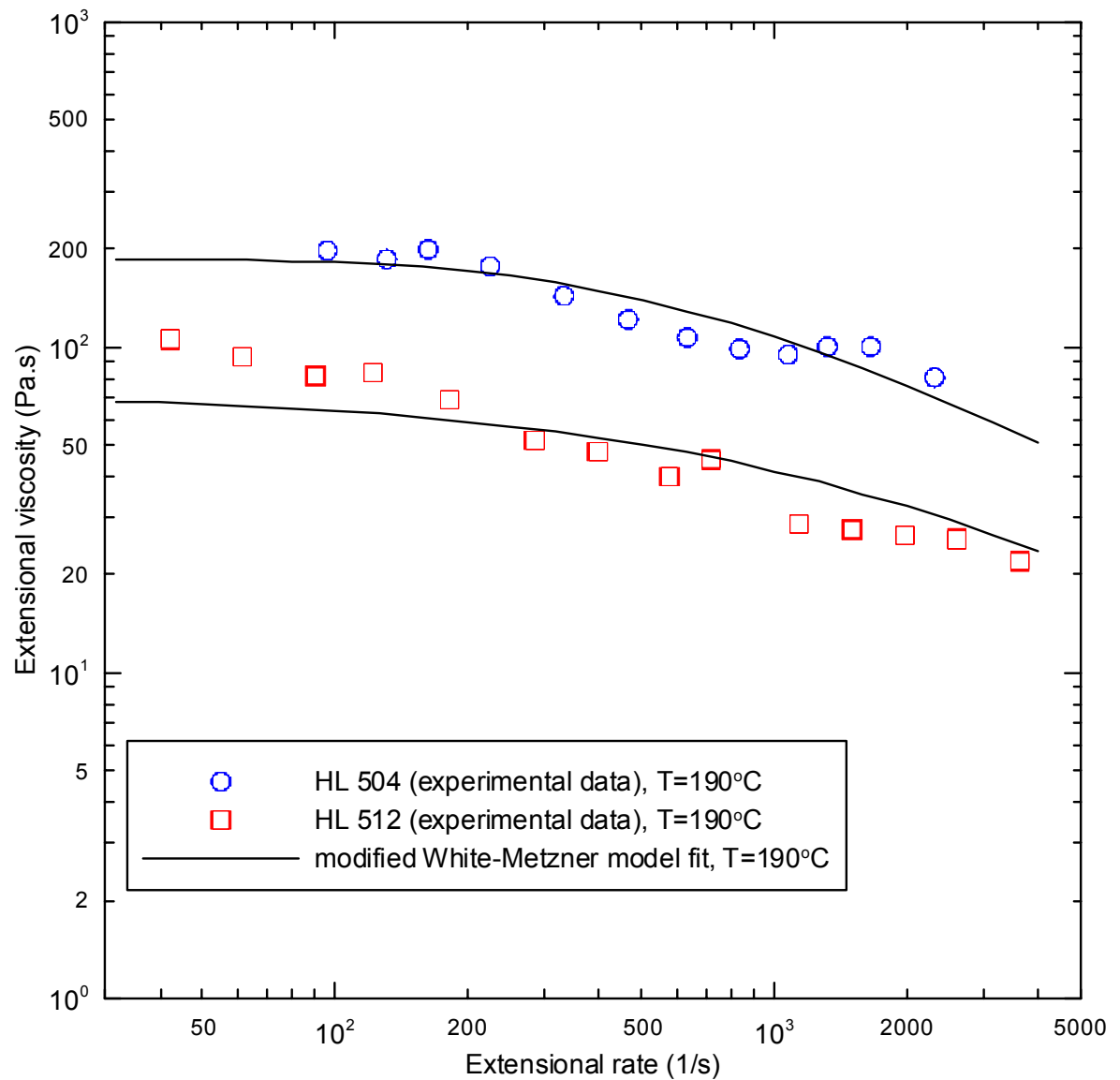
Fig. 53. Deformation rate dependent uniaxial extensional viscosity for HL 504 and HL 512 measured at 190ºC.
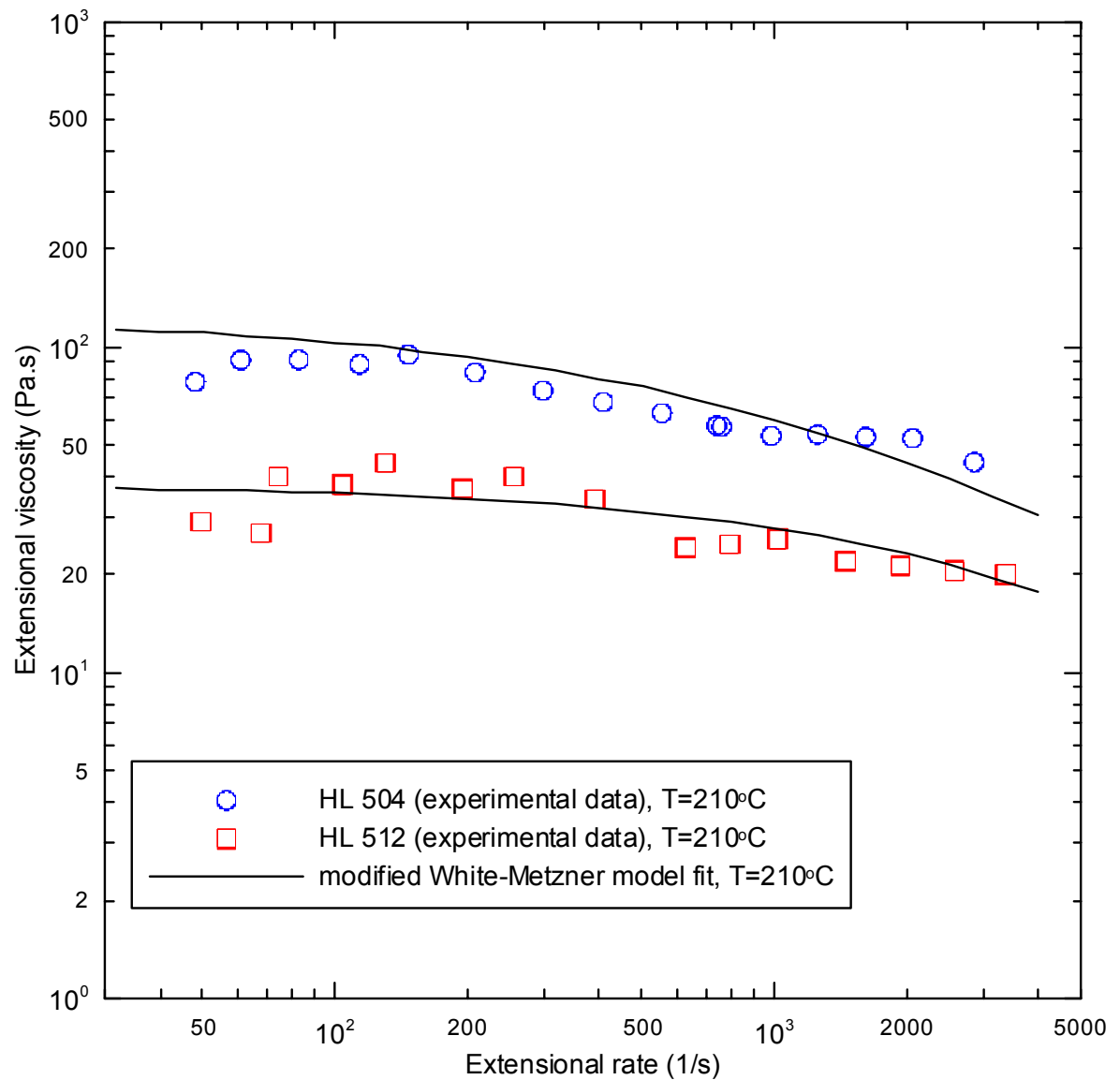
Fig. 54. Deformation rate dependent uniaxial extensional viscosity for HL 504 and HL 512 measured at 210°C.
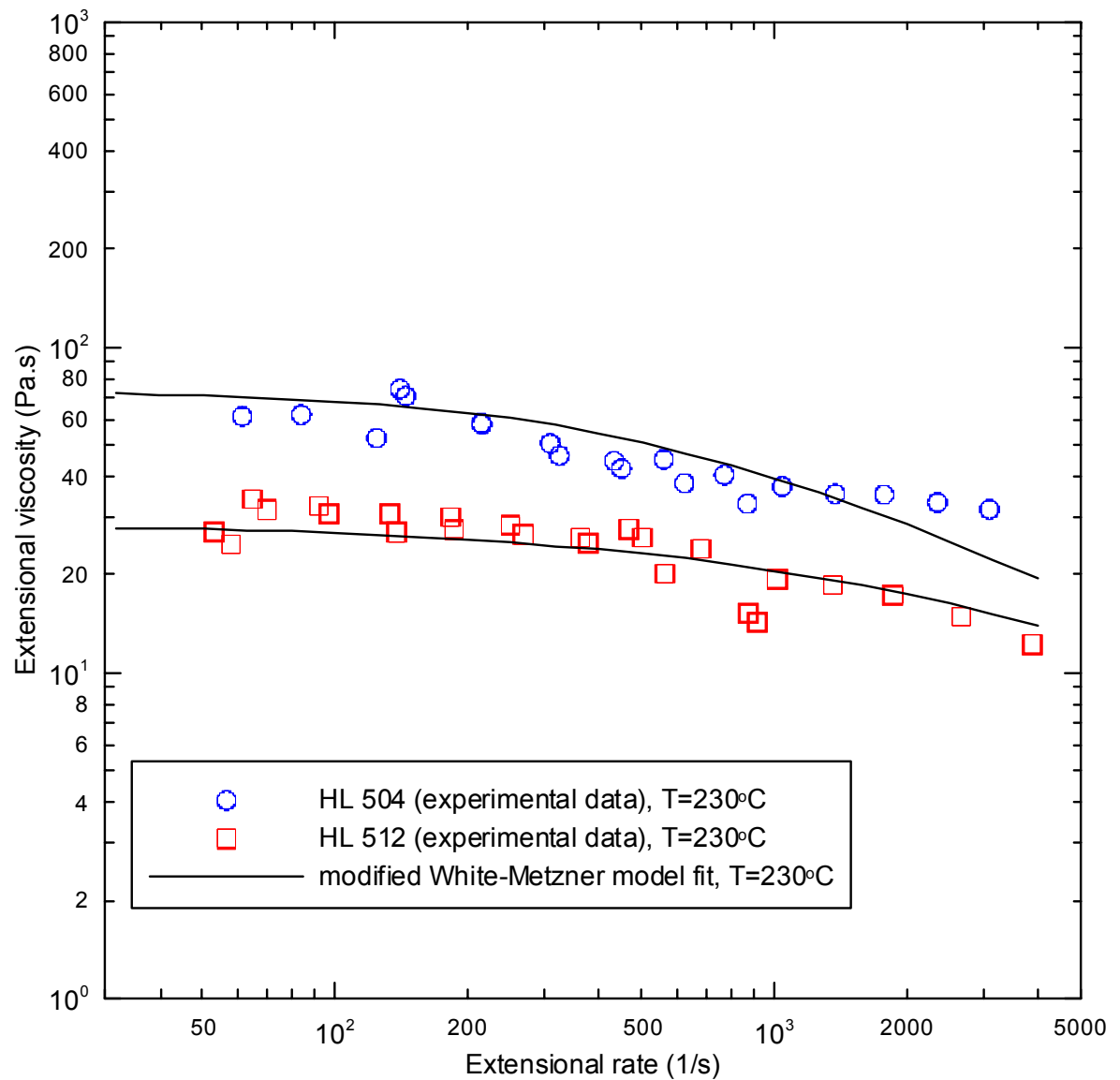
Fig. 55. Deformation rate dependent uniaxial extensional viscosity for HL 504 and HL 512 measured at $230^o C$.

CONCLUSION REMARKS

1. It has been concluded that the 500 PSI (long capillary)/250 PSI (short capillary) pressure transducer set-up should be preferred to measure basic rheological characteristics on the twin bore capillary rheometer for melt blown polymer samples.

2. Orifice die design with opened downstream region should only be preferred during entrance pressure drop/extensional viscosity measurements of melt blown samples; otherwise artificial increase of both variables may take place.

3. Physical rather than unphysical polynomial functions should be preferred during approximation function selection for the index of non-Newtonian behavior determination from the measured corrected shear stress vs. apparent shear rate data; otherwise shear as well as extensional viscosities might not be determined correctly, especially at low deformation rates.

4. It has been revealed that modified White-Metzner model [32, 33, 34] as well as Zatloukal model [30,31] can describe the measured shear as well as uniaxial extensional viscosity data of both melt blown samples very well, thus both model can be considered as good candidates for melt blown process modeling purposes.

5. PP HL 504 Newtonian viscosity (24.5-62.8 Pa.s), relaxation time (0.0012-0.0021) and index of non-Newtonian flow behavior (0.2870-0.3863) is higher than PP HL 512 Newtonian viscosity (7.8-18.9 Pa.s), relaxation time (0.001) and index of non-Newtonian flow behavior (0.18224-0.28128) within the investigated 190-230°C temperature range. This suggests that the diameter variation of the PP HL 504 based nanofibers can be expected to be smaller and fiber production more stable in comparison with PP HL 512 based nanofibers.

6. Extensional viscosity of PP HL 504 sample is higher than in the case of PP HL 512 i.e. PP HL 512 sample can be stretched more in post die area by the surrounding air and thus, it can be expected that the resulting fibers will have smaller diameter than PP HL 504 based fibers. On the other hand, specific care should be paid during melt blown die designing for PP HL 512 sample due to its high flow sensitivity to flow channel shape.

BIBLIOGRAPHY

[1] HUANG, Z.M., ZHANG, Y.Z., KOTAKI, M., RAMAKRISHNA, S.: Composites Science and Technology, Vol.63 (15), 2223-2253 (2003)

[2] SAMBAER, W., ZATLOUKAL, M., KIMMER, D.: 3D modeling of filtration process via polyuretane nanofiber based nonwoven filters prepared by electrospinning, DOI: doi:10.1016/j.ces.2010.10.035

[3] TAN, D. H., ZHOU, CH., ELLISON, CH. J., KUMAR, S., MACOSKO, CH. W., BATES, F. S.: Meltblown fibers: Influence of viskosity and elasticity on diameter distribution, D.H. Tanet al./J. Non-Newtonian Fluid Mech., Vol.165, 892-900 (2010)

[4] PINCHUK, L.S., GOLDADE, V.A., MAKAREVICH, A.V., KESTELMAN, V.N.: Melt blowing, equipment, technology, and polymer fibrous materials, Springer, United States of America, (2002)

[5] PODGRÓSKI, A., BALAZY, A., GRADÓN, L.: Application of nanofibers to improve the filtration efficiency of the most penetrating aerosol particles in fibrous filter, Chemical Engineering Science, Vol. 61, 6804-6815 (2006)

[6] DUTTON, K.C.: Overview and Analysis of the Meltblown Process and Parameters, JTATM, Vol.6, Issue 1, (2008)

[7] WANG, X., KE, Q.: Experimental Investigation of Adhesive Meltblown Web Production Using Accessory Air, Polymer Engineering and Science, Vol.46, 1-7 (2006)

[8] HEGDE, R. R., BHAT, G.S.: Nanoparticle effects on structure and properties of polypropylene Meltblown webs, Journal of Applied Polymer Science, Vol.115, 1062-1072 (2010)

[9] SUN, Q., ZHANG, D.: Analysis and Simulation of Non-Newtoian Flow in the Coat- Hanger Die of a Meltblown Process, Journal of Applied Polymer Science, Vol.67, 193-200 (1998)

[10] JOSEPH, E. G.: Structure and Properties of Multi-layer Melt Blown Microfiber Non-wovens, ANTEC, 1092-1095 (2010)

[11] MELT BLOWN TECHNOLOGY [online]. [cit. 2011-05-05]. Accessible from http://web.utk.edu/~mse/Textiles/Melt%20Blown%20Technology.htm

[12] LEE, Y. E., WADSWORTH, L. C.: Fiber and Web Formation of Melt-Blown Thermoplastic Polyuretane Polymers, Journal of Applied Polymer Science, Vol.105, 3723-3727 (2007)

[13] CHEN, T., ZHANG, CH., CHEN, X., Li, L.: Numerical Computation of the Fiber Diameter of Melt Blown Nonwovens Produced by the Inset Die, Journal of Applied Polymer Science, Vol.111, 1775-1779 (2009)

[14] LEE, Y., WADSWORTH, L.: Structure and Filtration Properties of Melt Blown Polypropylene Webs, Polymer Engineering and Science, Vol.30, 1413-1419 (1990)

[15] ELLISON, C.J., PHATAK, A., GILES, D.W., MACOSKO, C.W., BATES, F.S., Polymer, Vol. 48, 3306-3316 (2007)

[16] MACOSKO, CH. W., CHRISTOPHER, W.: Rheology – Principles, Measurements and Applications, New York, United States of America: John Wiley and Sons, (1994), ISBN 0-417-18575-2

[17] WARD, G. F., Meltblown nanofibers for nonwoven filtration applications, Filtration and Separation, Vol.38, 42-43 (2001)

[18] ZHAO, R., WADSWORTH, L. C., SUN, CH., ZHANG, D.: Properties of PP/PET bicomponent melt blown microfiber nonwovens after heat-treatment, Society of Chemical Industry, Vol. 52, 133-137 (2003)

[19] ZATLOUKAL, M.: Novel non-Newtonian fluid model for polymer melts, ANTEC, 92-96 (2011)

[20] WEI, Q., WANG, Y., WANG, X., HUANG, F., YANG, S.: Surface Nanostructure Evolutions of Functionalized Polypropylene Fibers, Journal of Applied Polymer Science, Vol. 106, 1243-1247 (2007)

[21] WANG, X., ZHAO, Q.: Effect of Processing Parameters on the Uniformity of Adhesive Meltblown Web, Polymer Engineering and Science, Vol.48, 2143-2146 (2008)

[22] CHEN, T., LI, L., HUANG, X.: Fiber Diameter of Polybutylene Terephthalate Melt-Blown Nonwovens, Journal of Applied Polymer Science, Vol. 97, 1750-1752 (2005)

[23] ELLISON, CH. J., PHATAK, A., GILDA, D. W., MACOSKO, CH. W., BATES, F. S.: Melt blown nanofibers: Fiber diameter distributions and onset of fiber breakup, Polymer, Vol. 48, 3306-3316 (2007)

[24] ZHANG, D., SUN, CH., BEARD, J., BROWN, H., CARSON, I., HWO, CH.: Development and Characterization of Poly(trimethylene terephthalate)- Based Bicomponent Meltblown Nonwovens, Journal of Applied Polymer Science, Vol. 83, 1280-1287 (2002)

[25] LIU, L., XU, Z., SONG, C., GU, Q., SANG, Y., LU, G., HU, H., LI, F.: Adsorption-filtration characteristics of melt-blown polypropylene fiber in purification of reclaimed water, Desalination, Vol. 201, 198-206 (2006)

[26] MALKIN, A. Y., ISAYEV, A. I.: Rheology-Concepts, Methods, and Applications, Toronto, Canada: ChemTec Publishing, (2006), ISBN 1-895198-33-X

[27] MORRISON, F. A.: Understanding rheology, New York, United States of America: Oxford university press, Inc., (2001), ISBN 0-19-514166-0

[28] MUSIL, J.: Development of improved entrance pressure drop techniques, Master thesis, Tomas Bata University in Zlín, (2008)

[29] SONG, W. N., XIA, Z. M.: A phenomenological viscosity model for polymeric fluid, J. Non-Newtonian Fluid Mech., Vol. 53, 151-163 (1994)

[30] ZATLOUKAL, M.: A simple phenomenological non-Newtonian fluid model, J. Non-Newtonian Fluid Mech., Vol.165, 592-595 (2010)

[31] ZATLOUKAL, M.: Novel non-Newtonian fluid model for polymer melts, ANTEC, 92-96 (2011)

[32] ZATLOUKAL, M.: Differential viscoelastic constitutive equations for polymermelts in steady shear and elongational flows, J. Non-Newtonian Fluid Mech., Vol. 113, 209-227 (2003)

[33] BARNES, H. A., ROBERTS, G. P.: A simple empirical model describing the steady-state shear and extensional viscosities of polymer melts, Journal of Non-Newtonian Fluid Mechanics, Vol. 44, 113-126 (1992)

[34] ZATLOUKAL, M.: Behavior of Constitutive Equations for polymer melts in different flow situations, Master thesis, Tomas Bata University in Zlín, (1997)

[35] ZATLOUKAL, M., MUSIL, J.: Analysis of entrance pressure drop techniques for extensional viscosity determination, Polymer Testing, Vol. 28, 843-853 (2009)

[36] MUSIL, J.: The effect of long chain branching on processibility of polymer melts, Bachelor thesis, Tomas Bata University in Zlín, (2006)

[37] COGSWELL, F. N.: Converging flow of polymer melts in extrusion dies, Polymer Engineering and Science, Vol.12, 64-73 (1972)

LIST OF ABBREVIATIONS

y	Air velocity	m/s
x	Distance from the die	m
A_1	Adjustable parameter from equation (1)	m/s
A_2	Adjustable parameter from equation (1)	m/s
x_0	Adjustable parameter from equation (1)	m
d_x	Adjustable parameter from equation (1)	m
$\dot{\gamma}$	Shear rate	s^{-1}
Ω	Rotation rate	rad. s^{-1}
R	Current radius	m
h	Distance between the parallel plates	m
N_1	First normal stress difference	Pa
N_2	Second normal stress difference	Pa
M	Torque	N.m
F_z	Normal force	N
$\underline{\underline{\tau}}$	Extra stress tensor	Pa
η_0	Newtonian viscosity	Pa.s
$\underline{\underline{D}}$	Stand for the deformation rate tensor	s^{-1}
η	Shear viscosity	Pa.s
a_t	Arrhenius equation for temperature-depend shift factor	1
η_∞	Limiting shear viscosity at infinite shear rate	Pa.s
Tr_1	Trouton ratio	1
I_d	First invariant of deformation rate tensor	s^{-1}
II_d	Second invariant of deformation rate tensor	s^{-1}

III_d	Third invariant of deformation rate tensor	s^{-1}
a	Adjustable parameter from equation (3,9,17)	1
n	Adjustable parameter from equation (3,7,9,17)	1
$Tr_{1\infty}$	Adjustable parameter from equation (4)	1
μ	Adjustable parameter from equation (4)	s
l	Adjustable parameter from equation (4)	1
E_a	Stand for activation energy	J
R	Universal gas constant	$J.mol^{-1}.K^{-1}$
T	Temperature	^oC
T_r	Reference temperature	^oC
m	Adjustable parameter from equation (7)	s^2
A	Constant from equation (8)	Pa.s
$\eta(II_D,T)$	Second invariant of deformation rate tensor and temperature dependent shear viscosity	Pa.s
$\bar{\lambda}(II_D,T)$	Stands for the deformation rate dependent relaxation time and second invariant	s
α	Adjustable parameter from equation (10)	s
ψ	Adjustable parameter from equation (10)	1
β	Adjustable parameter from equation (10)	1
ζ	Adjustable parameter from equation (10)	1
$\overset{\triangledown}{\underline{\underline{\tau}}}$	Upper convected tress tensor derivate	Pa. s^{-1}
K_2	Parameter with the dimension of time	s
λ_0	Constant from equation (18)	s
$\dfrac{D}{Dt}$	Substantial derivate	s^{-1}

L	Velocity gradient	s^{-1}
v	Velocity vector	m/s
η_E	Uniaxial extensional viscosity	Pa.s
L_{OC}	Length of the orifice capillary	m
D_{OC}	Diameter of orifice capillary die	m
L_{LC}	Length of the long capillary	m
D_{LC}	Diameter of long capillary die	m
τ_{xy}	Shear stress	Pa
P_{LC}	Stands for pressure drop measured on long capillary	Pa
P_{OC}	Stands for pressure drop measured on orifice capillary	Pa
R_C	Capillary die radius	m
$\dot{\gamma}_{APP}$	Apparent shear rate	s^{-1}
Q	Volume flow rate	s^{-1}
N	Represent index of non-Newtonian behavior in equation (23, 24, 26, 27, 30)	1
σ_E	Extensional stress	Pa
$\dot{\varepsilon}$	Extensional rate	s^{-1}
η_E	Extensional viscosity	Pa.s
σ_R	Rupture stress	Pa
D_B	Diameter of capillary rheometer barrel	m
b	Temperature sensitive parameter	${}^{o}C^{-1}$
λ	Adjustable parameter from equations (3,9,17)	s
Δp	Pressure drop in capillary	Pa

L	Length	m
L_c	Length capillary	m
ΔP_{EXIT}	Pressure drop on exit	Pa
ΔP_{CAP}	Pressure drop in capillary	Pa
ΔP_{ENTR}	Pressure drop on enter	Pa

LIST OF FIGURES

LIST OF TABLES

APPENDICES

Appendix A I: CD-ROM